General Disclaimer

One or more of the Following Statements may affect this Document

- This document has been reproduced from the best copy furnished by the organizational source. It is being released in the interest of making available as much information as possible.

- This document may contain data, which exceeds the sheet parameters. It was furnished in this condition by the organizational source and is the best copy available.

- This document may contain tone-on-tone or color graphs, charts and/or pictures, which have been reproduced in black and white.

- This document is paginated as submitted by the original source.

- Portions of this document are not fully legible due to the historical nature of some of the material. However, it is the best reproduction available from the original submission.

RESEARCH REPORT

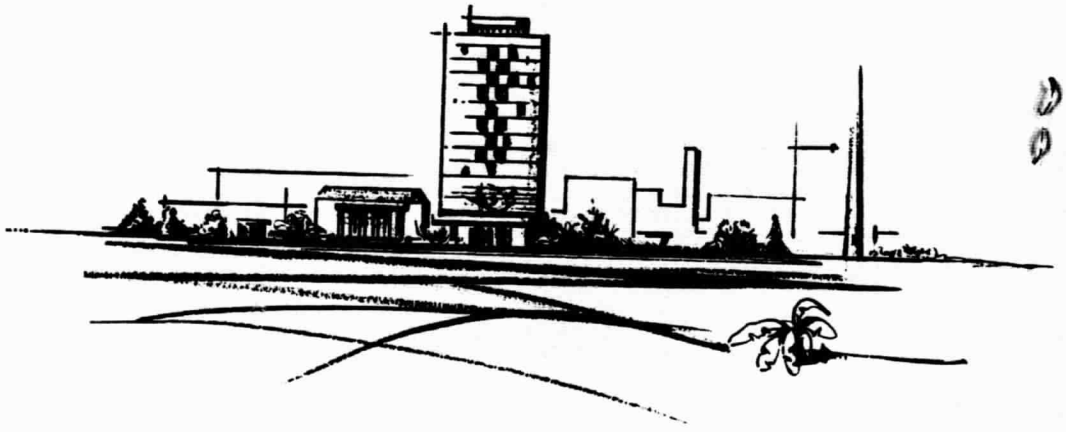

BATTELLE MEMORIAL INSTITUTE

COLUMBUS LABORATORIES

FINAL REPORT

on

AN ADVANCED THERMOELECTRIC LIFE TEST AND EVALUATION STUDY

(December 28, 1967 - September 28, 1968)

CONTRACT NO. NAS5-10497

GODDARD SPACE FLIGHT CENTER

Contracting Officer: Peter Videnieks
Technical Monitor: Joseph Fry

Prepared by:

BATTELLE MEMORIAL INSTITUTE
COLUMBUS LABORATORIES
505 King Avenue
Columbus, Ohio 43201

Project Manager: Philip E. Eggers

for

GODDARD SPACE FLIGHT CENTER
Greenbelt, Maryland

TABLE OF CONTENTS

TABLE OF CONTENTS
(Continued)

APPENDIXES

LIST OF TABLES

LIST OF FIGURES

LIST OF FIGURES
(Continued)

LIST OF FIGURES
(Continued)

AN ADVANCED THERMOELECTRIC
LIFE TEST AND EVALUATION STUDY

ABSTRACT

The tasks in this program involve diverse technologies and, consequently, are reported as separate chapters in this report. Under Task I, Development of Uniform Procedures for Tests and Measurements of Thermoelectric Materials and Components, a comprehensive study of the theory of the measurement of Seebeck coefficient, electrical resistivity, and electrical contact resistivity has been completed. On the basis of these studies, test apparatus have been designed and measurements have been performed in order to optimize measurement procedures and empirically derive the precision limits associated with the technique. In addition, a comprehensive study of life testing and efficiency measurement was performed which led to the design of new measurement techniques. In the development of the life-test and efficiency-measurement techniques, particular attention was placed on the applicability of the derived experimental data to the prediction of RTG performance. The work performed under Task II, RTG Analysis and Design, progressed to the point where the user-orientation of input/output formats of the existing RTG computer program was completed. In addition, the mathematical model used in the analysis was qualified by performing a three-dimensional heat-transfer analysis of a typical generator design case. Theoretical thermopile performance data were incorporated into a typical RTG design in order to predict the output power and efficiency of the system as a function of time. Under Task III, Thermoelectric Materials Studies, the Seebeck coefficient, electrical resistivity, and thermal conductivity have been measured for 2p-PbTe and

3p-PbSnTe materials in "nonstandard" conditions. The nonstandard conditions selected include oxygen-contaminated 2p-PbTe, copper-contaminated 2p-PbTe, and oxygen-contaminated 3p-PbSnTe. The experimental results indicate that the overall figure of merit associated with each nonstandard condition is significantly lower than that of normal 2p-PbTe and 3p-PbSnTe material. A similar relationship was observed on the power factor of 2p-PbTe, whereas, the calculated power factor for 3p-PbSnTe is relatively insensitive to the condition of the material. Under Task IV, Fabrication and Testing of SiGe-PbTe Thermoelectric Couples, the optimum sizes for the SiGe and PbTe segments were theoretically determined, eight segmented* couples have been fabricated, installed into life-test fixtures, and maintained on test for periods up to 3200 hr. The results of life testing indicate that the use of pressure-contacted junctions at the SiGe-PbTe interface provides acceptably low electrical contact resistance and a high degree of mechanical stability. However, the surface of the tungsten intermediate shoe adjacent to the PbTe usually became heavily oxidized after 500-1000 hr on test, hence, increasing the resistance of the intermediate junctions. The control of the formation of these oxide layers was complicated by the presence of Fiberfrax thermal insulation which releases significant amounts of water vapor when operated at elevated temperatures. The operating temperatures selected for life testing were 1200 K, 800 K, and 300 K for the hot junction, intermediate junction, and cold junction, respectively.

---

* The term segmenting refers to the thermal and electrical series operation of the thermoelectric materials.

INTRODUCTION

This is the final progress report issued under Contract NAS5-10497 by Battelle's Columbus Laboratories to National Aeronautics and Space Administration, Goddard Space Flight Center. Work under this program was initiated December 28, 1967, and has been performed in four tasks.

TASK I. DEVELOPMENT OF UNIFORM PROCEDURES FOR TESTS AND MEASUREMENTS OF THERMOELECTRIC MATERIALS AND COMPONENTS

The experience of thermoelectric systems contractors and experimental investigators has indicated the need for uniform procedures for tests and measurements of thermoelectric materials and components. In this task, BCL has undertaken work which addresses itself to this need by developing the measurement theory, accuracy, and precision limits which must be considered in the specification of the test and measurement techniques. Emphasis has been placed on the selection of "standards" (where applicable) for the calibration of the experimental apparatus. The establishment of a "standard" provides the laboratory reference necessary for direct comparison of experimental results obtained by various research groups. The test and measurement techniques investigated in this task include Seebeck coefficient measurement, electrical-resistivity measurement, contact-resistivity measurement, life testing, and conversion-efficiency measurement.

TASK II. RTG ANALYSIS AND DESIGN

The existing version of the Generalized Space Generator (GESPGN) computer program, developed under NASA-Goddard Contract NAS5-9160 for the weight optimization of radioisotope thermoelectric generators (RTG), has been "user-oriented" to permit more efficient data input compilation and output data reduction. The input data compilation and output data reduction have been simplified by (1) subdividing the input data into classes of variables according to frequency of change, (2) compilation of a "library" of permanent input data, (3) utilization of data generation subroutines to minimize the amount of data input, (4) reorganizing the tabular output according to logical classes of calculated data, and (5) providing graphical display of selected parameters using "printer-plotting" techniques. A three-dimensional heat-transfer analysis was performed to verify the temperature distribution assumed in the formulation of the analytical model. In addition, theoretical thermopile performance data were incorporated into an RTG design in order to predict output power and efficiency of the system as a function of time.

TASK III. THERMOELECTRIC MATERIALS STUDIES

A quantitative knowledge of the relationship of thermal conductivity to electrical properties for thermoelectric materials in "nonstandard" conditions would greatly increase the present ability to predict performance and/or explain the cause(s) of changing performance characteristics during thermopile operation. In the present task, the study of the interrelationship

of thermal and electrical properties has been restricted to 2p-PbTe and 3p-PbSnTe thermoelectric materials in a total of three nonstandard conditions, viz., oxygen-contaminated 2p-PbTe and 3p-PbSnTe and copper-contaminated 2p-PbTe.

TASK IV. FABRICATION AND TESTING OF SiGe-PbTe THERMOELECTRIC COUPLES

Combining two or more thermoelectric materials is a technique for achieving increased conversion efficiency since, by employing the proper design, each material operates in its optimum performance temperature range. The technique referred to as segmenting involves joining the thermoelectric materials in series electrically and thermally. Joining PbTe and SiGe materials in segmented element configurations is complicated by their widely differing mechanical and physical properties. This program, based on technology developed under NASA-Goddard Contract NAS5-10185, is being undertaken to continue long-term performance tests on selected SiGe-PbTe segmented couple configurations operating in the temperature range 300 to 1200 K.

The ensuing chapters are identified by task and have been performed by P. E. Eggers (Tasks I, II, IV), R. E. Best (Task II), and J. J. Mueller (Task III). The technical review of this report was performed by M. Pobereskin.

DISCUSSION

TASK I. DEVELOPMENT OF UNIFORM PROCEDURES FOR TESTS AND MEASUREMENTS OF THERMOELECTRIC MATERIALS AND COMPONENTS

Development of Seebeck Coefficient Measurement Technique

Theory

A comprehensive study of the theory of the Seebeck coefficient, supplemented by a survey of the literature[(1-12)*] regarding various measurement techniques, revealed that, in general, high-precision and high-accuracy measurements of the Seebeck coefficient can be achieved within the framework of presently accepted techniques. It is well known that the Seebeck coefficient, S, of thermoelectric materials is determined most commonly from the potential difference**, V, produced when the semiconductor is placed between two contacts with a known temperature difference $(T_1 - T_2)$. Based on the above parameters, the Seebeck coefficient is defined by the following equation:

$$S(\bar{T}) = \frac{V}{(T_1 - T_2)} \quad ,$$

where $\bar{T}$ is the mean temperature of the specimen. Therefore, conventional methods, i.e., the measurement of thermocouple and voltage probe emf values,

---

* See "Bibliography" at end of report.

** Commonly referred to as the Seebeck emf.

were adopted in the measurement of the specimen temperatures (T_1 and T_2) and the Seebeck emf (V) with special emphasis on the refinement of these methods.

The specific conclusions of this study were the basis for the development of the Seebeck coefficient measurement technique and are summarized below.

(1) The Seebeck emf can be assumed independent of the temperature distribution within the thermoelectric material and dependent only on the temperature at the junctions only if the thermoelectric material is chemically and physically homogeneous.

(2) The measured Seebeck emf is dependent on the chemical and physical homogeneity of the voltage-tap wires which lead to the potentiometer. Likewise, inhomogeneities in the thermocouple wires will result in erroneous temperature readings.

(3) The voltage taps and thermocouples should be positioned on the thermoelectric specimen so that heat flow between the thermocouple and specimen is minimized. The flow of heat across the interface between the thermocouple and specimen results in a temperature difference (hence, an error in the temperature reading) whose magnitude is a function of the total heat flow and the characteristic thermal contact resistance of the interface.

(4) The measurement of Seebeck coefficient using the "fixed cold-junction, variable hot-junction" technique (integral technique) is usually less accurate than the "fixed temperature difference, variable mean temperature" technique (differential technique).

In the integral technique, a differentiation of the data is performed to obtain the Seebeck coefficient, hence, small errors in the data which are obtained from the plot of Seebeck voltage versus temperature can lead to large errors in the derivative. In addition, compensation must be made for inevitable changes in T_c during the experiment.

(5) Large errors may result if current is allowed to flow during the measurement of the Seebeck emf, V, since a finite current flow produces an undesirable ohmic contribution to the measured potential difference.

Sensitivity of Measurement Technique

A sensitivity analysis was performed in order to isolate the major source(s) of error in the measurement of Seebeck coefficient. The results of this theoretical analysis indicate that the error associated with the measurement of the temperature difference across the specimen, i.e., the ΔT, is the dominant factor. As an illustration, the variation of the theoretical accuracy limits of Seebeck coefficient measurement for various ΔT values and thermocouple calibrations is presented in Table 1. These limits are based on the characteristic accuracy of uncalibrated and calibrated Pt-vs-Pt-Rh thermocouples and the voltage measurement error

TABLE 1. THEORETICAL ACCURACY LIMITS FOR SEEBECK COEFFICIENT MEASUREMENT FOR VARIOUS ΔT VALUES AND THERMOCOUPLE CALIBRATIONS

ΔT, C	ΔS_1 [(a)], percent	ΔS_2 [(b)], percent
20	20.6	9.13
30	13.7	6.13
40	10.3	4.53
50	8.23	3.63

(a) ΔS_1 corresponds to (1) uncalibrated Pt-vs-Pt-Rh thermocouples which typically exhibit an inaccuracy of ±0.25 percent of the measured temperature and (2) a digital voltmeter error of ±6 μvolts over the entire range of measurements.

(b) ΔS_2 corresponds to (1) calibrated Pt-vs-Pt-Rh thermocouples which typically exhibit an inaccuracy of ±0.1 C over the temperature range 20 C to 500 C and (2) a digital voltmeter error of ±6 μvolts over the entire range of measurements.

associated with the digital voltmeter. The computed accuracy limits shown in Table 1 suggest that maximum accuracy can be achieved by (1) maximizing the temperature difference, i.e., the ΔT, across the specimen and (2) calibrating the thermocouples used to determine the ΔT. It is noteworthy that the relative calibration of the ΔT thermocouples is considerably more critical than the absolute calibration. For example, two platinum-vs-platinum-rhodium thermocouples taken from two separate lots of wire with a rated inaccuracy of ±2 C would result in a ΔT measurement error (for $\Delta T \cong$ 30 C) of $\sim$13 percent. However, it has been experimentally confirmed that two platinum-vs-platinum-rhodium thermocouples taken from the same lot (at adjacent locations on a given spool of thermocouple wire) with a rated inaccuracy of ±2 C would result in a ΔT measurement error (for $\Delta T \cong 30$ C) of nominally 0.1 percent. This significant reduction in error is attributed to the localized uniformity of the thermocouple wire. Hence, the only consequence of the thermocouple error in the latter case is the uncertainty in the mean specimen temperature associated with the measured Seebeck coefficient value.

Design and Fabrication of Test Apparatus

The design of the Seebeck coefficient apparatus (see Figure 1) is based on the above considerations and features (1) a hermetically-sealed quartz test-fixture container insuring minimum environmental contamination of specimen, (2) the use of platinum, platinum-rhodium thermocouples which permit highly accurate temperature measurements and exhibit a high degree of stability at elevated temperatures in the presence of environmental contamination, e.g., oxygen, (3) the use of platinum emf leads since platinum

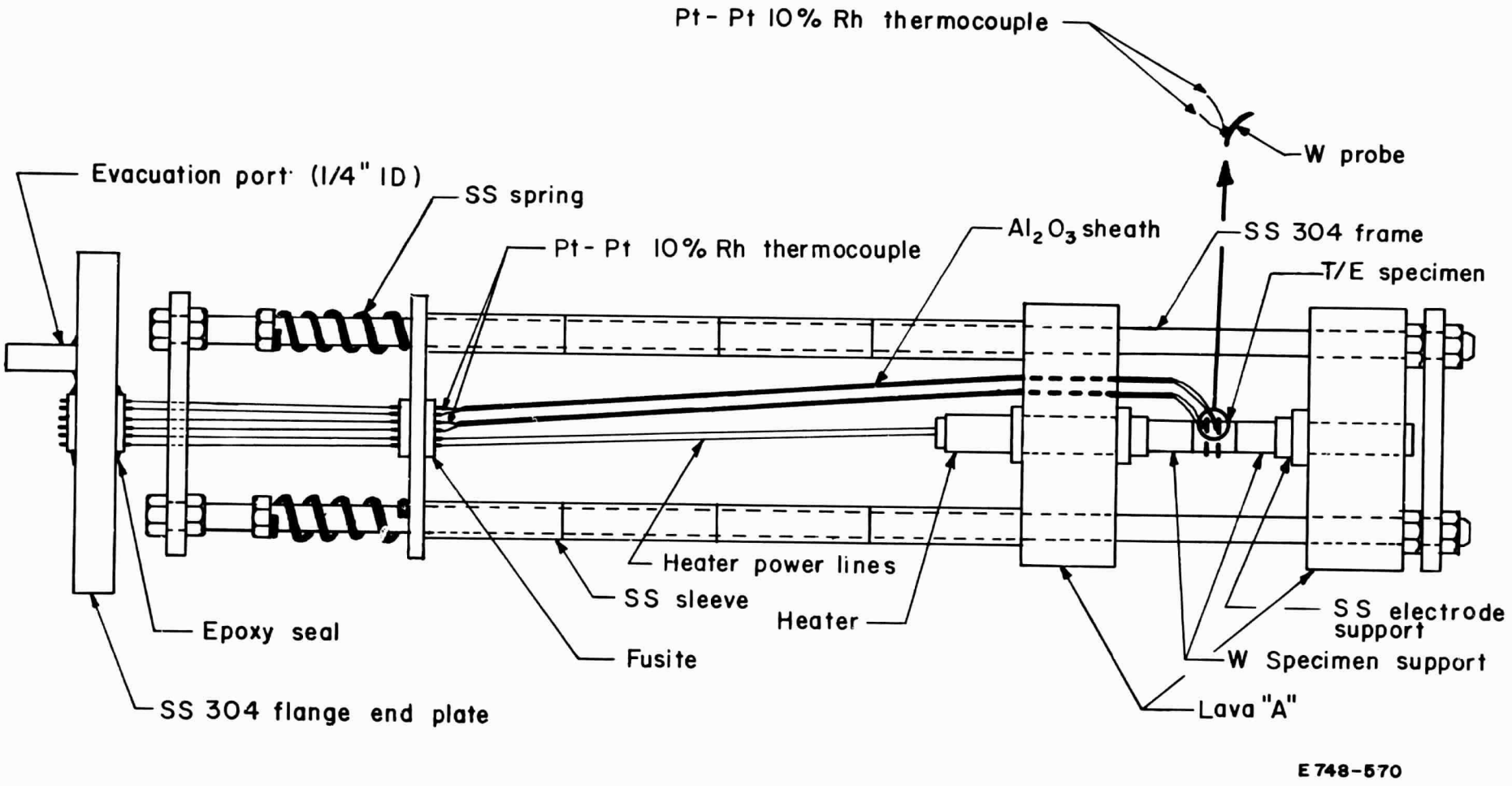

FIGURE 1. SEEBECK COEFFICIENT APPARATUS

is a universally accepted reference material for Seebeck emf measurements and exhibits a high degree of stability at elevated temperatures in the presence of environmental contamination, (4) the use of tungsten "voltage-thermocouple" probes and specimen supports (see Figure 1) in contact with the semiconductor surface to avoid "poisoning" the specimen, and (5) the use of a high impedance (10 MΩ) digital voltmeter to minimize current flow in the specimen during Seebeck emf measurements.

One test fixture has been fabricated according to the above specifications and is shown in Figure 2. This test fixture will be used to (1) optimize the measurement parameters, e.g., the temperature drop across the specimen (ΔT) and specimen heatup rate and (2) empirically derive the precision of the measurement technique selected.

Experimental Results

The Seebeck coefficient apparatus was subjected to pretest qualification to (1) ascertain the adequacy of the hermetic seals, e.g., quartz-to-metal seals and O-ring seal, and (2) ascertain the adequacy of bond between the tungsten probe and the platinum-vs-platinum-rhodium thermocouple. The hermetic seals were examined using a helium leak detector* and found to exhibit a leak rate of less than 1×10^{-9} atm-cc/sec (He). Prior to the installation of the PbTe element, the Seebeck coefficient apparatus was evacuated to 2×10^{-5} torr and operated for 60 hr at ~900 F. The Seebeck coefficient apparatus was disassembled and an examination revealed that the bond between the tungsten probe and the platinum-vs-platinum-rhodium thermocouple was unaffected.

---

* Consolidated Electrodynamic helium leak detector (Type 24-120B).

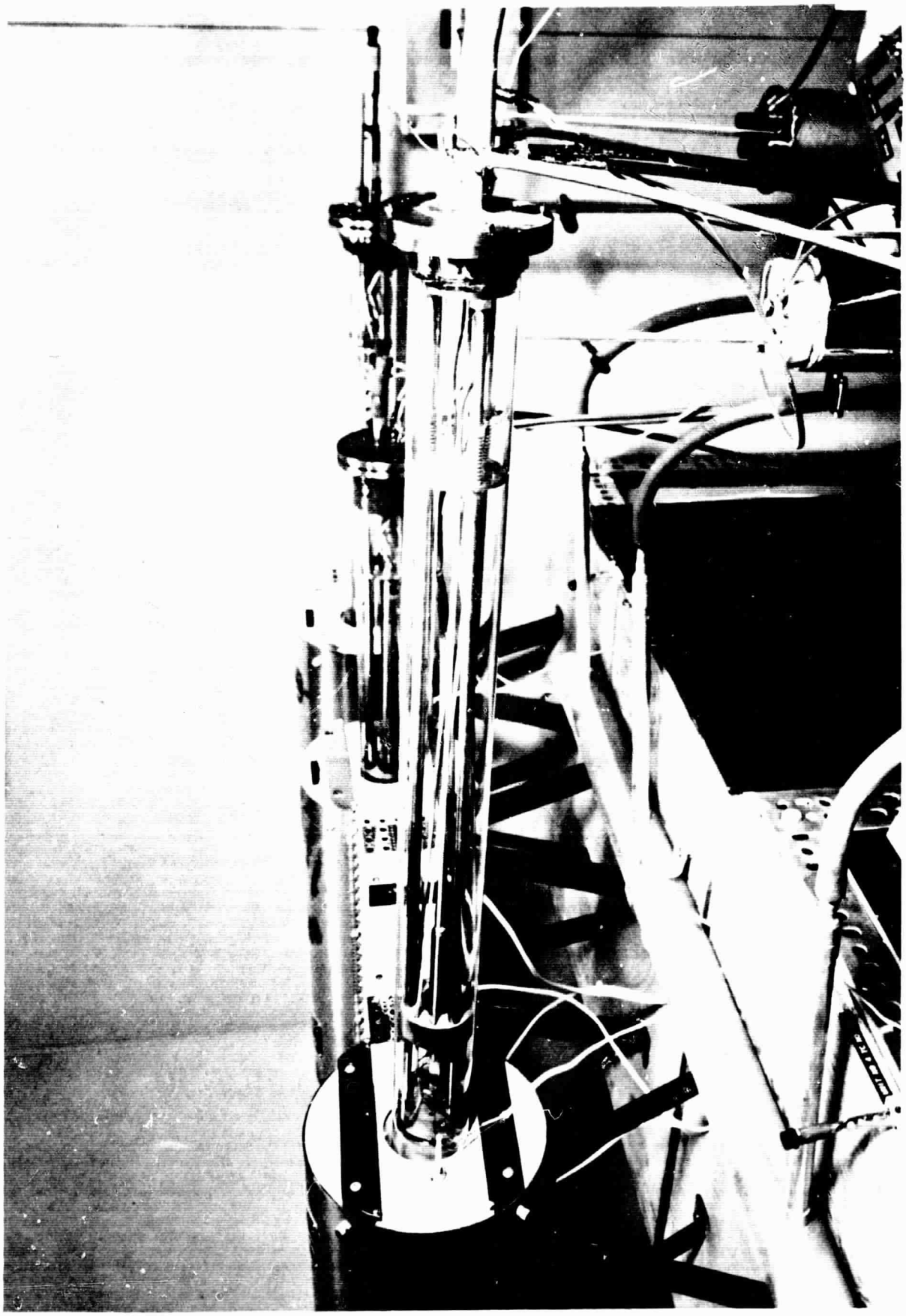

FIGURE 2. SEEBECK COEFFICIENT AND ELECTRICAL-RESISTIVITY-MEASUREMENT APPARATUS

Following the preliminary qualification tests, the Seebeck coefficient measurements were initiated. The measurement apparatus and instrumentation are shown in Figure 3. A total of 17 Seebeck coefficient measurements have been performed on two 2p-PbTe elements (Specimens 1 and 2) over the temperature range 20 to 527 C. Seven measurements were performed on Specimen 1 and ten measurements performed on Specimen 2.

In order to evaluate the effect on Seebeck coefficient measurement of heat transfer between the specimen and the environment, six of the measurements (on Specimen 1) were performed in argon (10-50 ppm 0_2) and one measurement was performed in vacuum. Although the specimen operated in vacuum was above 450 C for only 1 hr, a measurable increase in the Seebeck coefficient above 300 C was observed in subsequent measurements.

In the seven Seebeck coefficient measurements performed on Specimen 1, a ΔT of $\sim$40 C was used in the specimen temperature range 20 to 300 C followed by a monotonically decreasing ΔT value in the range 300 to 500 C with a ΔT of $\sim$20 C at a specimen temperature of 500 C. An analysis of the measurements on Specimen 1 revealed that measurements performed in argon yield results similar to the measurement performed in vacuo, however, the exposure of 2p-PbTe to vacuum conditions above 450 C for periods up to 1 hr appears to produce measurable increases in the Seebeck coefficient (20 μv/C increase at 500 C).

Ten additional Seebeck coefficient measurements were performed on Specimen 2 in argon ($<$10 ppm 0_2) since previous measurements performed in vacuum adversely affected the stability of the electrical properties.

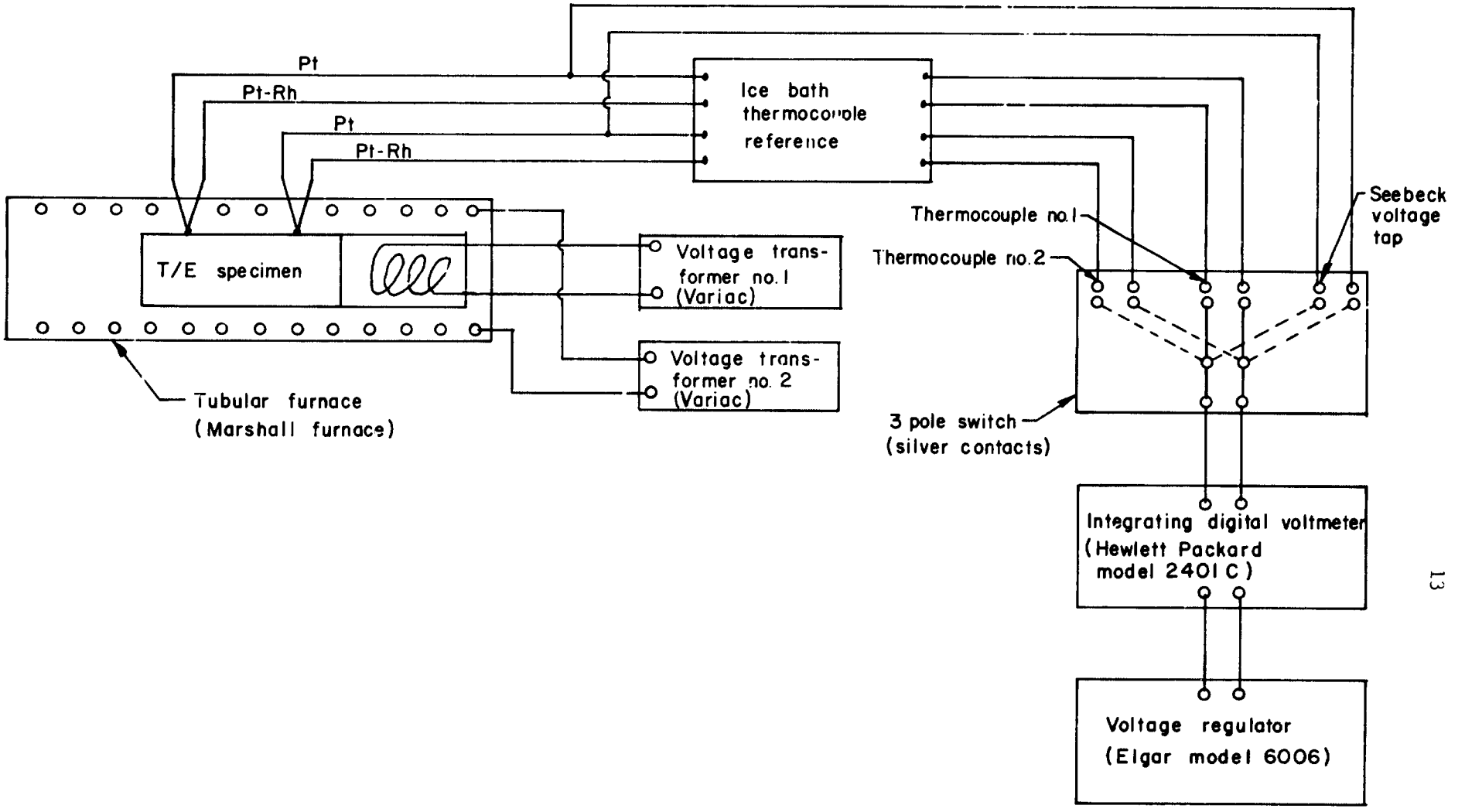

FIGURE 3. SCHEMATIC FOR SEEBECK-COEFFICIENT-MEASURING APPARATUS

An analysis of the experimental data gathered on Specimen 2 revealed that:

(1) Using specimen heatup rates of 3 C/min or less and digital voltmeter readout rates of ~3 channels/7 sec, dynamic measurements can be performed while introducing less than 1 percent error into the measurement

(2) Measurements performed in commercial-grade argon (nominally 10 ppm 0_2) above 500 C for periods up to 1 hr appear to produce no significant change in the Seebeck coefficient

(3) Reproducible measurements of Seebeck coefficient were achieved using a ΔT of 45 C in the range 20 to 300 C followed by a monotonically decreasing ΔT value in the range 300 to 500 C with a ΔT of ~30 C at a specimen temperature of 500 C.

The precision associated with the Seebeck coefficient measurement technique discussed above was empirically derived by calculating the standard deviation associated with the ten sets of measurements performed on Specimen 2. A total of 88 data points (obtained from ten sets of measurements) were statistically treated in order to achieve a seventh degree polynomial fit to the experimental data. The polynomial associated with the Seebeck coefficient measurements performed on Specimen 2 is given below:

$$S = -17449.8 + 224.801\,(T) - 1.22108\,(T^2) + 3.63893 \times 10^{-3}\,(T^3) - 6.42299 \times 10^{-6}\,(T^4) + 6.72873 \times 10^{-9}\,(T^5) - 3.88054 \times 10^{-12}\,(T^6) + 9.51399 \times 10^{-16}\,(T^7).$$

The deviation of the measured values from the mean (as defined by the above polynomial) is tabulated in Appendix I and results in a standard deviation, σ, of 1.683 microvolts/C, i.e., 68 percent of the data points lie in a "scatter" band width of 1 σ or ±1.683 microvolts/C and 95 percent of the data points lie in a "scatter" band width of 2 σ or ±3.366 microvolts/C.

The accuracy limits of the measurement technique described above appear in Table 2 as a function of specimen temperature. These limits were calculated (see Appendix II) based on (1) the use of calibrated Pt-versus-Pt-Rh thermocouples with a relative inaccuracy of ±0.1 C and an absolute inaccuracy of ±0.2 percent, (2) the use of a ΔT of 37 to 47 in the range 20 to 300 C with the ΔT value monotonically decreasing to a lower limit of 28.5 C at a specimen temperature of 500 C, and (3) the use of an integrating digital voltmeter (Hewlett-Packard Model 2401C) with microvolt resolution and a rated inaccuracy of ±6 microvolts over the entire range of measurement.

The Seebeck coefficient measurement technique described above has been selected as the optimum method based on the low level of the theoretically derived precision limits and calculated accuracy limits. The specifications for this measurement technique are summarized in Appendix V.

At this point, candidate calibration standards were installed in the test fixture in order to (1) qualify the calculated accuracy limits and (2) establish a reference material suitable for use as an interlaboratory "standard".

TABLE 2. THEORETICAL ACCURACY LIMITS FOR SEEBECK COEFFICIENT MEASUREMENT TECHNIQUE FOR VARIOUS $\triangle T$ VALUES AND ASSOCIATED SPECIMEN TEMPERATURES

T_M[(a)], C	$\triangle T$, C	$\triangle S$[(b)] (percent)	$\triangle S$[(b)] (microvolts/C)
100±0.3	36.8	±4.18	±4.94
200±0.5	46.7	±4.07	±7.00
300±0.7	44.7	±3.73	±8.53
400±0.9	37.2	±4.28	±11.62
500±1.1	28.5	±5.50	±16.73

(a) The uncertainty limits for the mean specimen temperature T_M are based on the inaccuracy of ice bath thermocouple reference (±0.1 C) and the absolute inaccuracy of the Pt-versus-Pt-Rh thermocouples (±0.2 percent).

(b) See Appendix II for details of Seebeck coefficient error analysis.

Selection of Calibration Standard

A literature survey was performed in order to select materials suitable for use as calibration standards for the Seebeck coefficient measurement. The metals and semimetals surveyed and selected properties are summarized in Table 3. Ideally, the "standard" should (1) be homogeneous and reproducible, (2) be chemically and physically stable with respect to time at temperature, (3) possess a Seebeck coefficient comparable to thermoelectric materials (50-200 μv/C), (4) possess a thermal conductivity comparable to thermoelectric materials ($\sim$0.02 watt/cm-C), (5) be operable over a temperature regime comparable to that of thermoelectric materials, and (6) resist the formation of surface oxide layers which may affect both

TABLE 2. SUMMARY OF PROPERTIES FOR METALS AND SEMICONDUCTORS

	Candidate Material	Seebeck Coefficient (μV/°C) 300 K	Seebeck Coefficient (μV/°C) 800 K	Thermal Conductivity (watts/cm-°C) at 300 K	Cost for Specimen (1/2 Dia. x 1 in.)	Purity or Reproducibility	Oxidation Resistance Up to 800 K	Composition	Ref.
(1)	n-type PbTe	-90.0	-220.	0.025	Nominal	Fair-Poor	Fair	PbTe, Pb, I	
(2)	SAE 1040	- 1.7	--	0.250	Nominal	Good	Good	C = 0.36 - 0.44% P = 0.040% Fe-residue Mn = 0.60 - 0.90% S = 0.05%	1,2,3
(3)	Chromel-P	+22.0	+ 25.8	0.120	Nominal	Good	Excellent	Ni - 90, Cr - 10%	1,2,3
(4)	Constantan	-41.0	- 54.8	0.247	Nominal	Good	Good	Ni - 43%, Cu - 57%	1,2,3
(5)	Advance II	-41.0	- 54.8	0.247	Nominal	Good	Good	Ni - 43%, Cu - 57%	1,2,3
(6)	Alumel	-18.9	- 16.7	0.420	Nominal	Good	Excellent	Ni - 94%, Mn - 3%, Al - 2%, Si - 1%	1,2,3
(7)	Nichrome V	+ 5.4	+ 11.8	0.112	Nominal	Good	Excellent	Ni - 80%, Cr - 20%	1,2,3
(8)	Nichrome	+ 2.5	+ 8.8	0.133	Nominal	Fair	Excellent	Ni - 60%, Fe - 24%, Cr - 16%	1,2,3
(9)	Au-9% Ni	-76.0	--	0.400	~$100	Fair-Good	Excellent	Au - 91%, Ni - 9%	
(10)	Au	- 3.0	- 3.0	2.850	~$70	Excellent	Excellent		2
(11)	Ni	-20.0	- 26.0	0.900	Nominal	Excellent	Excellent		
(12)	Mo	+ 4.71	+ 16.1	1.410	Nominal	Excellent	Excellent		2
(13)	Pd	- 9.00	- 25.1	0.704	~$40	Excellent	Fair-Poor		2
(14)	Pt	- 4.50	- 14.9	0.696	~$300	Excellent	Excellent		2
(15)	W	+ 1.0	+ 14.65	1.600	Nominal	Excellent	Excellent		2
(16)	Fe	+13.0	+ 0.3	0.592	Nominal	Good	Poor		2
(17)	Bi*	-71.0	--	0.0795	Nominal	Excellent	Excellent*		3,5
(18)	Co	-21.0	--	0.6900	Nominal	Excellent	Poor		5
(19)	Sb*	+42.0	--	0.1880	Nominal	Excellent	Excellent*		3,5
(20)	Si	+44.0	--	0.835	Nominal	Excellent	Fair		3,5,6
(21)	Te	+49.0	--	0.0585	Nominal	Excellent	Poor		3,5

* Can be used at room temperature only.

(1) Weber, R. L., Heat and Temperature Measurement, Prentice-Hall, Inc., New York, pp 396, 397 (1950).
(2) Cusack, N. and Kendall, P., The Absolute Scale of Thermoelectric Power at High Temperature, Proceedings of the Physical Society of London, 72, page 898 (1958).
(3) Rosebury, Fred, Handbook of Electron Tube and Vacuum Techniques, Addison-Wesley Publishing Co., Inc., Reading, Mass., pp 521-537 (1965).
(4) Heikes, R. R. and Ure, R. W., Thermoelectricity: Science and Engineering, Interscience Publishers, New York (1961).
(5) Ioffe, A. F., Physics of Semiconductors, Academic Press, Inc., New York, pp 288-305 (1957).
(6) Frankl, D. R., Electrical Properties of Semiconductor Surfaces, Pergamon Press, New York, pp 174-181 (1967).

the temperature measurement and the Seebeck coefficient of the surface layer of the thermoelectric specimen.

None of the metals and semimetals included in the survey possess all of the qualities listed above. Bismuth appears to be a suitable standard for room-temperature calibration and nickel or platinum may be suitable for elevated-temperature calibration. The elemental metals are preferred because of the assured purity and reproducibility although certain alloys (e.g., Nichrome V) feature a significant reduction in thermal conductivity and other alloys (e.g., Advance II) feature a significant increase in the Seebeck coefficient.

Constantan* (Advance) was tentatively selected as a "standard" and was evaluated for use in the calibration of the Seebeck coefficient apparatus. The measured values of the Seebeck coefficient of Constantan are compared with the vendor-supplied data in Figure 4. The results of these measurements indicate that (1) Constantan is suitable for use as a calibration standard for Seebeck coefficient apparatus, (2) multiple measurements (ten or more) may be necessary to obtain a representative curve of Seebeck coefficient versus temperature based on the observed scatter in the data, and (3) the deviation of the measured Seebeck coefficient data from the reference data is in the range 0.5 to 4.5 μv/C which is in agreement with the deviation predicted based on precision measurements and accuracy calculations for thermoelectric specimens.

---

* Constantan specimen supplied by Driver-Harris Company, Harrison, New Jersey.

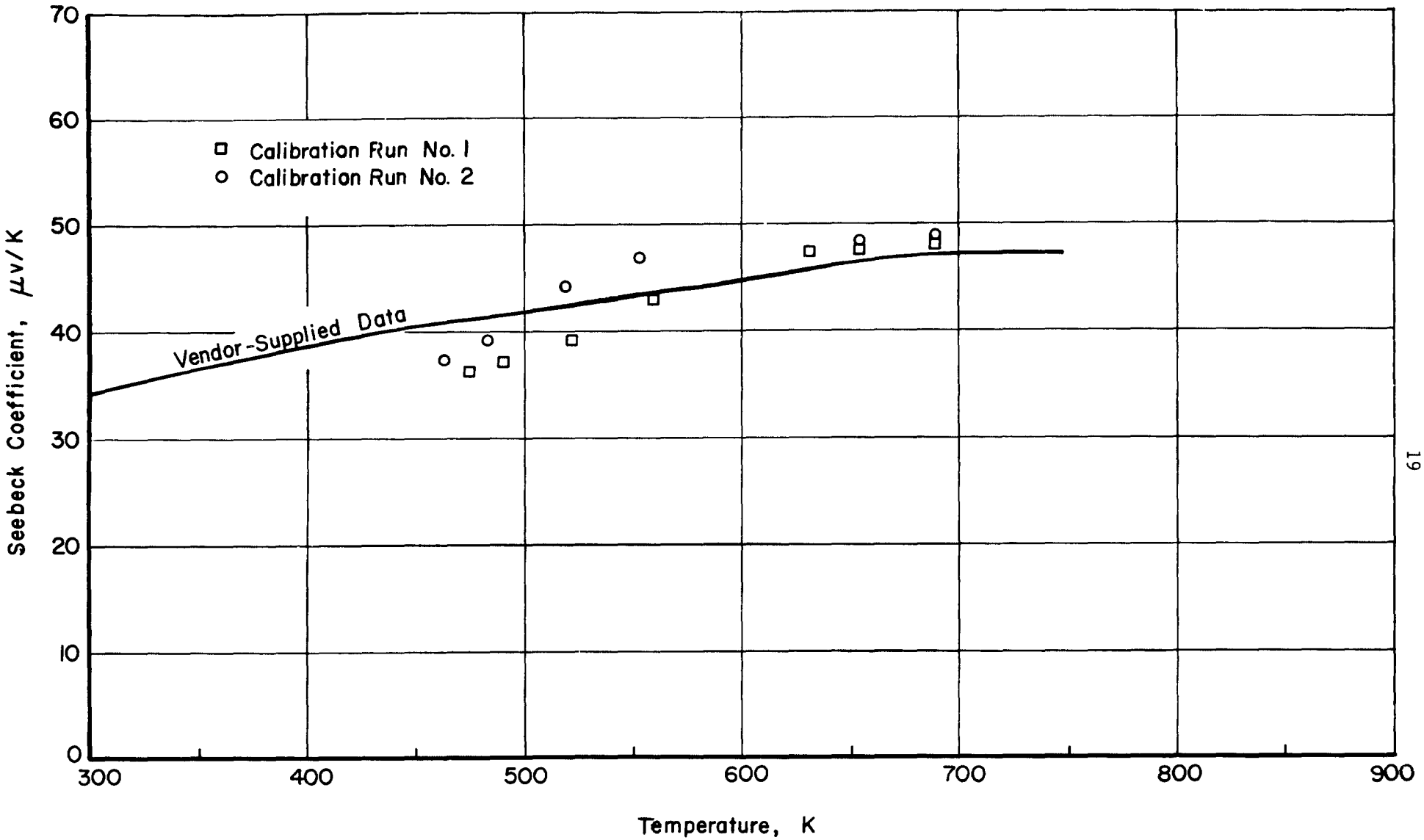

FIGURE 4. COMPARISON OF VENDOR-SUPPLIED SEEBECK COEFFICIENT DATA WITH EXPERIMENTAL MEASURED VALUES FOR CONSTANTAN VERSUS PLATINUM

Development of Electrical-Resistivity-Measurement Technique

Theory

A comprehensive study of the theory of the electrical resistivity supplemented by a survey of the literature[13-21]* regarding various measurement techniques revealed that, in general, high-precision and high-accuracy measurements of the electrical resistivity can be achieved within the framework of presently accepted techniques. The electrical resistivity, ρ, of thermoelectric materials is usually measured by the well-known method of passing a known current, I, through the specimen and measuring the voltage drop between two probes on the specimen. The resistivity is then given by the following equation:

$$\rho(T) = (V/I)_T \cdot (A/L) \quad ,$$

where A is the measured cross-sectional area of the sample, L is the measured distance between the probes measured parallel to the axis of the specimen, and T is the specimen temperature. Therefore, conventional methods were adopted in the measurement of the specimen temperature (T), current (I), voltage drop (V), and dimensions (A and L) with special emphasis on the refinement of these methods.

The specific conclusions of this study were the basis for the development of the electrical-resistivity-measurement technique and are summarized below.

---

* See Bibliography at end of report.

(1) The resistance at the junctions between the thermoelectric specimen and the current electrodes is one of the major sources of error in the measurement of electrical resistivity. An excessive junction resistance may result from insufficient area of contact and/or barrier layers at the junction arising from the difference in the contact potential between the electrode material and the thermoelectric material.

(2) Significant errors may result from inhomogeneities in the thermoelectric specimen since the current is determined by the mean electrical resistivity over the whole specimen cross section while the potentials are determined by the surface layers. Ideally, the equipotential surfaces are supposed to be planar and normal to the axis of the specimen.

(3) Seebeck voltages resulting from thermal gradients in the thermoelectric specimen may be the source of significant errors when using direct-current resistance measurement techniques. The thermal gradients are developed in thermoelectric materials when a direct current is used (commonly referred to as Peltier cooling).

(4) The contact resistance between the crystal grains of a polycrystalline thermoelectric specimen will result in significant errors if the working frequency is above a certain threshold level.

(5) High-current fluxes will cause Joulean heating which may result in errors in the measurement of specimen temperature.

(6) The shape factor of the thermoelectric element has a significant effect on the accuracy of the measurement of electrical resistivity since the current distribution is assumed unifo m and the current assumed parallel to the axis of the specimen. Hence, for specimens with L/A values as low as the order of unity, the current distribution is uniform only when the resistance between the specimen and the electrodes is uniform or low over the entire area of the contact. The anisotropy exhibited by certain materials, e.g., Bi_2Te_3, requires even larger L/A values in order to insure uniform current distribution and current flow parallel to the specimen axis.

(7) Considerable errors may result from polycrystalline specimens whose bulk material density is considerably less than that of single crystal specimens. Specifically, the individual semiconductor crystallites, i.e., powder particles, are generally covered by a surface layer whose electrical properties are significantly different from those in the interior of crystallite. These surface layers may be due to slow diffusion of impurities or imperfections in or out when the sample is not in equilibrium with its atmosphere. Another cause of surface layer effects

> is the presence of an electrical charge on the surface of the crystallites balanced by a space charge of the opposite sign in the material just beneath the surface. For example, a positive surface charge often results from reducing conditions in the atmosphere which is balanced out by a negative space charge of conduction electrons or by ionized acceptors. Consequently, the material close to the surface becomes more n-type or less p-type than the bulk material. Conversely, an oxidizing atmosphere results in a surface layer which is less n-type or more p-type than the bulk material.

A sensitivity analysis was performed in order to isolate the major source(s) of error in the measurement of electrical resistivity. The results of this theoretical analysis indicate the measurement error can be minimized by (1) utilizing large specimen aspect ratios, i.e., ratio of the specimen length (included between the voltage probes) to specimen cross-sectional area, and (2) maximizing the operating current.

Design and Fabrication of Test Apparatus

The design of the electrical-resistivity apparatus (see Figure 5) is based on the above considerations, and features: (1) a hermetically sealed quartz test-fixture container insuring minimum environmental contamination of the specimen, (2) the use of tungsten voltage probes and current electrodes in contact with the semiconductor surface to avoid "poisoning" the specimen and to provide a low-resistance junction between the specimen and the current electrode, (3) the use of an a-c signal whose frequency is high enough to minimize the effects of Peltier cooling on the temperature

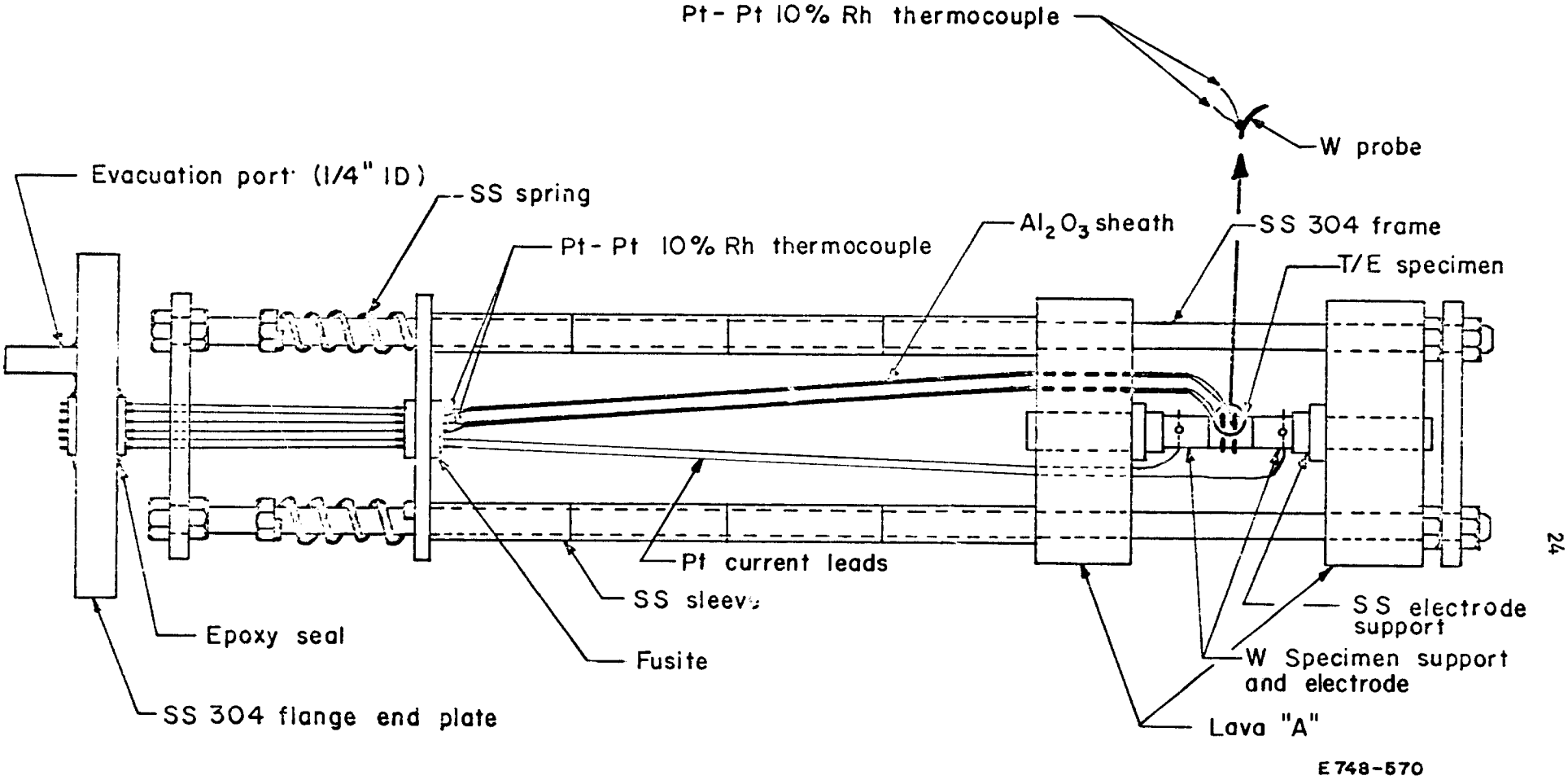

FIGURE 4. ELECTRICAL-RESISTIVITY APPARATUS

distribution of the specimen but whose frequency is low enough to avoid capacitive effects resulting from the polycrystalline nature of the specimen, (4) the use of a low-current flux to minimize the effects of Joulean heating on the temperature distribution of the specimen, and (5) the use of platinum, platinum-rhodium thermocouples which permit highly accurate temperature measurements and exhibit a high degree of stability at elevated temperatures in the presence of environmental contamination, e.g., oxygen.

One test fixture was fabricated according to the above specifications and is shown in Figure 2.

Experimental Results

The electrical-resistivity measurements were performed in order to determine (1) the voltage-probe separation yielding maximum reproducibility of measurements, (2) the maximum specimen heatup rate (C/unit time) which can be used without significantly affecting the accuracy of the measurement, (3) the optimum frequency range for the a-c signal to minimize Peltier cooling effects and capacitive effects in the specimen, and (4) the optimum current minimizing Joulean heating effects but sufficiently high to permit an accurate measurement.

A total of 12 sets of electrical-resistivity measurements were performed on a 2p-PbTe element (Specimen 2). All of the tests were performed in an argon atmosphere at a pressure of 3 psig. The results of the first two sets of measurements (Runs 1 and 2) indicated that an extraneous voltage was interfering with the measurement of the specimen voltage since the empirically determined value of the electrical

resistivity was 10 to 15 percent higher than expected. A close inspection of the voltage-probe arrangement used in these two measurements revealed that a slight misalignment in the probes existed as illustrated by Probe B in Figure 6. Ideally, the probe should be positioned such that the points of contact coincide with the same voltage potential as illustrated by Probe A in Figure 6. This misalignment of the probe ends results in a potential difference between the points of contact and, consequently, a circulating current flow within the "C"-shaped probe. The flow of current across the junction of the voltage probe and the semiconductor can superimpose significant extraneous voltages onto the specimen voltage measured between the two sets of probes. The misalignment problem was corrected by inserting a sheet (10 mils thick) of mica electrical insulation between one side of the voltage probes and the specimen as shown in Figure 6. Subsequent measurement indicated that this corrective measure had eliminated the extraneous voltage encountered in earlier measurements.

Ten sets of electrical-resistivity measurements (Runs 3-12) were performed which incorporated the modified voltage-probe attachment technique discussed above. An analysis of the experimental data gathered from these measurements revealed that:

(1) Using specimen heatup rates of 3 C/min or less and digital readout rates of $\sim$3 channels/7 sec, dynamic measurements can be performed while introducing less than 1 percent error into the measurement

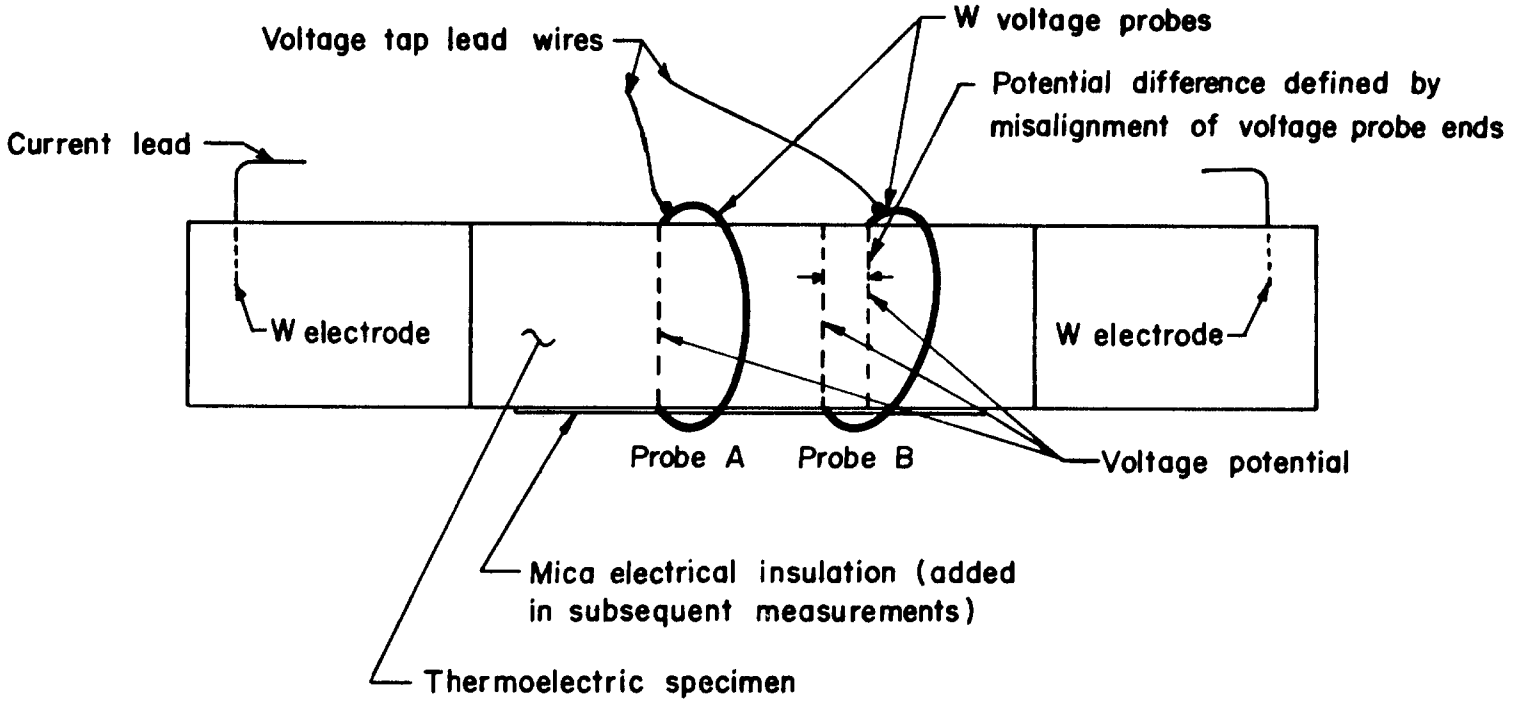

FIGURE 6. DETAILED VIEW OF VOLTAGE-PROBE ATTACHMENT TECHNIQUE FOR THE ELECTRICAL-RESISTIVITY APPARATUS

(2) Reproducible measurements of electrical resistivity were achieved using a voltage-probe separation-to-specimen cross-sectional area ratio of 0.935 cm^{-1} (2.37 $in.^{-1}$)

(3) The measured values of electrical resistivity appear to be independent (within the limits of experimental precision) of the signal frequency in the range 100 to 1000 Hz for specimen temperatures of 20 to 500 C

(4) Measurements performed in commercial-grade argon (nominally 10 ppm) at temperatures above 500 C for periods up to 1 hr appear to produce no significant change in the electrical resistivity

(5) Using a current flux of 1.5 amp/cm^2 or less results in a Joulean-induced specimen heatup rate of $<8 \times 10^{-4}$ C/sec at 20 C and $<8 \times 10^{-3}$ C/sec at 500 C.

The precision of the electrical-resistivity-measurement technique discussed above was empirically derived by calculating the standard deviation associated with the ten sets of measurements (Runs 3-12) performed on Specimen 2. A total of 81 data points (obtained from the ten sets of measurements) were statistically treated in order to achieve an eighth degree polynomial fit to the experimental data. The polynomial associated with the electrical-resistivity measurements performed on Specimen 2 is given below:

$$\rho = - 176990 + 2894.45\ (T) - 20.2911\ (T^2) + 7.98969 \times 10^{-2}\ (T^3) - 1.93253 \times 10^{-4}\ (T^4) + 2.9385 \times 10^{-7}\ (T^5) - 2.73859 \times 10^{-10}\ (T^6) + 1.42887 \times 10^{-13}\ (T^7) - 3.19541 \times 10^{-17}\ (T^8).$$

The deviation of the measured values from the mean (as defined by the above polynomial) is tabulated in Appendix III and results in a standard deviation, σ, of 24.5 $\mu\Omega$-cm, i.e., 68 percent of the data points lie in a "scatter" band width of 1 σ or $\pm$24.5 $\mu\Omega$-cm and 95 percent of the data points lie in a "scatter" band width of 2 σ or $\pm$49.0 $\mu\Omega$-cm.

The accuracy limits of the measurement technique described above appear in Table 4 (Case I) as a function of specimen temperature. The details of the electrical-resistivity error analysis appear in Appendix IV. These limits were calculated based on (1) the use of calibrated Pt-versus-Pt-Rh thermocouples with an absolute inaccuracy of $\pm$0.2 percent, (2) the use of a standard four-terminal resistor (Guideline Model No. 9221) with a maximum error of less than $\pm$0.03 percent, (3) the use of a precision a-c power supply (Optimation, Inc. Model AC-15) with less than 0.05 percent distortion and less than 1.5 milliwatts of noise, (4) the use of an integrating digital voltmeter (Hewlett-Packard Model 2401C) in conjunction with an a-c/d-c converter (Hewlett-Packard Model 2410B) with microvolt resolution and a rated inaccuracy of $\pm$(0.10 percent of reading + 0.05 percent of full scale), (5) an operating current flux of 1.5 amp/cm^2, and (6) a voltage-probe separation to specimen cross-sectional area ratio, i.e., length/area ratio of $\sim$1.0 cm^{-1}.

TABLE 4. THEORETICAL ACCURACY LIMITS FOR ELECTRICAL-RESISTIVITY-MEASUREMENT TECHNIQUE AT VARIOUS SPECIMEN TEMPERATURES AND FOR SEVERAL OPERATING CONDITIONS

T_M (a), C	$\Delta\rho$, percent		
	Case I [J = 1.5 amp/cm^2, L/A = 1.0 cm^{-1}]	Case II [J = 3.0 amp/cm^2, L/A = 1.0 cm^{-1}]	Case III [J = 1.5 amp/cm^2, L/A = 2.0 cm^{-1}]
100±0.3	±10.5	±5.57	±4.44
200±0.5	±6.87	±3.98	±2.84
300±0.7	±4.90	±2.87	±1.72
400±0.9	±4.08	±2.44	±1.30
500±1.1	±3.64	±2.28	±1.19

(a) The uncertainty limits for the mean specimen temperature T_M are based on the inaccuracy of the ice bath thermocouple reference (±0.1 C) and the absolute inaccuracy of the Pt-versus-Pt-Rh thermocouples (±0.2 percent).

The theoretically derived uncertainty limits associated with the measurement technique discussed above were found to be undesirably large, particularly at low specimen temperatures (100 to 200 C). Therefore, accuracy limits were calculated based on two alternate measurement procedures, viz., operating current flux of 3.0 amp/cm^2 and length/area ratio of 2.0 cm^{-1}. The equations used in these calculations appear in Appendix IV and the results are compared with the previously calculated accuracy limits (see Table 4). The calculated limits appearing in Table 4 indicate that acceptably low uncertainty limits can be achieved by performing measurements at a current flux of 1.5 amp/cm^2 and a length/area ratio of 2.0 cm^{-1} (Case III).

Similar gains in measurement accuracy may be realized by operating at the original L/A ratio but at an increased current flux, viz., 3.0 amp/cm^2 (Case II). However, it appears that Joulean heating effects become significant above 1.5 amp/cm^2 since the equilibrium specimen temperatures were found to be 28, 33, and 52 C for current fluxes of 0, 1.5, and 3.0 amp/cm^2, respectively. The observed Joulean-induced temperature increase is undesirable since it may result in significant errors in the measurement of the mean specimen temperature, particularly if the pressure-contacted specimen-electrode junctions exhibit high resistance relative to the resistance of the specimen. Therefore, the electrical-resistivity-measurement technique involving a current flux of $\sim$1.5 amp/cm^2 and a length/area ratio of $\sim$2.0 cm^{-1} has been selected as the optimum method based on the theoretically derived accuracy limits. Although larger length/area ratios offer improved measurement accuracies, the specimen may become (1) difficult to fabricate and/or install into the measurement apparatus, (2) sensitive to surface defects as a result of small specimen cross-sectional area, and (3) sensitive to inhomogeneities as a result of the increased length of thermoelectric material located between the voltage probes. The specifications for this measurement technique are summarized in Appendix V.

Calibration of Electrical-Resistivity Apparatus

The calibration of the electrical-resistivity apparatus using Constantan* and platinum** standards was performed in order to (1) qualify

* Constantan specimen supplied by Driver-Harris Company, Harrison, New Jersey.

** Platinum specimen procured from Engelhard Industries, Chemical Division, Newark, New Jersey.

the calculated accuracy limits and (2) establish a reference material suitable for use as an interlaboratory "standard". The measured values of the electrical resistivity of the Constantan standard are compared with the vendor-supplied data in Figure 7. In this calibration run, the ratio of voltage-probe separation to specimen cross-sectional area was 18.1 cm^{-1}. The results of the measurements on the Constantan specimen indicate that (1) the measured values of resistivity appear to be increasing monotonically with temperature at a rate slightly larger than the vendor-supplied data indicate, and (2) the deviation of the measured electrical-resistivity data from the reference data is in the range 1.5 to 8 percent. However, the reproducibility of electrical properties in Constantan is inherently lower than that of pure metals, e.g., platinum. In addition, Constantan is also undesirable from the standpoint that the electrical resistivity is nearly independent of temperature, hence, prohibiting the calibration of the temperature-measurement technique.

In order to confirm the trend observed above, viz., the monotonic increase of the measured electrical resistivity at a rate slightly larger than that of the reference values, an additional calibration run was made using a platinum standard (99.995 percent purity). The ratio of voltage-probe separation to cross-sectional area of this specimen was 2.84 cm^{-1}. The measured values of the electrical resistivity of the platinum standard are compared with reference values and indicate that (1) platinum is suitable for use as a calibration standard for electrical-resistivity apparatus and (2) the measured values of resistivity correlate well with published data with the deviation of the measured data from the reference data in the range 1 to 6 percent. Based on the above results, platinum

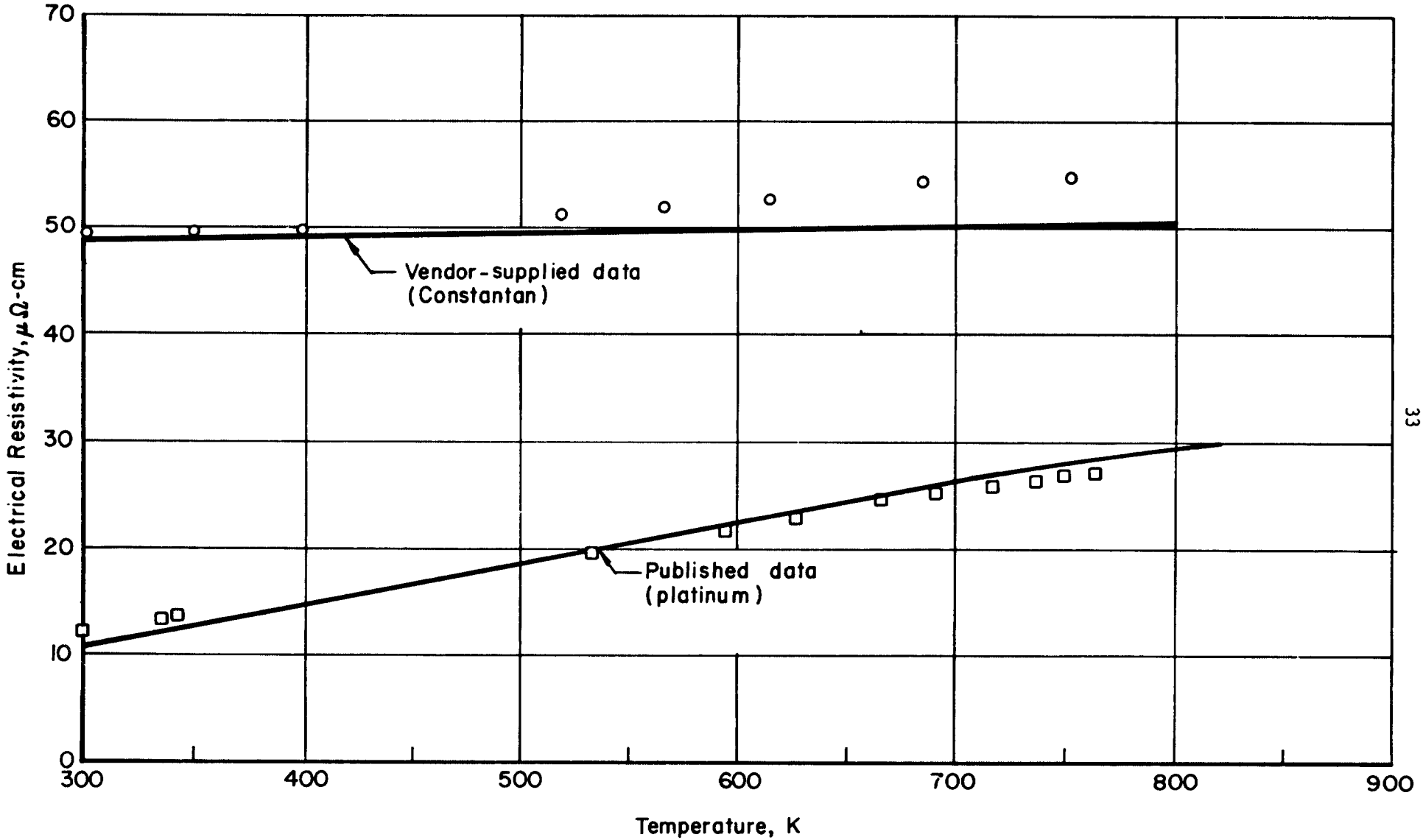

FIGURE 7. COMPARISON OF VENDOR-SUPPLIED ELECTRICAL-RESISTIVITY DATA WITH EXPERIMENTAL MEASURED VALUES FOR CONSTANTAN VERSUS PLATINUM

appears more suitable for use as a calibration standard because of its availability in pure forms and its temperature-dependent electrical resistivity which provides the data necessary for calibrating the temperature-measurement technique.

Development of Electrical-Contact-Resistivity-Versus-Time-Measurement Technique

Theory

A comprehensive study supplemented by a survey of the literature[14,15,22-26]* regarding the electrical-contact-resistivity-versus-time-measurement technique revealed that, in general, high-precision measurements of electrical contact resistivity versus time can be achieved within the framework of presently developed techniques**. The electrical contact resistivity (for time-dependent studies), ρ_c, of a metal-semiconductor junction is measured by passing a known current, I, through the specimen and measuring the voltage drop across the metal-semiconductor junction, V_J, as well as the voltage drop across the bulk material, V_B (see Figure 8 for a description of these parameters). The contact resistivity is then given by the following equation:

$$\rho_c = (V_J - \frac{X}{Y} V_B) \frac{A}{I} \quad ,$$

where A is the measured cross-sectional area of the sample, X is the length of semiconductor included between the pair of probes spanning the junction, and Y is the length of semiconductor included between

---

* See Bibliography at end of report.

** Developed under AEC Contract W-7405-eng-92.

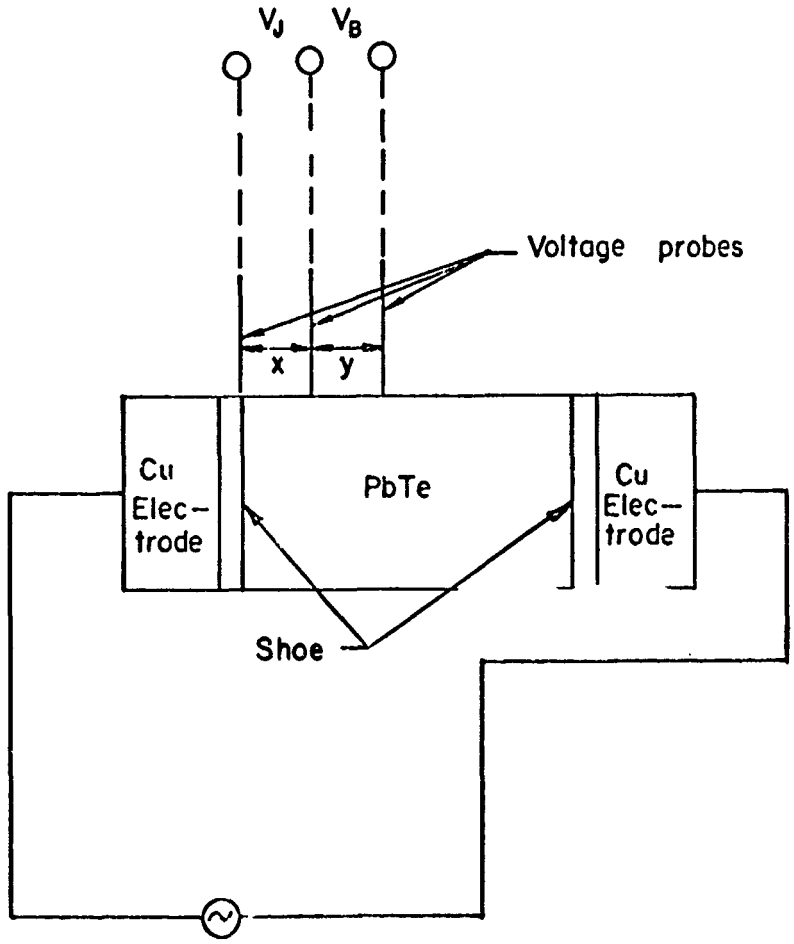

$$\rho_c = \left(V_J - \frac{X}{Y} V_B\right) \frac{A}{I}$$

FIGURE 8. SCHEMATIC OF CONTACT-RESISTIVITY-VERSUS-TIME APPARATUS

the pair of probes spanning only the bulk semiconductor (see Figure 8). Therefore, conventional methods were adopted in the measurement of specimen temperature, current, voltage drop, and dimensions with special emphasis on the refinement of these methods and the selection of measurement conditions, e.g., current flux, test atmosphere, etc.

The specific conclusions of this study were the basis for the development of the electrical-contact-resistivity-measurement technique and are summarized below.

(1) Seebeck voltages resulting from thermal gradients in the thermoelectric specimen may be the source of significant errors when using direct-current resistance-measurement techniques. The thermal gradients are developed in thermoelectric materials due to direct-current-induced Peltier cooling.

(2) High-current fluxes will cause Joulean heating which may result in errors in the measurement of specimen temperature.

(3) The shape factor of the thermoelectric element - electrode composite has a significant effect on the accuracy of the contact-resistivity measurement since the current distribution is assumed uniform and current assumed parallel to the axis of the specimen. Hence, for voltage-probe separations with length/area ratios as low as the order of unity, the current distribution is

uniform only when the resistance between the specimen and the electrodes is uniform or low over the entire area of the contact.

(4) The inaccuracy associated with the measurement of voltage-probe separations may lead to large errors, particularly if the magnitude of the separations is small.

(5) Environmental contamination (e.g., oxidation) may lead to significant errors since the objective of this measurement is the evaluation of contact resistivity and bulk resistivity as a function of time.

(6) Significant errors may result from the sublimation of the bulk semiconductor material and/or dopant with a subsequent change in electrical properties and/or specimen dimensions.

Design and Fabrication of Test Apparatus

The above considerations were the basis for the development of the electrical-resistivity-measurement technique. The design of the measurement apparatus is shown in Figure 9 and features (1) a hermetically sealed quartz test-fixture container insuring minimum environmental contamination of the specimen, (2) the use of argon cover gas to minimize sublimation effects in the thermoelectric materials, (3) the use of tungsten voltage probes in contact with the semiconductor surface to avoid "poisoning" the specimen as a result of chemical incompatibility,

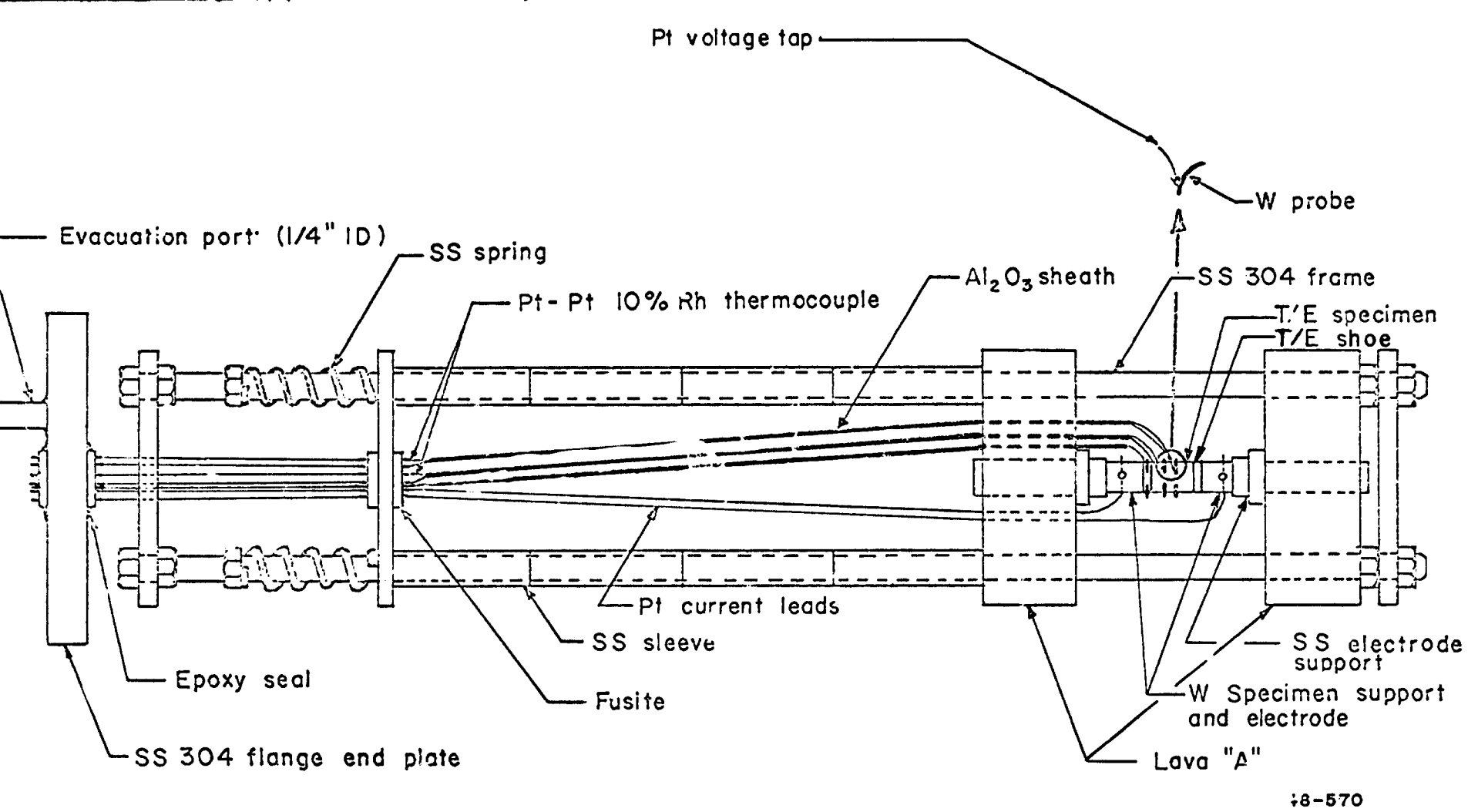

FIGURE 9. CONTACT-RESISTIVITY-VERSUS-TIME APPARATUS

(4) the use of an a-c signal whose frequency is high enough to minimize the effect of Peltier cooling on the temperature distribution of the specimen but whose frequency is low enough to prevent the occurrence of significant capacitive voltage components in the vicinity of the junction, and (5) the use of low-current flux to minimize the effect of Joulean heating on the temperature distribution of the specimen, particularly in the vicinity of the junction.

Experimental Results

Electrical-contact-resistivity-versus-time measurements were performed in order to determine (1) the voltage-probe separation yielding maximum reproducibility of measurements, (2) the optimum frequency range for the a-c signal to minimize Peltier cooling effects and capacitive effects at the junction, and (3) the optimum current minimizing Joulean heating effects but sufficiently high to permit an accurate measurement.

A total of five groups of electrical-contact-resistivity-versus-time measurements have been performed on a 2n-PbTe element (Specimen 3) which involved 138 individual sets of readings. All of the measurements were performed in an argon atmosphere (3 psig) at a specimen temperature of 537 C (1000 F). A complete description of the electrical-contact-resistivity apparatus used in these measurements has been reported previously. A sheet of mica electrical insulation was inserted between one side of the specimen and the three voltage probes to eliminate the extraneous voltages and perturbations in the current flux which arise from circulating currents in the "C"-shaped tungsten probes.

The objective of the first four groups of measurements (125 sets of readings) was to empirically derive the precision of the technique over a range of a-c signal frequencies (100 to 1000 Hz) and operating current fluxes (1.5 to 3.0 amp/cm^2). An analysis of the experimental data gathered from these measurements reveals that:

(1) Reproducible measurements of electrical contact resistivity were achieved using a voltage-probe separation-to-specimen cross-sectional area ratio of 0.935 cm^{-1} (2.37 $in.^{-1}$)

(2) No significant improvement in measurement precision is achieved by increasing the current flux from 1.5 to 3.0 amp/cm^2 or by increasing the signal frequency from 100 to 1000 Hz

(3) Based on the empirically derived precision, the specimen temperature must be maintained within 0.5 C of the initial (reference) temperature in order to compare the contact resistivity measured at time t with the initial value measured at time t_o.

The precision of the electrical-contact-resistivity-measurement technique discussed above was empirically derived by calculating the standard deviation associated with the variation in the measured contact resistivity for each of the first four groups. The deviation of the measured values from the mean is tabulated in Appendix I and results in standard deviations ranging from 0.707 $\mu\Omega$-cm^2 to 2.047 $\mu\Omega$-cm^2, i.e., 68 percent of

the data points lie in a "scatter" band width of 1 σ or ±0.707 to ±2.047 $\mu\Omega$-cm^2 and 95 percent of the data points lie in a "scatter" band width of 2 σ or ±1.414 to ±4.094 $\mu\Omega$-cm^2.

The objective of the fifth group of measurements (15 sets of readings) was to measure the contact resistivity as a function of the a-c signal frequency at a fixed current flux of 1.5 amp/cm^2. The results of these measurements indicate that the contact-resistivity value increases slightly with increasing a-c signal frequency (3.5 percent increase in contact resistivity for a frequency increase from 100 to 1000 Hz). The observed increase in contact resistivity may be caused by the polycrystalline nature of the pressed and sintered specimen since the contact resistance between the crystal grains of semiconductors can result in significant errors if the working frequency is above a certain threshold level.

The results of the five groups of contact-resistivity measurements indicate that high precision can be achieved using (1) current fluxes of 1.5 amp/cm^2, (2) a-c signal frequencies in the range 100 to 1000 Hz, (3) voltage-probe separation/cross-sectional area ratios of 1 or greater, (4) the use of a standard four-terminal resistor (Guideline Model No. 9221) with a maximum error of less than ±0.03 percent, (5) the use of a precision a-c power supply (Optimation, Inc. Model AC-15) with less than 0.05 percent distortion, less than 1.5 milliwatts of noise, and an amplitude instability of less than 0.01 percent, and (6) the use of an integrating digital voltmeter (Hewlett-Packard Model 2401C) in conjunction with an a-c/d-c converter (Hewlett-Packard Model 2410B) with microvolt resolution and a rated inaccuracy of ±(0.10 percent of reading + 0.05 percent of full scale). The specifications for the measurement technique are summarized in Appendix V.

The calculation of the accuracy limits associated with the measurement of electrical contact resistivity has not been included in this study since this technique was developed only for measuring changes in contact resistivity as a function of time. The accurate measurement of contact resistivity can be accomplished, however, using the contact-resistivity-traverse technique discussed below.

Development of Electrical-Contact-Resistivity-Traverse-Measurement Technique

Theory

A comprehensive study supplemented by a survey of the literature[14,15,22-26]* regarding the electrical-contact-resistivity-traverse technique revealed special methods would need to be developed to permit the accurate measurement of low-contact-resistivity junctions (<100 $\mu\Omega$-cm^2). Conventional traverse techniques, which were the basis for the development of the traverse technique discussed below, involve the measurement of an a-c potential drop taken at small intervals on either side of the metal-semiconductor junction. In these measurements, one probe remains fixed in position and the other is repositioned for each measurement at small intervals along a line parallel to the longitudinal axis of the sample. A typical plot of the resulting data appears in Figure VI-1 (Appendix VI). Because of the low resistivity of the metal electrode, little, if any, discernible increase in potential drop is observed as measurements are made with the movable probe at successively greater distances from the fixed probe. Potential drop as a function of

* See Bibliography at end of report.

distance into the semiconductor is measurable because of its higher resistivity. The discontinuity in voltage drop, ΔV, occurring at the metal-semiconductor interface is a result of the contact resistivity associated with that junction. The electrical contact resistivity, ρ_c, for the traverse-measurement technique is, hence, defined by the equation:

$$\rho_c = \frac{\Delta V}{I} \cdot A \ ,$$

where A is the cross-sectional area of the specimen and I is the a-c current used in the measurement. Since the current and the cross-sectional area are maintained constant, contact resistivity is proportional to the potential drop across the interface. Moreover, the slope of the potential-drop curve in the semiconductor is proportional to the semiconductor resistivity. This fact makes it possible in some cases to identify alterations in semiconductor properties in the vicinity of the junction such as might arise from bonding procedures and other factors.

The specific conclusions of this study were the basis for the development of the electrical-contact-resistivity-traverse technique and are summarized below.

(1) Seebeck voltages resulting from thermal gradients in the thermoelectric specimen may be the source of significant errors when using direct-current resistance-measuring techniques. The thermal gradients are developed in thermoelectric materials due to direct-current-induced Peltier cooling.

(2) High-current fluxes will cause Joulean heating which may result in errors in the measurement of the specimen temperature.

(3) The shape factor of the thermoelectric element - electrode composite has a significant effect on the accuracy of the contact-resistivity measurement since the current distribution is assumed uniform and current assumed parallel to the axis of the specimen when defining contact resistivity, ρ_c. Hence, for specimens with length/area ratios as low as the order of unity, the current distribution is uniform only when the resistance between the specimen and the electrodes is uniform or low over the entire area of the contact.

(4) The uncertainty associated with the actual location of the metal-semiconductor junction (based on the traverse increment size may lead to large errors, particularly if the magnitude of the contact resistivity is small.

(5) The shape of traversing probe tip and the pressure applied during voltage measurement as well as the brittleness of the specimen surface have a significant effect on the lower limit of the traverse increment size.

(6) Environmental contamination of the specimen and the probes (e.g., oxidation) may lead to significant errors caused by changes in the electrical properties of the specimen, changes in the planar contact resistivity (especially pressure-contacted junctions), and loss of electrical continuity across the voltage-probe specimen interface.

Development of Measurement Technique

The above considerations were the basis for the development* of the electrical-contact-resistivity-traverse-measurement technique. The design of the measurement apparatus is shown schematically in Figure 10 and features (1) a hermetically sealed (O-ring) quartz test-fixture container insuring minimum environmental contamination of the specimen, (2) the use of tungsten voltage probes to avoid "poisoning" the specimen as a result of chemical incompatibility, (3) the use of an a-c signal frequency of 100 Hz which is high enough to minimize the effects of Peltier cooling on the temperature distribution of the specimen but is low enough to avoid capacitive effects resulting from the polycrystalline nature of the specimen, (4) the use of a low-current flux (1.5 to 3.0 amp/cm^2) to minimize the effects of Joulean heating on the temperature distribution of the specimen and, in particular, the temperature of the metal-semiconductor junction, (5) the application of a calibrated spring-loading pressure in the range 0 to 120 psi to permit the simulation of conditions

---

* Initially developed under AEC Contract W-7405-eng-92.

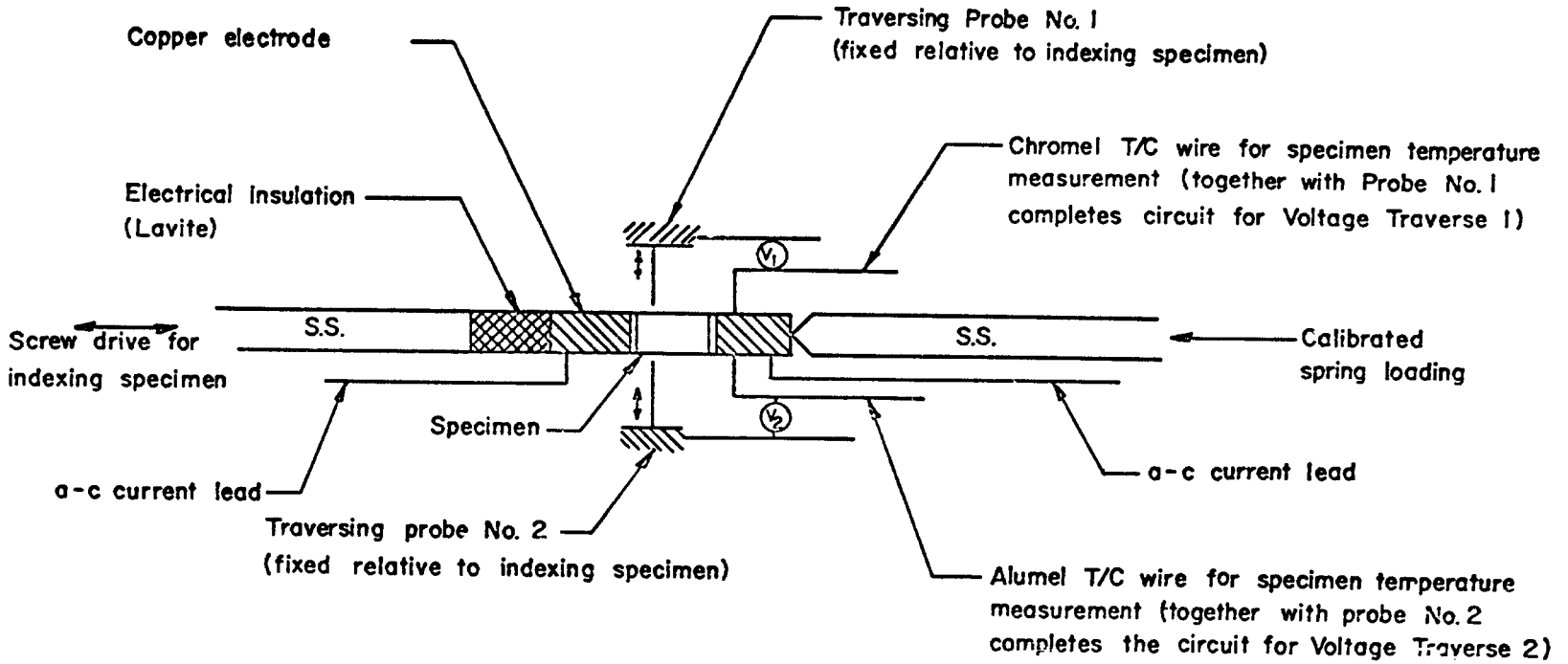

FIGURE 10. TRAVERSE APPARATUS FOR ELEVATED-TEMPERATURE CONTACT RESISTIVITY

typical of thermoelement operation in actual devices, and (6) the use of two electrically independent traverse probes located on opposite sides of the specimen in order to qualify the homogeneity of the metal-semiconductor junction.

Experimental Results

Electrical-contact-resistivity-traverse measurements were performed in order to determine the magnitude of the traverse increment yielding (1) maximum resolution of the location of the metal-semiconductor junction, hence, the resolution of the contact-resistivity value while (2) minimizing the specimen surface damage (local cracking, chipping, etc.) resulting from insufficient separation between successive voltage-probe-induced defects. The latter consideration in the optimization procedure depends primarily on the density and elastic modulus of the specimen being traversed. In addition, replicate traverse measurements will be performed in order to empirically derive the precision of the measurement technique.

A total of ten sets of electrical-contact-resistivity-traverse measurements were performed which involved 860 individual readings. The junction under study contained tungsten pressure contacted to 2p-PbTe (100-psi spring loading) and the traverse measurements were performed at 920 F (493 C) in argon at 3-4 psig. The type of junction and operating conditions were arbitrarily selected in order to empirically determine the reproducibility of the traverse-measurement technique. A signal frequency of 100 Hz and a current flux of 1.5 amp/cm^2 were selected for use in these traverse measurements based on the results of empirical studies performed for the contact-resistivity-versus-time apparatus and

the electrical-resistivity-versus-temperature apparatus. The traverse increment size was minimized in order to minimize the uncertainty associated with the location of the junction. However, surface deformation of the semiconductor resulting from voltage-probe contact and voltmeter resolution prohibit traverse increment sizes less than 5 mils.

The precision of this measurement technique was empirically derived by calculating the standard deviation associated with the observed variation about the mean of each of the individual measurements comprising the voltage profile. These limits of variation together with those resulting from the uncertainty associated with the actual location of the metal-semiconductor junction resulted in a standard deviation of $\pm 18.87\ \mu\Omega\text{-cm}^2$, i.e., 68 percent of the data points lie in a "scatter" band width of $1\ \sigma$ or $18.87\ \mu\Omega\text{-cm}^2$. Likewise, 95 percent of the data points lie in a scatter band width of $2\ \sigma$ or $37.74\ \mu\Omega\text{-cm}^2$.

Over 90 percent of the total observed scatter is the result of the uncertainty associated with the location of the metal-semiconductor junction within the confines of a 5-mil increment (see Appendix VI, Figure VI-1). However, this component was minimized by examining the vicinity of the junction (aided by a microscope) at the completion of the traverse measurement, thereby identifying the actual position of the junction. The standard deviation associated with this modified measurement procedure (including the posttest microscopic examination of the junction) is $\pm 1.87\ \mu\Omega\text{-cm}^2$, i.e., 68 percent of the data points lie in a "scatter" band width of $1\ \sigma$ or $1.87\ \mu\Omega\text{-cm}^2$. Likewise, 95 percent of the data points lie in a scatter band width of $2\ \sigma$ or $3.74\ \mu\Omega\text{-cm}^2$.

The accuracy limits associated with the modified measurement technique described above are ±3.3 percent or ±10.1 $\mu\Omega\text{-cm}^2$ and were calculated based on (1) the use of a traverse increment of 5 mils, (2) the use of calibrated Pt-versus-Pt-Rh thermocouples with an absolute inaccuracy of ±0.2 percent, (3) the use of a standard four-terminal resistor (Guideline Model No. 9221) with a maximum error of less than ±0.03 percent, (4) the use of a precision a-c power supply (Optimation, Inc. Model AC-15) with less than 0.05 percent distortion and less than 1.5 milliwatts of noise, (5) the use of an integrating digital voltmeter (Hewlett-Packard Model 2401C) in conjunction with an a-c/d-c converter (Hewlett-Packard Model 2410B) with microvolt resolution and a rated inaccuracy of ±(0.10 percent of reading + 0.05 percent of full scale), and (6) the use of a microscope at completion of traverse in order to accurately locate the position of the metal-semiconductor junction. The details of the electrical-contact-resistivity error analysis appear in Appendix VI and the specifications for the measurement technique are summarized in Appendix V.

Development of Life-Testing Technique

Theory

A comprehensive study of life-test-measurement techniques, i.e., the measurement of the output power of one or more couples as a function of time, was performed. Particular attention was given to the applicability of the derived life-test data to the prediction of RTG performance. The results of this study revealed that, in general, the acquisition of

meaningful life-test data cannot be achieved within the framework of conventional life-testing techniques, viz., testing under conditions of (1) constant cold- and hot-junction temperatures and (2) unknown thermal input.

The specific conclusions of this study were the basis for the development of the life-testing technique and are summarized below.

(1) Output power stability measured under conditions of constant cold- and hot-junction temperature (thermal input not monitored) is not applicable to the reliable prediction of RTG performance if the p-type and/or n-type thermoelectric elements are undergoing changes in thermal conductivity.

(2) Monitoring thermal input power using heat meters at the hot end of the thermoelectric couple(s) is complicated by the high hot-junction temperatures (1700-1800 F) associated with the testing of SiGe thermoelectric materials.

(3) Monitoring thermal input power using heat meters or heat-flux transducers at the cold end of the thermoelectric couple(s) is practical only if heat losses from the periphery of the thermoelectric couple are low and constant with respect to time.

(4) Monitoring thermal input power using electrical input power measurements may be feasible if the ratio of the heat flow through the thermoelectric couple(s) to the total heat input can be maintained

above about C.85 to 0.90. In addition, the parasitic heat losses would have to remain nearly constant with time (less than 5 percent variation).

(5) The computation of couple output power, P. using the relation $P = V_{oc}^2/4R$ (where V_{oc} and R are the measured open-circuit voltage and internal resistance, respectively) may indicate lower output power degradation than the computation at fixed external load using the relation $P = I \cdot V_{cc}$ (where I and V_{cc} are the measured current and closed-circuit voltage).

(6) The use of volatile and/or reactive materials in the life-test apparatus which are not otherwise present in RTG systems may result in misleading performance stability. For example, life testing performed in fixtures employing graphite support electrodes at the hot junction of the elements may be actively "gettering" the oxygen from the thermoelectric elements and the atmosphere in their vicinity and, hence, represent test conditions significantly different from normal operation in RTG systems. However, getters and reducing atmospheres may be effectively employed in life-test experiments designed to isolate the cause(s) of output power degradation, e.g., oxidation.

(7) The electrical output power of an individual couple (or an array of couples) operating at fixed cold- and hot-junction temperatures will <u>increase</u> with increasing parasitic heat losses from the periphery of the thermoelectric elements. The increase in the electrical output power is the result of a decrease in the internal resistance caused by parasitic heat-loss-induced changes in the temperature distribution along the length of the thermoelectric elements.

The disparity between the two methods of output power computation cited above is the result of the difference in the apparent external load. Specifically, the output power derived from the computation of $V_{oc}^2/4R$ represents power delivered under conditions of <u>matched</u> load, i.e., internal couple resistance equals external load resistance, whereas the output power derived from the computation of $I \cdot V_{cc}$ represents power delivered under conditions of <u>fixed</u> external load, which is matched for either "beginning-of-life" or "end-of-life" conditions. The magnitude of the difference between these two methods is illustrated in Table 5. It is noteworthy that P_1 always represents the "matched-load" operating condition, hence, the maximum output power of the couple. This calculation of output power is particularly useful for prediction of maximum output power at "end-of-life" conditions, e.g., after 6124 hr on test, the maximum output power is 0.650 watt (see Table 5). However, the output power stability indicated by the $V_{oc}^2/4R$ calculation is not representative of actual RTG operation in which the external load remains fixed and matches the internal

resistance of the thermopile at only one point in time (usually at the end of life of the RTG). In contrast, the output power, P_2, represents the power delivered to a fixed external load and its variation with time is typical of that exhibited by an RTG system. The comparison of the normalized output powers, ΔP_1 and ΔP_2, in Table 5 illustrates the inadequacy of the output power calculations based on the $V_{oc}^2/4R$ relation for the purpose of predicting performance stability. The ΔP_2 values represent the normalized power delivered to the external load and indicate a 3.3 percent decrease after 6124 hr on test in contrast to the ΔP_1 which represent the normalized values of the maximum power available and indicate no change after 6124 hr on test.

TABLE 5. COMPARISON OF SEVERAL COMPUTATION METHODS FOR THERMOELECTRIC COUPLE OUTPUT POWER BASED ON MEASURED PERFORMANCE DATA[a]

Hours on Test	T_C, C	T_H, C	R, mΩ	$P_1 = \frac{V_{oc}^2}{4R}$, watts	$P_2 = I \cdot V_{cc}$, watts	$\Delta P_1 = \frac{P_1}{P_o}$	$\Delta P_2 = \frac{P_2}{P_o}$
0[b]	20	538	14.81	0.650	0.650	1.000	1.000
1081	20	538	12.98	0.685	0.673	1.05	1.035
3097	20	538	12.35	0.702	0.685	1.080	1.050
4108	20	538	12.48	0.675	0.649	1.040	1.001
5116	20	538	12.48	0.664	0.640	1.020	0.985
6124	20	538	12.84	0.650	0.629	1.000	0.967

(a) Couple composed of 3p-PbSnTe and 2n-PbTe operated in argon atmosphere.

(b) External load adjusted for peak output power, P_o, initially.

Design of Life-Test Apparatus

The design of the life-test apparatus, which was based on the above considerations, is shown schematically in Figure 11 and features (1) the measurement of output power stability under conditions of constant thermal input power (regulated d-c input electrical power), (2) monitoring cold-, intermediate-, and hot-junction temperature during life test, and (3) computation of couple output power, P, using the relation $P = I \cdot V_{cc}$ under conditions of fixed external load (where I and V_{cc} are the measured current and closed-circuit voltage). In addition, the thermoelectric couple may be encapsulated in a hermetically sealed container in order to minimize the effect of oxidation and sublimation on the output power stability of thermoelectric materials, particularly PbTe. The specifications for the test atmosphere, materials used in test fixture, electrical-measurement equipment, and test procedure are summarized in Appendix V.

Development of Efficiency-Measurement Technique

Theory

A comprehensive study of efficiency-measurement techniques, i.e., the measurement of the ratio of electrical output power of one or more couples to their thermal input power, was performed. Particular attention was given to maximizing the accuracy of the measurement while minimizing the complexity of the technique. The results of this study revealed that, in general, high-accuracy measurements of conversion efficiency can be achieved within the framework of presently accepted techniques. The

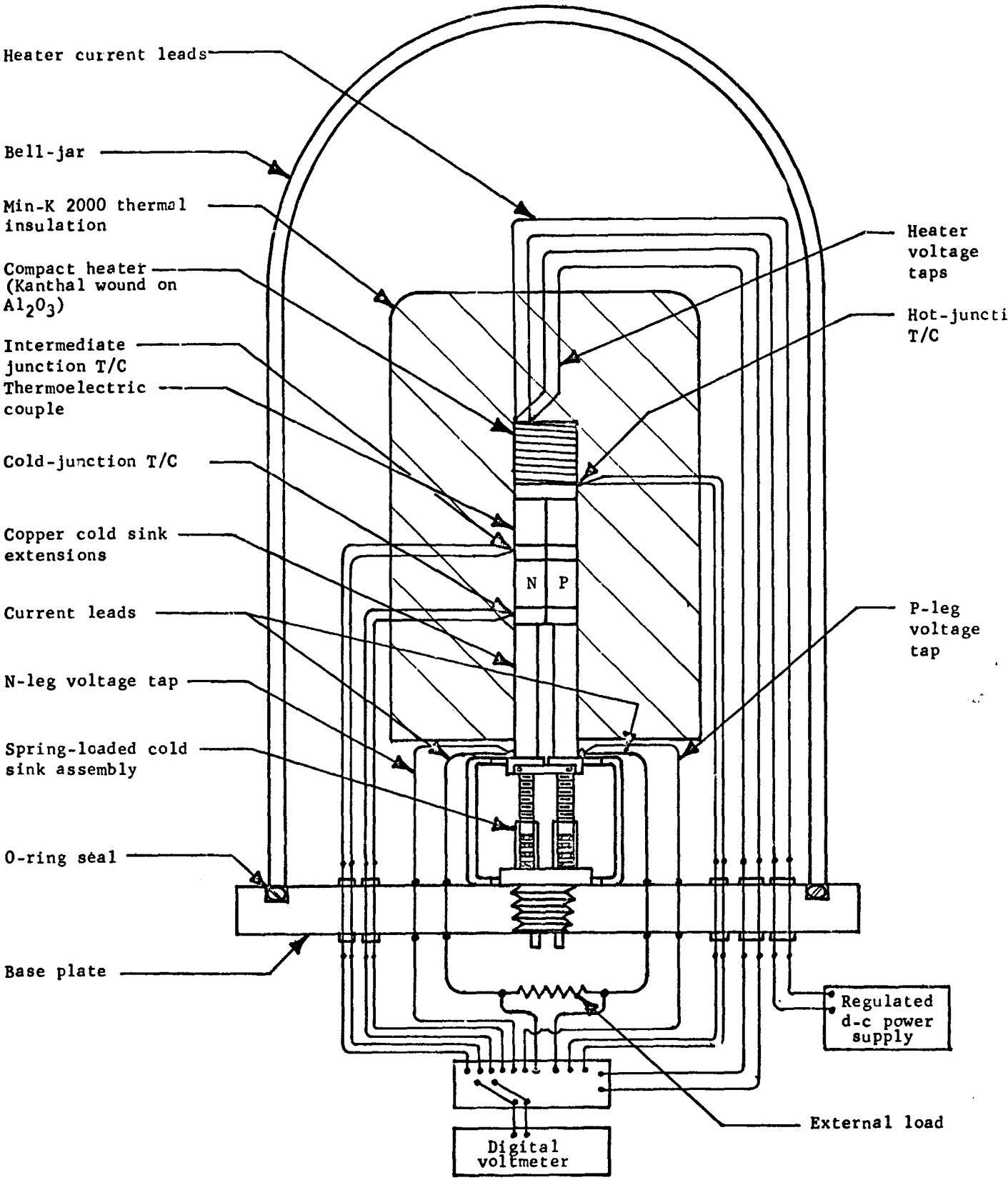

FIGURE 11. SCHEMATIC OF LIFE-TEST APPARATUS

conversion efficiency of one or more thermoelectric couples is usually measured by the well known method of operating the couple(s) at a particular cold- and hot-junction temperature while monitoring the electrical output power, $P_{out}(e)$, and the thermal input power, $P_{in}(th)$. The electrical output power is the product of the measured current flow in the couple and the closed-circuit voltage of the couple. The thermal input power is usually measured using heat meters at either the cold or hot junction of the couple and often requires a complicated arrangement of "guard rings" which are matched to the measured temperature profile of the heat meter and, hence, minimize parasitic heat losses from the periphery of the heat meter.

The specific conclusions of this study were the basis for the development of the efficiency-measurement technique and are summarized below.

(1) Monitoring thermal input power using heat meters at the hot end of the thermoelectric couple(s) is complicated by the high hot-junction temperatures (1700-1800 F) associated with the testing of SiGe thermoelectric materials.

(2) Monitoring thermal input power using heat meters or heat-flux transducers at the cold end of the thermoelectric couple(s) may be practical if heat losses from the periphery of the thermoelectric couple are low.

(3) The use of a heat-meter calibration standard, e.g., Pyroceram 9606, would permit a more accurate assessment of parasitic heat losses and actual thermal flux through the thermoelectric couple(s).

(4) The electrical output power of an individual couple (or an array of couples) operating at fixed cold- and hot-junction temperatures will increase with increasing parasitic heat losses from the periphery of the thermoelectric elements and, therefore, these parasitic losses should be minimized. The increase in the electrical output power is the result of a decrease in the internal resistance caused by parasitic heat-loss-induced changes in the temperature distribution along the length of the thermoelectric elements.

Design of Efficiency-Measurement Apparatus

The design of the efficiency-measurement apparatus was based on the above considerations. This design closely resembles that of the life-test apparatus (shown schematically in Figure 12) and features (1) the measurement of conversion efficiency under conditions of either constant thermal input power or fixed hot- and cold-junction temperatures, (2) the measurement of thermal input power using a thermal-flux transducer at the cold junction of the thermoelectric couple, (3) the calibration of the heat-monitoring transducer using a Pyroceram 9606 thermal conductivity

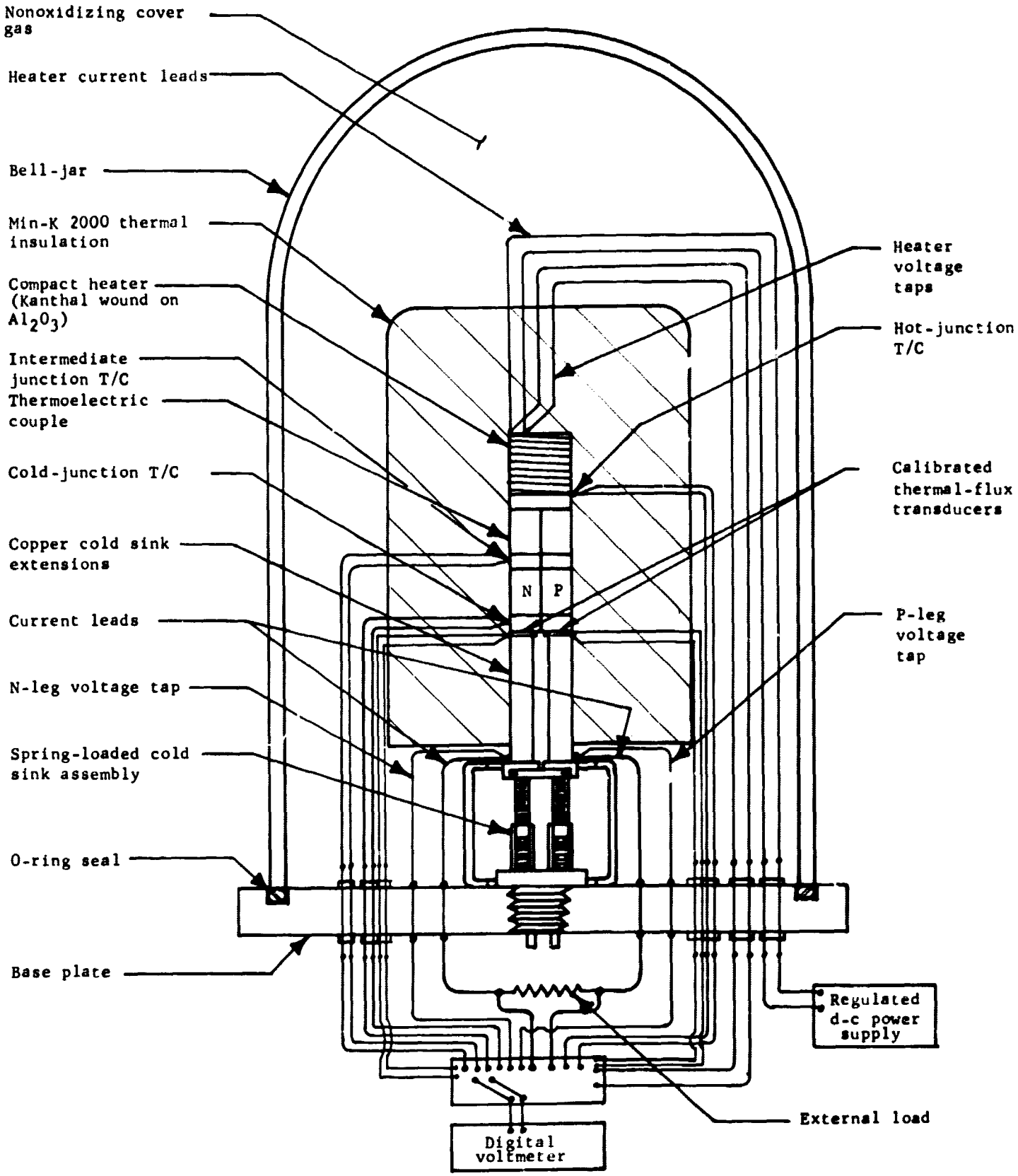

FIGURE 12 . SCHEMATIC OF EFFICIENCY-MEASUREMENT APPARATUS

standard (in order to correct for parasitic losses through the thermal insulation surrounding the thermoelectric couple), and (4) the computation of couple output power, P, using the relation $P = I \cdot V_{cc}$ (where I and V_{cc} are the measured current and closed-circuit voltage). The specifications for the test atmosphere, materials used in test fixture, electrical-measurement equipment, and test procedure are summarized in Appendix V.

It is noteworthy that the above design for the measurement of conversion efficiency does not include the use of a thermal "guarding" technique which is conventionally employed to minimize parasitic losses normal to the direction of heat flow. This is made possible through the use of vendor-calibrated thermal-flux transducers in conjunction with a well established thermal conductivity standard, viz., Pyroceram 9606, whose dimensions, emissivity, and thermal conductivity are closely matched to those of the thermoelectric couple to be tested. The elimination of thermal guarding simplifies the measurement of conversion efficiency, particularly at the high temperatures associated with couples containing SiGe ($\sim$1500 to $\sim$1700 F).

The accuracy of this measurement technique is principally a function of (1) the error associated with the measurement of thermal input power and (2) the ability to correct for unavoidable thermal losses from the periphery of the thermoelectric couples. Based on present information, the error associated with this efficiency-measurement technique may be as low as 3 to 4 percent.

TASK II. RTG ANALYSIS AND DESIGN

User Orientation of Input/Output Formats

The user-orientation of the input format for the GESPGN (Generalized Space Generator) computer program has been completed during this reporting period. The input format has been modified to (1) eliminate the use of all acronyms, (2) organize the input data into functional groups, e.g., radiator-fin inputs, thermopile inputs, fuel-form inputs, etc., (3) eliminate all input-data values of a "subjective" nature, e.g., iteration delta functions (increment size), iteration epsilon functions (tolerances), maximum number of iterations permitted, etc., and (4) include a permanent library of optimized radiator-fin parameters, viz., fin-length parameters, fin-thickness parameters, and fin-weight parameters. The compilation of radiator-fin data includes the parameters associated with magnesium, beryllium, magnesium M1A, magnesium HM21A-T8, aluminum A356-T6, copper, and chromium-copper. The compilation of other classes of input data (e.g., thermopile conversion efficiencies, thermal conductivities, etc.) into similar libraries would lessen the flexibility of the computer program since these classes of inputs are subject to frequent change as more reliable data become available. In addition, standard data forms (see Appendix VII) have been drafted in order to simplify compilation of input data.

The user-orientation of the output format for the GESPGN computer program has also been completed during this reporting period. The output format has been modified to (1) eliminate the use of acronyms, (2) organize the output data into functional groups, e.g., dimensions, weights, heat

losses, etc., (3) provide the option for either a detailed or abstracted display of tabular output data, and (4) provide the option for a graphical display of generator component weights versus radiator temperature or generator length. A "printer-plotter" subroutine was developed for the graphical display of output data in order to minimize the complications associated with the application of alternative graphical display techniques, viz., the CALCOMP X-Y plotters. An example of the input/output tabular format and "printer-plotter" appears in Appendix VIII. The detailed output data in this sample display (following the Summary of Output Data) and the printer-plot are optional and are specified in the input data.

The RTG computer program GESPGN has been translated from FORTRAN IV (Control Data Corporation 6400 version) to FORTRAN IV (IBM 360/91 version) to permit operation of the computer program at NASA-Goddard's computer center. The final phase of the translation will be performed at NASA-Goddard's computer center within the next few months. The delivery of the computer program to NASA-Goddard will be subject to the results of the three-dimensional heat-transfer analysis of the RTG (discussed in the following section) which may suggest inadequacies in the present model and, hence, necessitate corrections to the present computer program.

Heat-Transfer Analysis of RTG Mathematical Model

The three-dimensional heat-transfer analysis of the RTG model used in GESPGN was completed during this reporting period. The purpose of this analysis is to compute the longitudinal temperature profile of the generator model. In the analytical model of the computer program,

this temperature was considered constant along the length of the generator. This heat-transfer analysis was performed in two parts:

(1) The transverse temperature profile was calculated for a cross section of a generator shell and radiator located at the midpoint of the generator length

(2) The longitudinal temperature profile was calculated for the heat source, generator shell, and radiator fin.

The calculations of the transverse and longitudinal temperature profiles were based on the analytical models shown in Figures 13 and 14. The dimensions and thermal fluxes of the model are those of the minimum-weight design case for a selected 250-watt(e) RTG. The following assumptions have been included in both heat-transfer analyses:

(1) The modes of heat transfer between any subregion and the remainder of the model are radiation and/or conduction

(2) The thermal fluxes incident on the inside surface of the generator shell are calculated based on PbTe thermoelectric modules operating between 800 K and 500 K and Min-K 2000 thermal insulation

(3) The thermal conductivity of the radiator fin and generator shell was assumed to be 1.37 watts/cm-K (Magnesium H21A-T8)

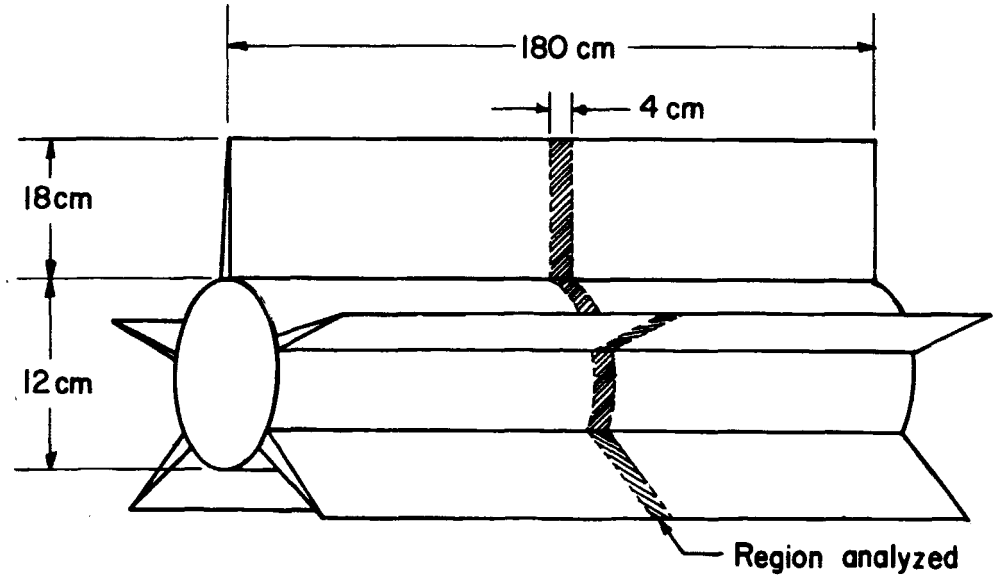

a. Longitudinal view of RTG

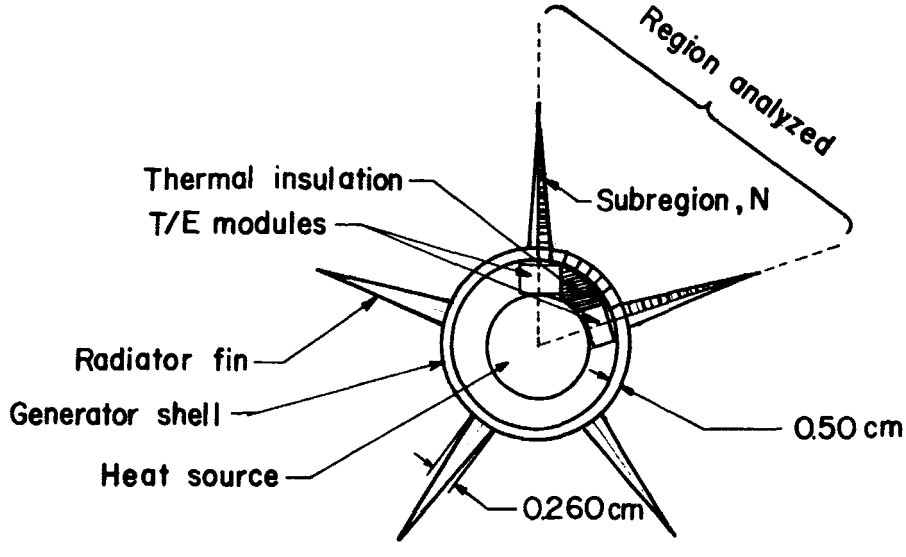

b. Cross-sectional view of RTG

FIGURE 13. ANALYTICAL MODEL FOR THREE-DIMENSIONAL HEAT-TRANSFER ANALYSIS OF RTG TRANSVERSE PROFILE

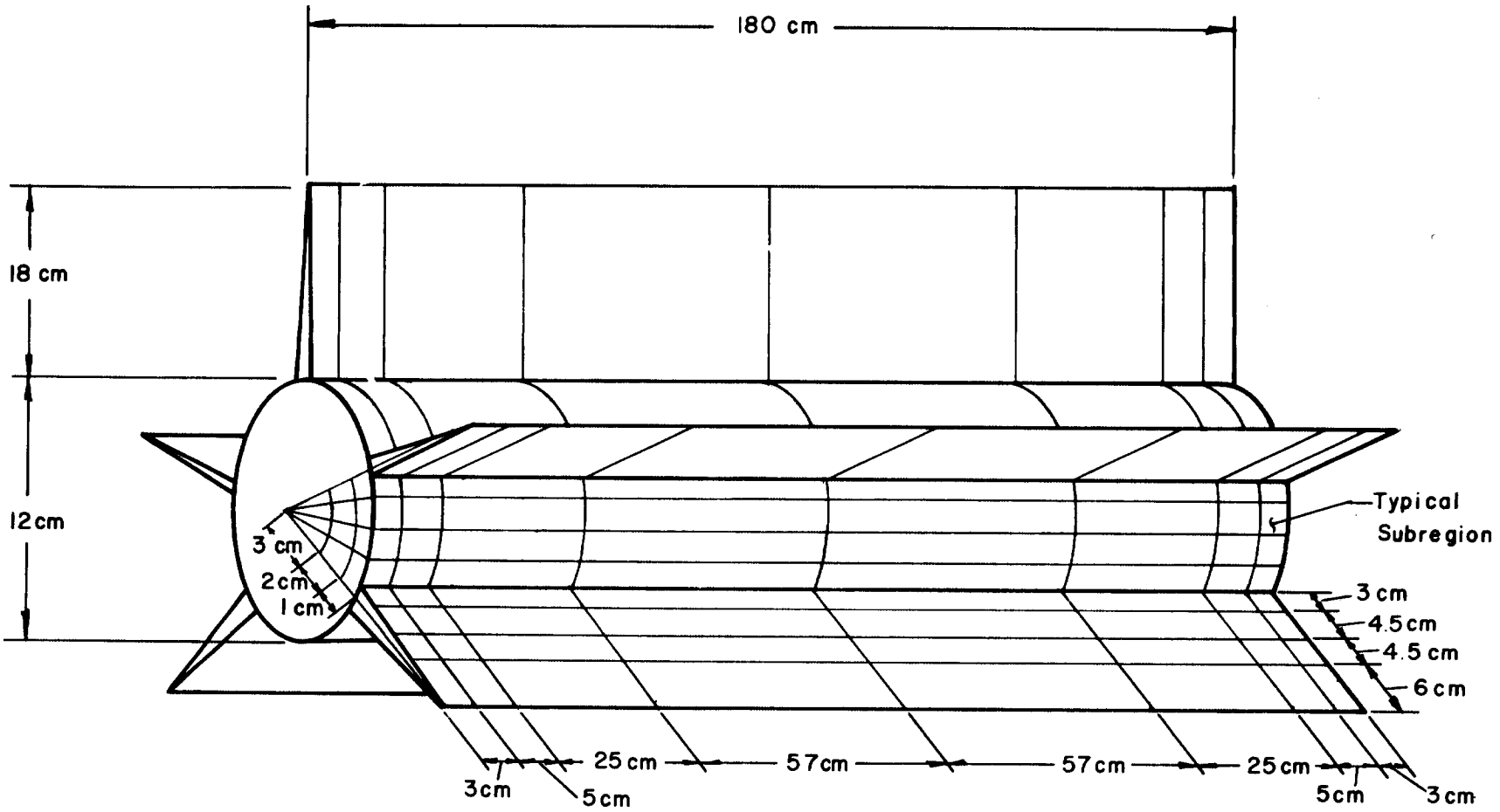

FIGURE 14. NODAL NETWORK FOR ANALYSIS OF RTG LONGITUDINAL TEMPERATURE PROFILE

(4) The generator was assumed to include five radiator fins and five thermoelectric modules (each module aligned with a radiator fin as shown in Figure 13).

(5) The radiator fin emissivity was assumed 0.90.

The thermal radiation interaction between any subregion and the remainder of the RTG model, i.e., the configuration factors, were calculated using the CONFAC II* computer program. These configuration factors as well as the calculated thermal conduction coupling between adjacent subregions, subregion surface areas, emissivities, and imposed thermal fluxes comprise the input data for the heat-transfer computer program TASIB**.

The heat-transfer analysis of the transverse profile closely approximates that of an infinitely long cylindrical generator since the enhanced radiation interchange between the generator ends and space, i.e., "end effects", has been neglected. Consequently, the computed transverse temperature distribution represents the "peak" radiator temperatures. The results of the transverse profile analysis are to be used as guidelines in establishing the dimensions of the nodal network for the longitudinal heat-transfer analysis. The computed transverse temperature profile is shown in Figure 15 and indicates that the choice of 0.5-cm generator shell thickness is sufficient to insure nearly constant surface temperatures in the region between adjacent radiator fins.

---

* Toups, K. A., A General Computer Program for the Determination of Radiant Interchange Configuration and Form Factors - CONFAC II, SID-65-1043-2, North American Aviation, Inc., October, 1965.

** Hultberg, J. A., Thermal Analyzer System - TASIB, Jet Propulsion Laboratories, 1966.

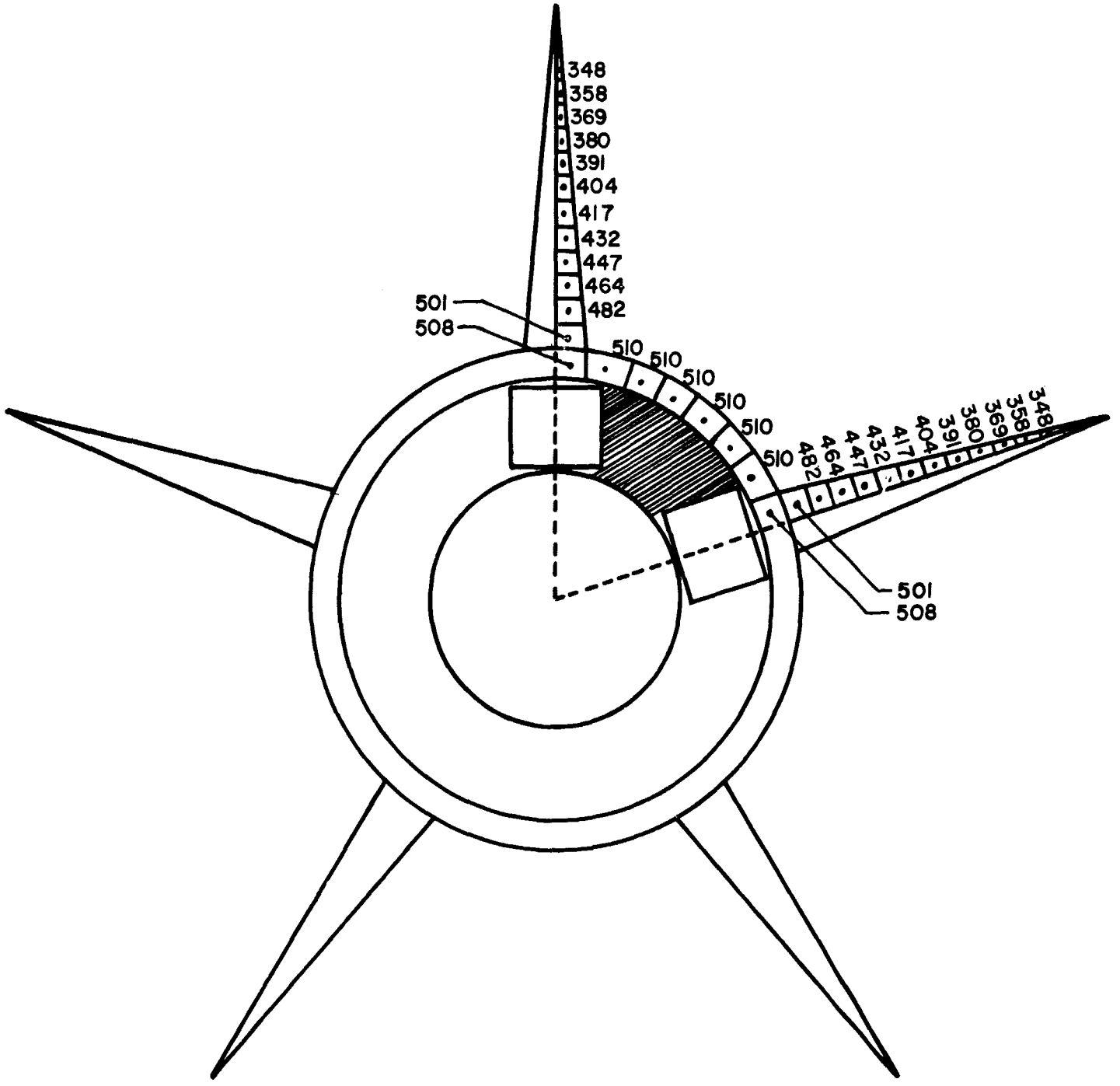

FIGURE 15. COMPUTED TEMPERATURE PROFILE FOR TRANSVERSE PROFILE OF RTG (TEMPERATURE IN DEGREES K)

The calculation of the longitudinal temperature profile was based on the analytical model shown in Figure 14. The dimensions for the nodal network, which subdivides the generator into "subregions" of nearly constant ΔT, are based on the results of the transverse profile analysis. The computed longitudinal temperature profile is shown in Figure 16 and indicates that (1) the choice of 0.5-cm generator shell thickness is sufficient to insure a nearly constant longitudinal temperature profile for generators possessing length-to-diameter (generator shell) ratios of 15 or less and (2) the radiator fin-base temperature in the regions adjacent to the thermoelectric modules ranges from 492 K to 483 K (assuming end effects) as compared with 484 K predicted by the radiator analysis used in the computer program. The calculated output power of the RTG is reduced by approximately 1 percent because of the difference between the uniform temperature profile assumed in the GESPGN computer program (484 K) and the profile predicted from the results of the three-dimensional heat-transfer analysis (483 K - 492 K).

In addition to the generator shell and radiator fin heat-transfer analyses, the longitudinal temperature profile of the heat source was calculated. This heat-transfer analysis was performed in order to determine the separation between adjacent thermoelectric modules (distributed along the length of the heat source) resulting in heat-source peak surface temperatures of less than 35 K above the assumed value. An excursion of 35 K (in the region between modules) above the assumed temperature profile of the heat-source surface would result in less than a 0.3 percent increase in the parasitic heat losses and can, therefore, be neglected. The results of this analysis indicate that for a combined fuel tube - heat-source

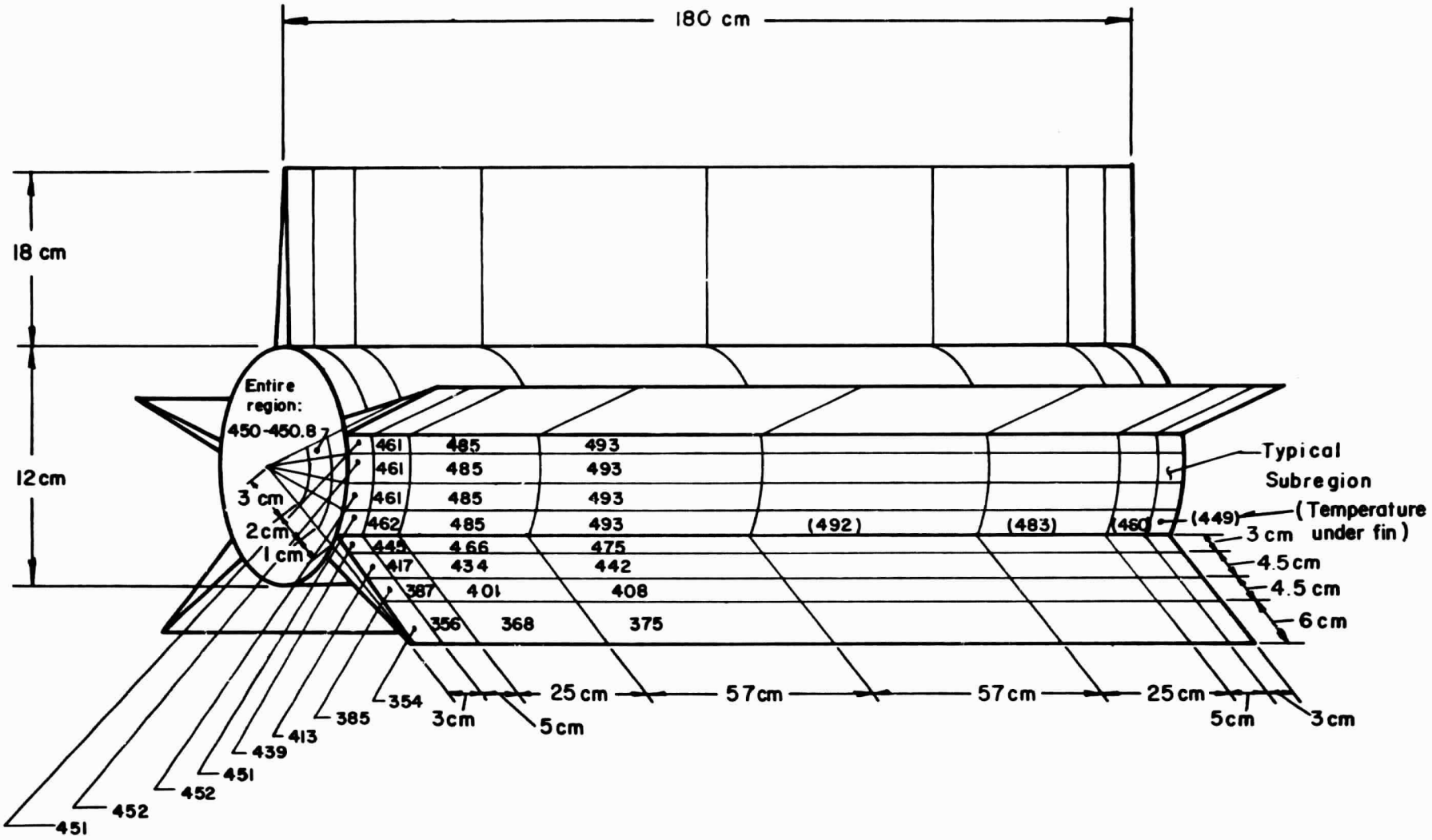

FIGURE 16. COMPUTED TEMPERATURE PROFILE FOR LONGITUDINAL PROFILE OF RTG (TEMPERATURE IN DEGREES K)

cladding thickness of 0.4 cm and radioisotope materials exhibiting low thermal conductivity, i.e., less than 0.05 watt/cm/C, (1) module-to-module separation should not exceed one heat-source diameter and (2) module-to-end-of-heat-source separations should not exceed one-half heat-source diameter.

Based on the results of the above heat-transfer analyses, no changes are required in the basic mathematical model used in the GESPGN computer program. The computer program will be modified, however, to indicate when the separation from end of module to end of heat source exceeds one-half heat-source diameter.

Study of Output Power and Efficiency of RTG System as a Function of Time

A study was performed in order to evaluate different approaches to the prediction of RTG thermopile performance using theoretical and/or empirical performance data. An examination of the possible modes of thermopile degradation revealed that the required performance data could be divided into the following three categories:

(1) Contact resistivity versus time at temperature

(2) Bulk thermoelectric properties (Seebeck coefficient, electrical resistivity, and thermal conductivity) versus time at temperature

(3) Radioisotopic decay rate.

Data for the first and third category above can be readily acquired and applied to the prediction of RTG performance using energy-balance techniques*. However, the measurement of bulk thermoelectric properties as a function of time at temperature is complicated by the fact that (1) under fixed thermal-input conditions typical of RTG operation, a change in the thermal conductivity of the thermoelectric material results in a change in the hot-junction temperature of the thermopile, hence, affecting the temperature-dependent degradation rates for the bulk thermoelectric properties and (2) the accurate measurement of thermal conductivity as a function of time at temperature under environmental conditions representative of actual RTG thermopile operation is extremely difficult. In addition, the theoretical prediction of thermopile performance based on individual measurements of Seebeck coefficient, electrical resistivity, thermal conductivity, and contact resistivity as a function of time at temperature for the case of varying hot-junction temperatures (induced by changes in thermal conductivity) is a formidable analysis task incorporating many experimental uncertainties. An alternative approach to the prediction of RTG thermopile performance for the case of changing bulk thermoelectric properties involves the direct measurement of the electrical output power and thermal input power of the thermopile (single or multiple couples).

Sample calculations of RTG performance involving the above three categories of degradation modes have been performed. These

---

* Computer program, OFF-OPT, was developed under USAEC Thermoelectric Contract W-7405-eng-92, "Development of Segmented Thermoelectric Modules Fabricated by Hot Isostatic Pressing".

calculations were based on a 50-watt(e) RTG containing a PbTe (2n-PbTe and 2p-PbTe) thermopile with (1) an initial fuel inventory of 1000 watts(th), (2) 10 percent parasitic heat losses, and (3) operating between 500 and 800 K initially. In this study, each of the three modes of degradation were analyzed separately in order to determine their effect on the RTG performance parameters.

Degradation Due to Contact-Resistivity Increase

The variation in hot-junction temperature and output power with increasing electrical contact resistivity and constant thermal inventory has been calculated using energy-balance techniques and is summarized in Table 6. These calculations were based on a ~50-watt(e) RTG containing a PbTe thermopile with (1) 10 percent parasitic heat losses, (2) no degradation of bulk thermoelectric properties, and (3) the external load matched to internal resistance at beginning of life, i.e., for contact resistivity equal to 200 $\mu\Omega$-cm^2. The results indicate that an increase in contact resistivity is accompanied by an increase in the hot-junction temperature and a decrease in the total electrical output power in the presence of constant thermal inventory and nondegrading bulk thermoelectric properties.

Degradation Due to Changes in Bulk Thermoelectric Properties

The magnitude and the direction of change in the hot-junction temperature and output power with degrading bulk thermoelectric properties and constant thermal inventory will depend on the change in the thermopile

thermal conductance with time. For example, the degradation of a thermopile containing 3p-PbSnTe often results in (1) a decrease in the Seebeck coefficient and electrical resistivity and (2) an increase in the thermal conductivity of the bulk thermoelectric material. Under conditions of constant thermal input, the thermopile would experience (1) a decreasing hot-junction temperature, (2) a constant cold-junction temperature, and (3) a decreasing electrical output power. However, the degradation of a thermopile containing 2p-PbTe often results in (1) an increase in Seebeck coefficient, (2) an increase in electrical resistivity, and (3) a decrease in thermal conductivity. Under conditions of constant thermal input, this thermopile would experience (1) an increasing hot-junction temperature, (2) a constant cold-junction temperature, and (3) a decreasing electrical output power. In the latter case, the increase in hot-junction temperature will tend to offset the decrease in output power due to bulk material degradation.

TABLE 6. HOT-JUNCTION TEMPERATURE, THERMAL INVENTORY, AND OUTPUT POWER AS A FUNCTION OF INCREASING ELECTRICAL CONTACT RESISTIVITY

Electrical Contact Resistivity, microhm-cm^2	Q_{Total}, watts(th)	T_{Cold}, K	T_{Hot}, K	Output Power, watts(e)
200	1000	500	800.0	49.51
500	1000	500	800.7	48.83
1000	1000	500	802.1	47.69
1500	1000	500	803.4	46.53
2000	1000	500	804.8	45.39

Degradation Due to Radioisotope Decay

The variation in the hot-junction temperature, cold-junction temperature, and output power with decreasing thermal input, i.e., decaying radioisotope heat source, has been calculated for a 50-watt(e) RTG containing a PbTe thermopile and is summarized in Table 7. These calculations were based on a ~50-watt(e) RTG containing a PbTe thermopile with (1) an initial fuel inventory of 1000 watts(th), (2) 10 percent parasitic heat losses, and (3) no thermopile degradation. The results indicate that, for a 50-watt(e) RTG, the cold junction is relatively insensitive (1 percent decrease) to a 10 percent decrease in the thermal inventory while the hot-junction temperature and, particularly the electrical output power experience a significant decrease, viz., 3.1 percent decrease and 15.2 percent decrease, respectively.

The above theoretical results serve as the rationale for the design and development of a life-testing technique (Task I) which provides meaningful data with respect to the prediction of typical RTG performance. Specifically, the results of this study indicate that life testing should be performed under conditions of constant thermal input or decaying thermal input (in order to simulate natural radioisotope decay) since the hot-junction temperature, which is usually maintained constant in most life testing, tends to increase or decrease depending on the mode of degradation.

TABLE 7. RTG OPERATING TEMPERATURES, THERMOPILE EFFICIENCY, AND OUTPUT POWER AS A FUNCTION OF RADIOISOTOPE DECAY

eat-Source Thermal nventory, atts(th)	Elapsed Time Required for Radioisotope Decay to Present Thermal Inventory			Thermopile Temperatures		Thermopile Conversion Efficiency, percent	Thermopile Output Power, watts(e)
	Plutonium-238, years	Polonium-210, years	Curium-244, years	Cold Junction, K	Hot Junction, K		
1000	0	0	0	500.11	800.093	5.50117	49.5115
995	.643747	2.74858 E-3	.130196	499.818	798.908	5.48618	49.1178
990	1.29074	5.51101 E-3	.261048	499.525	797.721	5.47118	48.7255
985	1.941	8.28742 E-3	.392562	499.23	796.534	5.45616	48.3344
980	2.59458	.011078	.524746	498.934	795.346	5.44112	47.9446
975	3.25149	1.38828 E-2	.657605	498.637	794.156	5.42607	47.5561
970	3.91179	.016702	.791148	498.338	792.965	5.41101	47.1688
965	4.5755	1.95358 E-2	.925381	498.037	791.773	5.39593	46.7829
960	5.24265	2.23844 E-2	1.06031	497.736	790.58	5.38084	46.3983
955	5.91329	2.52478 E-2	1.19595	497.432	789.385	5.36573	46.0149
950	6.58745	2.81262 E-2	1.33229	497.128	788.19	5.3506	45.6328
945	7.26517	3.10198 E-2	1.46936	496.821	786.993	5.33546	45.252
940	7.94648	3.39288 E-2	1.60715	496.514	785.795	5.3203	44.8725
935	8.63143	3.68533 E-2	1.74568	496.204	784.595	5.30513	44.4943
930	9.32005	3.97935 E-2	1.88495	495.893	783.395	5.28994	44.1174
925	10.0124	4.27495 E-2	2.02498	495.581	782.193	5.27474	43.7418
920	10.7085	4.57215 E-2	2.16576	495.267	780.989	5.25951	43.3674
915	11.4083	4.87098 E-2	2.3073	494.951	779.785	5.24428	42.9944
910	12.1121	5.17144 E-2	2.44963	494.634	778.579	5.22902	42.6227
905	12.8196	5.47355 E-2	2.59274	494.315	777.371	5.21375	42.2522
900	13.5311	5.77734 E-2	2.73664	493.995	776.163	5.19846	41.8831

TASK III. THERMOELECTRIC MATERIALS STUDIES

Material Selection and Preparation

Material Selection

The thermoelectric materials to be evaluated in nonstandard compositional conditions were chosen according to the following criteria:

(1) The thermoelectric alloy should be one notably sensitive to the contaminants of an operating couple environment

(2) The thermoelectric alloy should be one commonly used for power generation and of a standard commercial grade.

Accordingly, the materials were selected to be of p-type, specifically, 2p-PbTe and 3p-PbSnTe which are produced commercially by Minnesota Mining and Manufacturing Company (3M). Two contaminants, oxygen and copper, were selected as representative of contaminants frequently cited as causes of unstable behavior of operating thermoelements. The following specific combinations of thermoelectric material and contaminant were evaluated:

(1) 2p-PbTe - oxygen

(2) 2p-PbTe - copper

(3) 3p-PbSnTe - oxygen.

Material Preparation

The thermoelectric materials used to prepare the "nonstandard" conditions were commercially available formulations purchased in powder form. The powder which was initially minus 100 mesh was screened to produce the following mesh fractions:

(1) Minus 100-plus 325 mesh

(2) Minus 325 mesh.

These mesh fractions were used either singularly or in blended proportions to obtain the desired products which are discussed below.

The thermoelement specimens for property measurement were prepared by cold-die pressing at 60,000 to 100,000 psi followed by sintering. The elements were approximately 0.3 in. in diameter by 3/4 in. long. The details of the formulation of the nonstandard conditions are discussed below.

Oxygen Contamination

Oxygen was introduced into the element through the use of fine powder (minus 325 mesh) having a large amount of surface area with an attendant large content of surface oxide. The amount of oxygen added was varied by varying the amount of minus 325-mesh powder added to the coarser (minus 100-plus 325) mesh fraction. Sintering was performed in a nonreducing atmosphere to insure retention of the oxygen. The sintering treatment was of 2-hr duration at 1200 F in argon in a Vycor chamber. The elements produced in this manner were found to have stable electrical properties during elevated-temperature measurements.

Initially, in order to assess the effects of oxygen, test specimens were prepared with varying amounts of fine powder (minus 325 mesh). The Seebeck coefficients were measured at a nominal temperature of 50 C by means of the Seebeck probing apparatus described in Appendix III. The resulting data for 2p-PbTe and 3p-PbSnTe are plotted in Figures 17 and 18, respectively. The data show an increase in Seebeck coefficient with additions of fines in 2p-PbTe and a decrease for 3p-PbSnTe.

It should be noted that the effects attributed to oxygen from addition of fines is confirmed by the fact that the 2p-PbTe properties can be restored to normal levels by treatment in hydrogen. This is not the case, however, for 3p-PbSnTe since the oxide formed is probably a manganese oxide which is not reducible by hydrogen at the normal sintering temperatures.

The selection of the specific additions of fines to be made to the 2p-PbTe and 3p-PbSnTe for property characterization was made on the basis of accumulated analyses made on couples oxidized during life testing. Additions of 20 and 40 w/o minus 325 mesh were chosen for 2p-PbTe yielding Seebeck coefficients (at 50 C) of approximately 50 and 100 percent higher than that of the normal material, respectively. The addition for the 3p-PbSnTe was chosen to be 45 w/o on the basis of cursory resistivity measurements. The resistivity at this level of addition was approximately half that of the normal material at 500 C.

A group of six elements of each type were prepared according to the procedures described above. No attempt was made to ascertain the

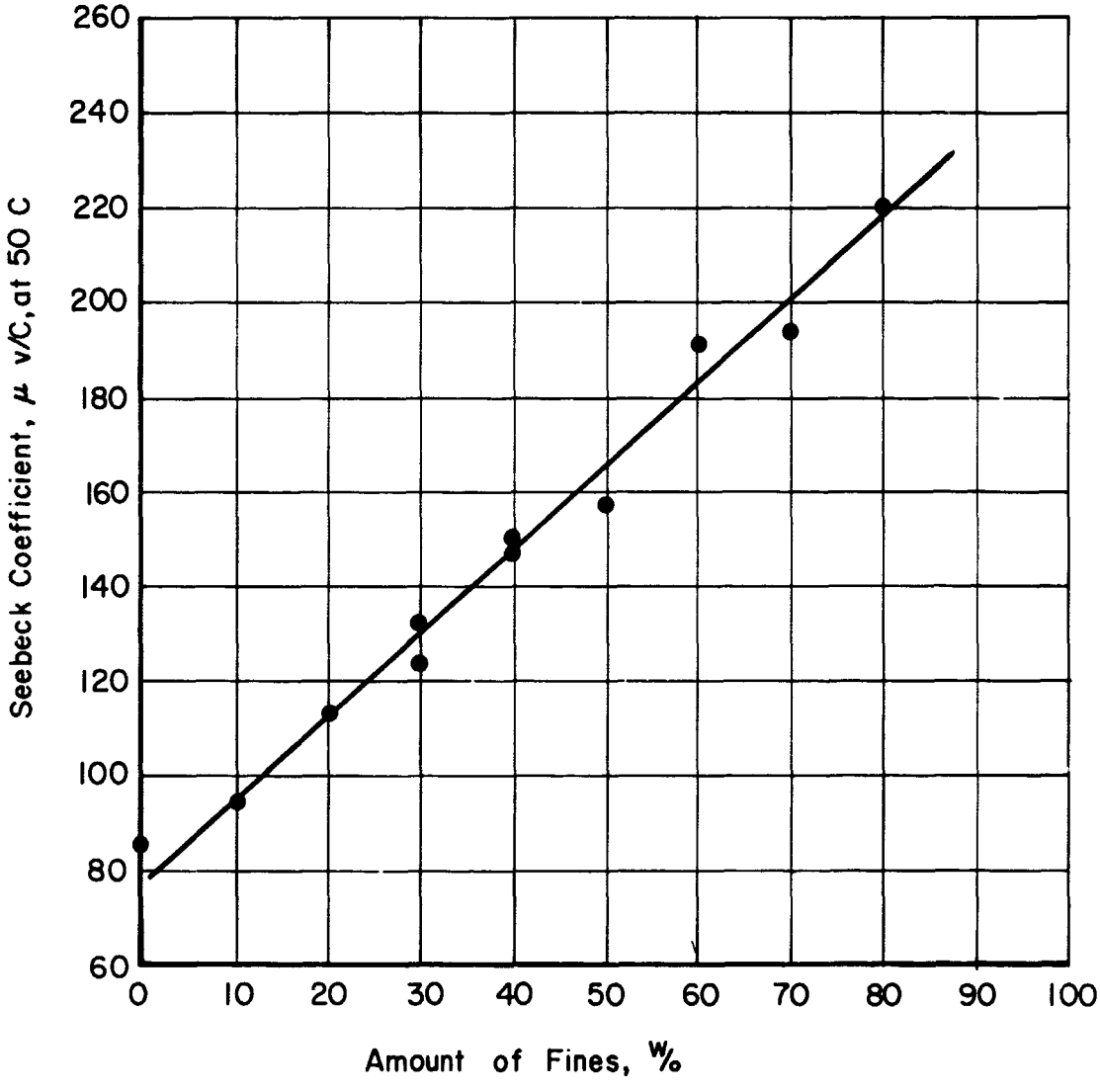

FIGURE 17. EFFECTS ON SEEBECK COEFFICIENT OF ADDITIONS OF FINE POWDER TO COARSE 2p-PbTe POWDER

Weighed amounts of fines (minus 325 mesh) were added to coarse 2p-PbTe powder and blended. The mixture was green pressed then sintered 2 hr at 1200 F in an argon atmosphere. The data show the effects of oxygen from particle surfaces on the Seebeck coefficient.

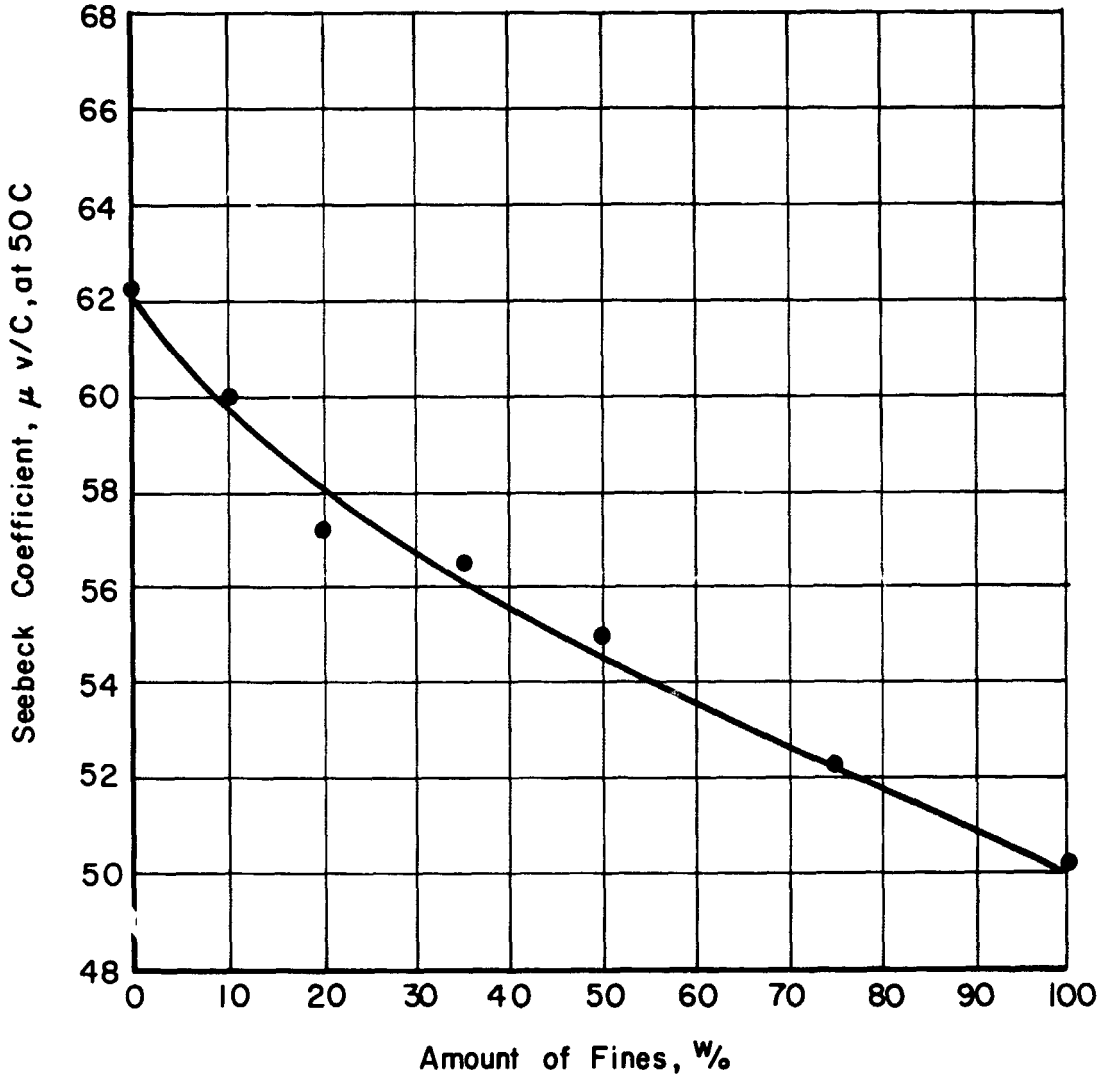

FIGURE 18. EFFECTS ON SEEBECK COEFFICIENT OF ADDITIONS OF FINE POWDER TO COARSE 3p-PbSnTe POWDER

Weighed amounts of fines (minus 325 mesh) were added to coarse 3p-PbSnTe powder and blended. The mixture was green pressed then sintered 2 hr at 1200 F in an argon atmosphere. The data show the effects of oxygen from particle surface on the Seebeck coefficient.

oxygen contents of these elements because of poor reproducibility in previous analyses. Alternate methods of analysis are being reviewed in an attempt to achieve a direct analysis for oxygen content.

Copper Contamination

The level of copper addition made to 2p-PbTe was 0.1 w/o. This amount was selected on the basis of accumulated analyses made on elements poisoned during couple testing. The copper analyses determined spectrographically were generally grouped about the 0.1 w/o level.

The copper contaminant was introduced by blending an accurately weighed amount of copper powder into the 2p-PbTe powder before processing into elements. The elements pressed from this mixture were sintered for 1 hr at 1200 F in hydrogen to produce sintering and diffusion of the copper into the PbTe. It was necessary, however, to process the elements further because the electrical properties were found to be unstable during the preliminary elevated-temperature measurements. This instability was attributed to inadequate distribution of the copper throughout the elements. To insure homogenization of the copper, the elements were crushed and reprocessed as above. The reworking of the material provided both mechanical and chemical homogenization effects. The resulting elements were found to have very stable electrical characteristics.

A group of six elements were prepared according to the procedures described above. Figure 19 shows typical photomicrographs of the three categories of materials in as-polished condition.

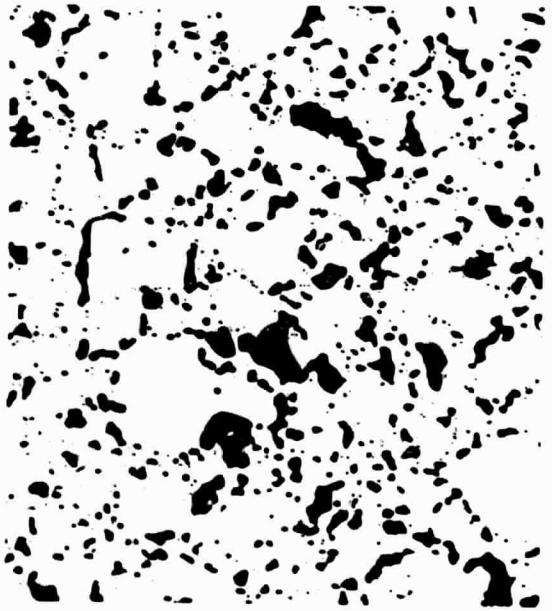

100X OD 485

(a) 2p-PbTe containing oxygen

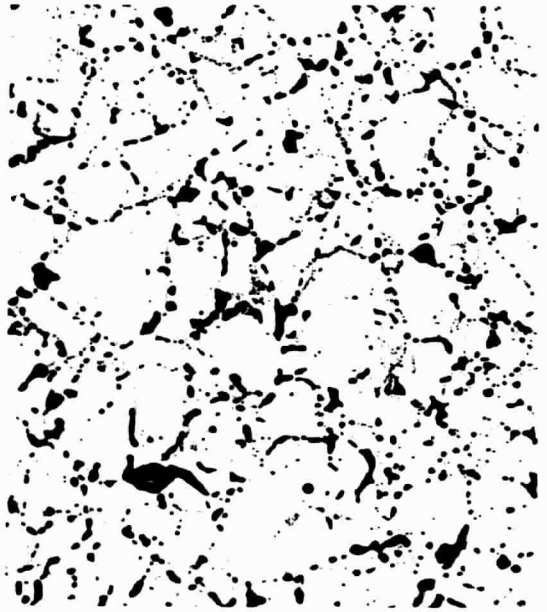

100X OD 486

(b) 2p-PbTe containing 0.1 w/o copper

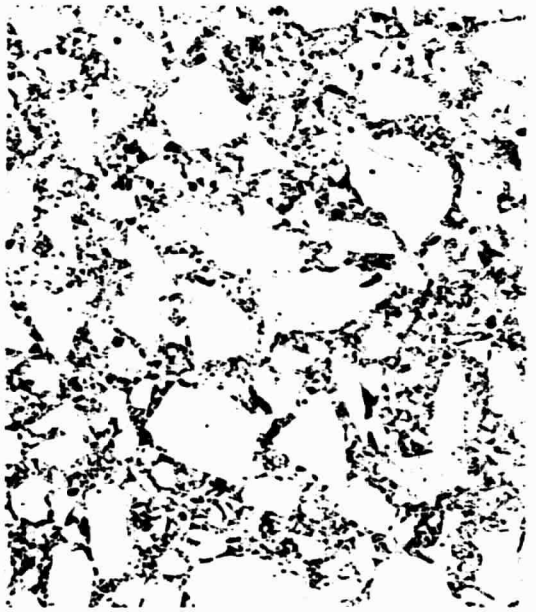

100X OD 484

(c) 3p-PbSnTe containing oxygen

FIGURE 19. AS-POLISHED PHOTOMICROGRAPHS OF 2p-PbTe AND 3p-PbSnTe IN NONSTANDARD COMPOSITIONAL CONDITIONS

The 2p-PbTe specimens exhibit rounded pores typical of the pressed and sintered product made from relatively fine powder. The specimen containing 0.1 w/o copper contains a finely dispersed phase attributable to the copper which is clearly evident at the particle boundaries. The 3p-PbSnTe specimen shows clearly the combination of coarse and fine powder. The coarse particles exhibit their characteristic irregular shape resulting from cleavage fracture during comminution.

Characterization of Electrical Properties

The temperature dependence of Seebeck coefficient and electrical resistivity of the three types of elements were measured from room temperature to a minimum of 550 C. The equipment used to make the Seebeck coefficient and electrical-resistivity measurements has been reported previously.* The Seebeck coefficient and electrical-resistivity-measurement techniques under development in Task I of this program could not be implemented in this task because of the concurrent nature of the two efforts. Argon was used as a protective cover gas during measurements at elevated temperature. Three or more measurements of both the Seebeck coefficient and electrical resistivity were made on different elements from each group. These data were used to calculate the average values for each group and to assess the scatter of measured values among the group of elements. In general, the scatter of the data within each group of elements was within acceptable limits as will be apparent from review of the data given below.

---

* An Advanced Thermoelectric Component Development Program Final Summary Report, February 18, 1966, Contract NAS5-9160, page 21.

Oxygen-Contamina'ed 2p-PbTe

The Seebeck-coefficient and electrical-resistivity data for one of the oxygen-contaminated conditions (40 w/o, minus 325 mesh powder addition) of 2p-PbTe are summarized in Tables 8 and 9, respectively. Included in these tables are the calculated average values and the maximum deviation (in percent) of a single curve from the average curve at each 100 C increment of temperature. The maximum deviation from the mean value observed was 6.1 percent.

The average values of Seebeck coefficient and resistivity are plotted in Figures 20 and 21, respectively, with data for the 2p-PbTe in both the normal and oxygen-contaminated conditions. These data show the following:

(1) The Seebeck coefficients of the oxygen-contaminated materials reach a higher maximum value than that of the normal material and become intrinsic at a significantly lower temperature as indicated by the position of their maxima (from 350 to 400 C).

(2) The resistivity of the oxygen-contaminated materials is significantly higher over the entire temperature range. The resistivities range from two to four times higher at about 450 C than that of the normal material.

TABLE 8. SEEBECK COEFFICIENT OF 2p-PbTe CONTAMINATED WITH OXYGEN*

	Seebeck Coefficient (microvolts/C)				
	Temperature (C)				
Specimen	100	200	300	400	500
2230P2	145	232	305	316	233
2226P2	153	241	322	317	234
2227P2	150	241	318	304	214
Average	150	238	315	312	227
Maximum deviation from average (%)	-3.3	-2.5	-3.2	-2.6	-6.1

* Mixture of 60% minus 100 plus 325 mesh powder and 40% minus 325 mesh powder.

TABLE 9. ELECTRICAL RESISTIVITY OF 2p-PbTe CONTAMINATED WITH OXYGEN*

	Resistivity (microhm-cm)				
	Temperature (C)				
Specimen	100	200	300	400	500
2230P2	2000	6400	13,500	19,600	18,800
2226P2	2300	6900	14,800	20,500	19,850
2227P2	2050	6500	13,500	18,700	18,000
Average	2120	6600	13,950	19,600	18,900
Maximum deviation from average (%)	+5.6	+4.6	+6.1	±4.6	+5.0

* Mixture of 60% minus 100 plus 325 mesh powder and 40% minus 325 mesh powder.

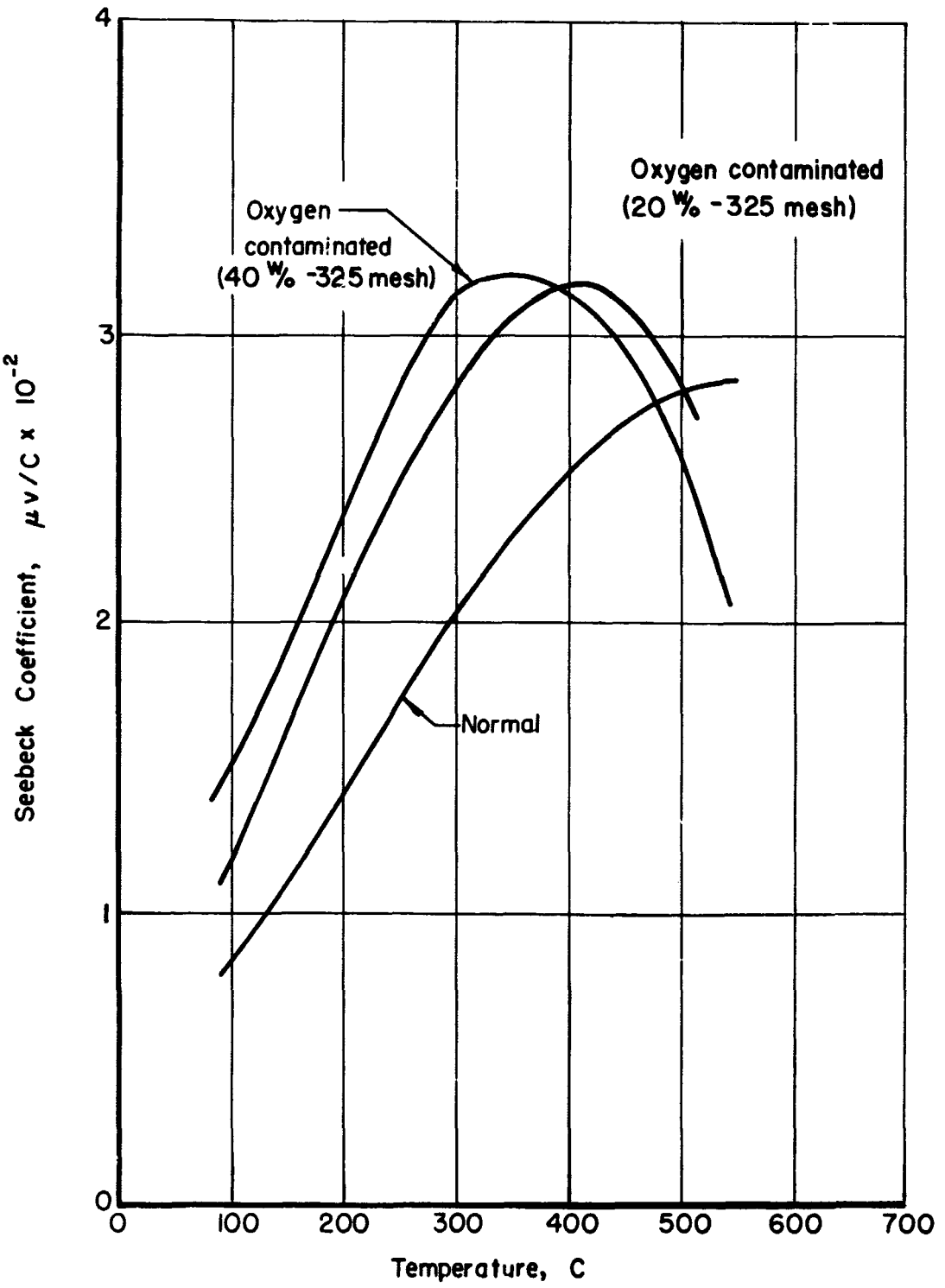

FIGURE 20. SEEBECK COEFFICIENT OF OXYGEN-CONTAMINATED AND NORMAL 2p-PbTe

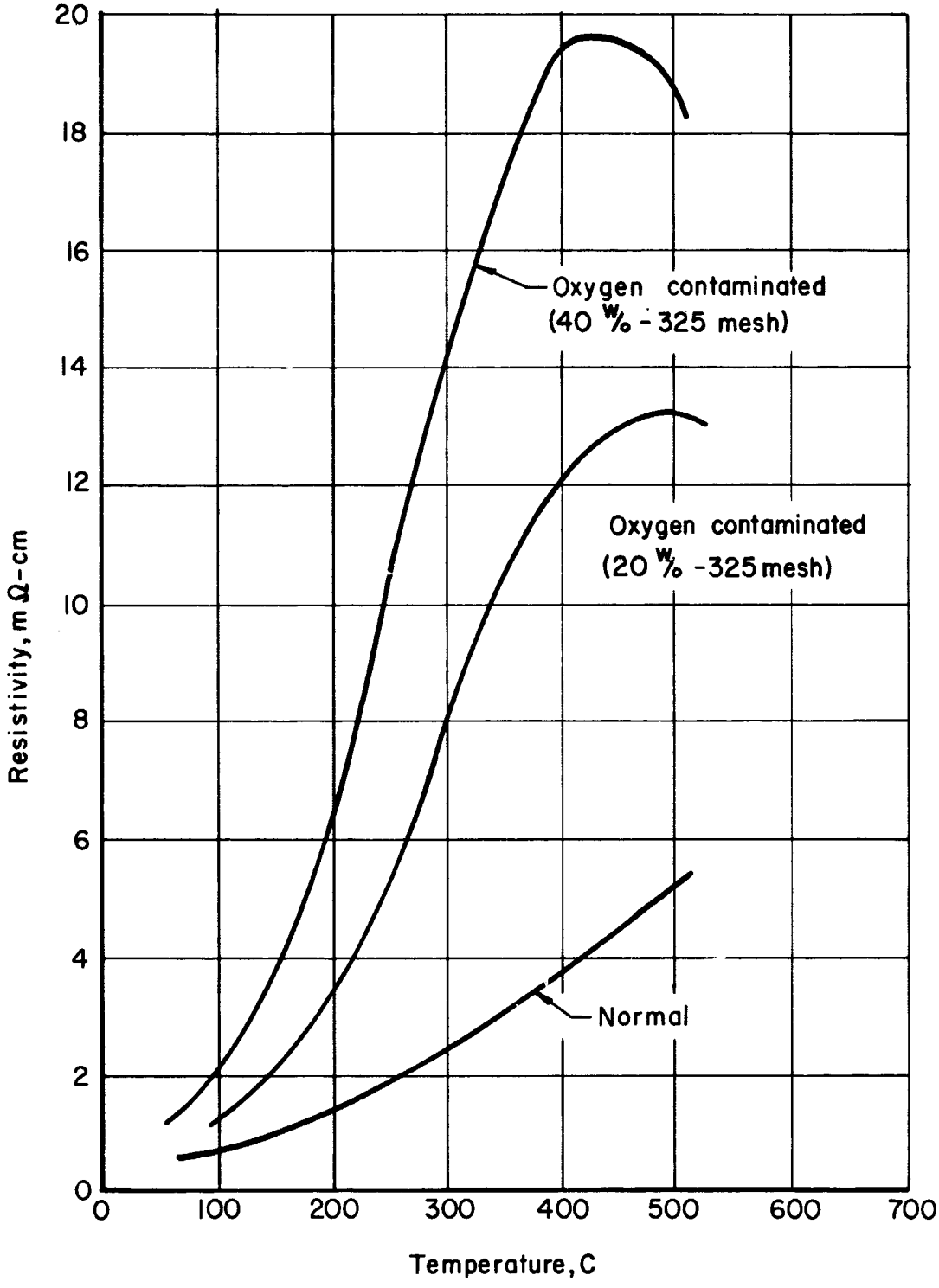

FIGURE 21. ELECTRICAL RESISTIVITY OF OXYGEN-CONTAMINATED AND NORMAL 2p-PbTe

The calculated power factors (S^2/ρ) for the oxygen-contaminated and normal 2p-PbTe are compared in Figure 22. The power factors of the oxygen-contaminated materials are depressed over most of the range from 100 to 500 C with the maximum difference from normal values occurring at the higher temperatures. The average power factors over the range 100 to 500 C are 6.8, 8.7, and 15.6 $\left((\text{volts/C})^2/\text{ohm-cm} \times 10^{-6}\right)$ for 2p-PbTe containing 40, 20, and 0 w/o, -325 mesh powder, respectively.

Oxygen-Contaminated 3p-PbSnTe

The Seebeck-coefficient and electrical-resistivity data for the oxygen-contaminated condition of 3p-PbSnTe are summarized in Tables 10 and 11, respectively. Included in these tables are the calculated average values and the maximum percent deviation of a single curve from the average curve at each 100 C increment of temperature. The maximum deviation from the mean property value is 6.0 percent for the Seebeck coefficient and 2.3 percent for the resistivity.

The average values of each property are plotted in Figures 23 and 24 with data for 3p-PbSnTe in both the normal and oxygen-contaminated condition. These data show a general depression in values of both properties over most of the range from 100 to 600 C. The resistivity data exhibit an unusual dip in values at about 550 C which appears to be peculiar to this material.

The calculated power factors (S^2/ρ) for the oxygen-contaminated and normal 3p-PbSnTe are compared in Figure 25. The average power factors over the range 100 to 600 C are 8.3 and 9.2 $(\text{volts/C})^2/\text{ohm-cm} \times 10^{-6}$)

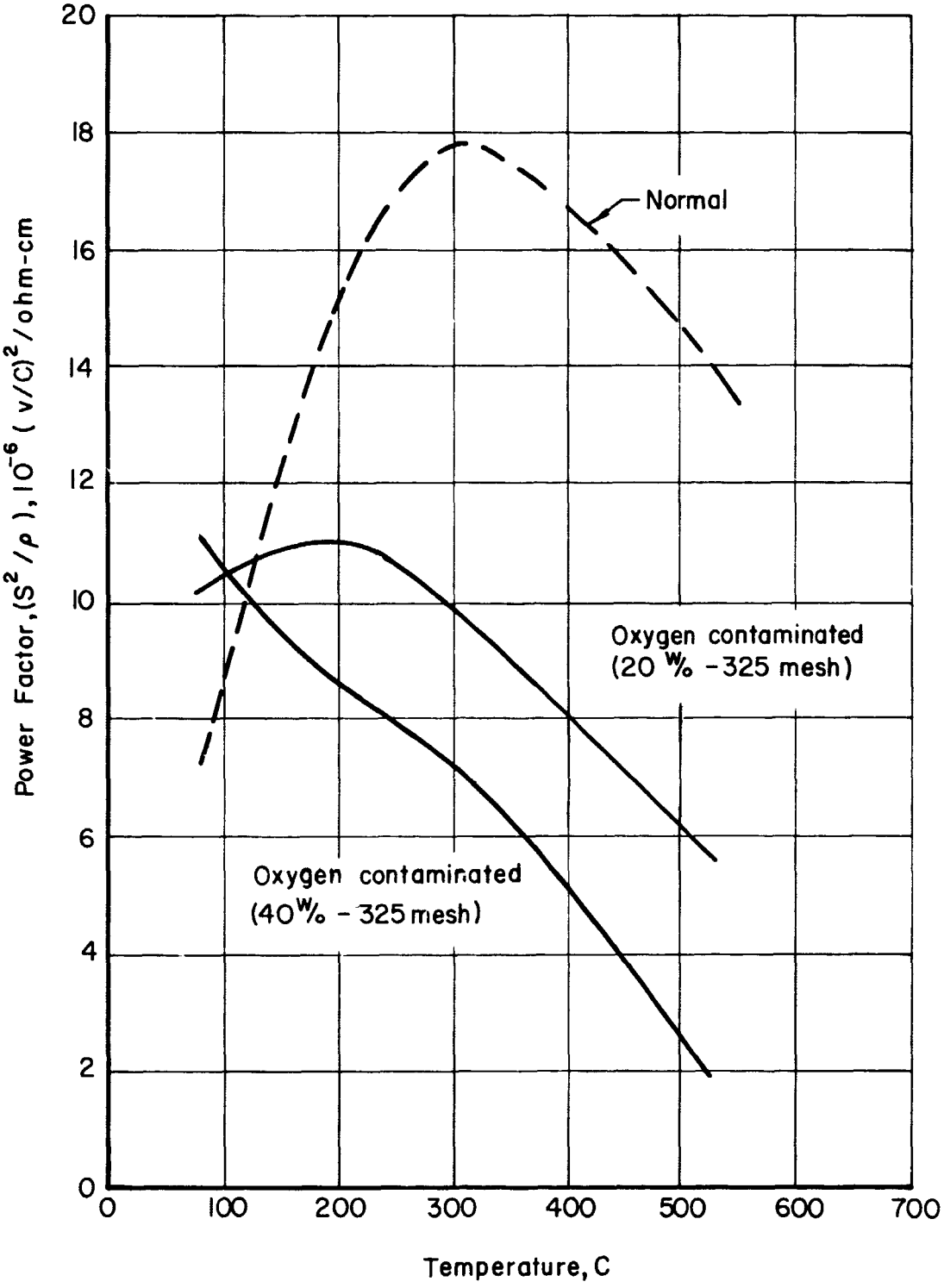

FIGURE 22. POWER FACTOR AS A FUNCTION OF TEMPERATURE FOR 2p-PbTe CONTAMINATED WITH OXYGEN

TABLE 10. SEEBECK COEFFICIENT OF 3p-PbSnTe CONTAMINATED WITH OXYGEN*

	Seebeck Coefficient (microvolts/C)						
	Temperature (C)						
Specimen	100	200	300	400	500	550	600
2255P3	59	84	113	143	167	168	166
2254P3	59	83	113	146	168	171	171
2256P3	59	87	116	145	170	173	168
Average	59	85	114	145	168	171	168
Maximum deviation from average (%)	±0	±2.3	+1.8	-1.4	+1.2	-1.8	+1.8

* Mixture of 55% minus 100 plus 325 mesh and 45% minus 325 mesh.

TABLE 11. ELECTRICAL RESISTIVITY OF 3p-PbSnTe CONTAMINATED WITH OXYGEN*

	Resistivity (microhm-cm)						
	Temperature (C)						
Specimen	100	200	300	400	500	550	600
2257P3	940	1250	1700	2200	2500	2426	2600
2253P3	950	1250	1850	2325	2450	2450	2600
2254P3	950	1350	1875	2425	2575	2450	2600
Average	945	1285	1810	2315	2510	2440	2600
Maximum deviation from average (%)	±0.7	+5.2	-6.0	-5.0	+2.7	-0.7	±0

* Mixture of 55% minus 100 plus 325 mesh and 45% minus 325 mesh.

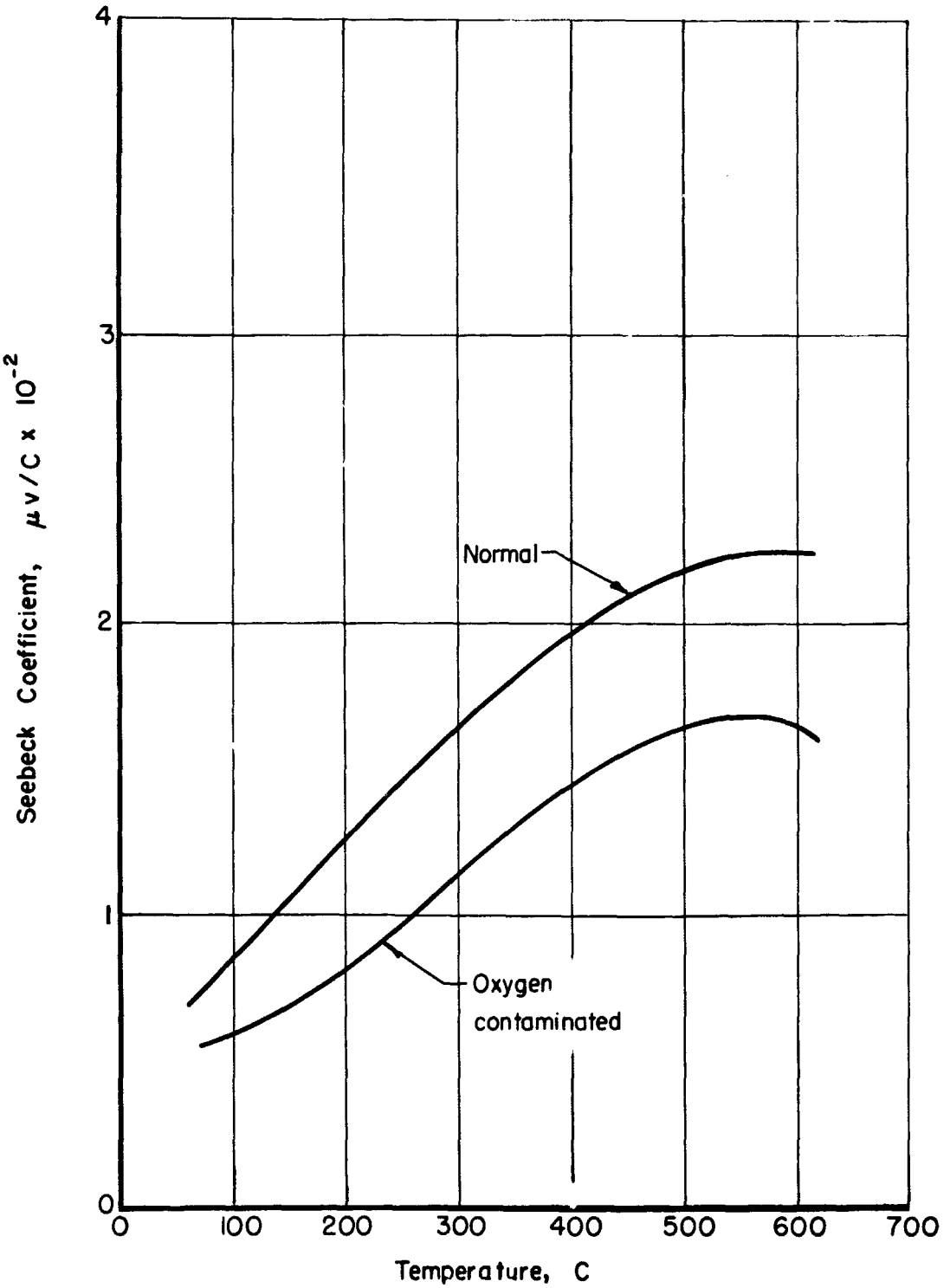

FIGURE 23. SEEBECK COEFFICIENT OF OXYGEN-CONTAMINATED AND NORMAL 3p-PbSnTe

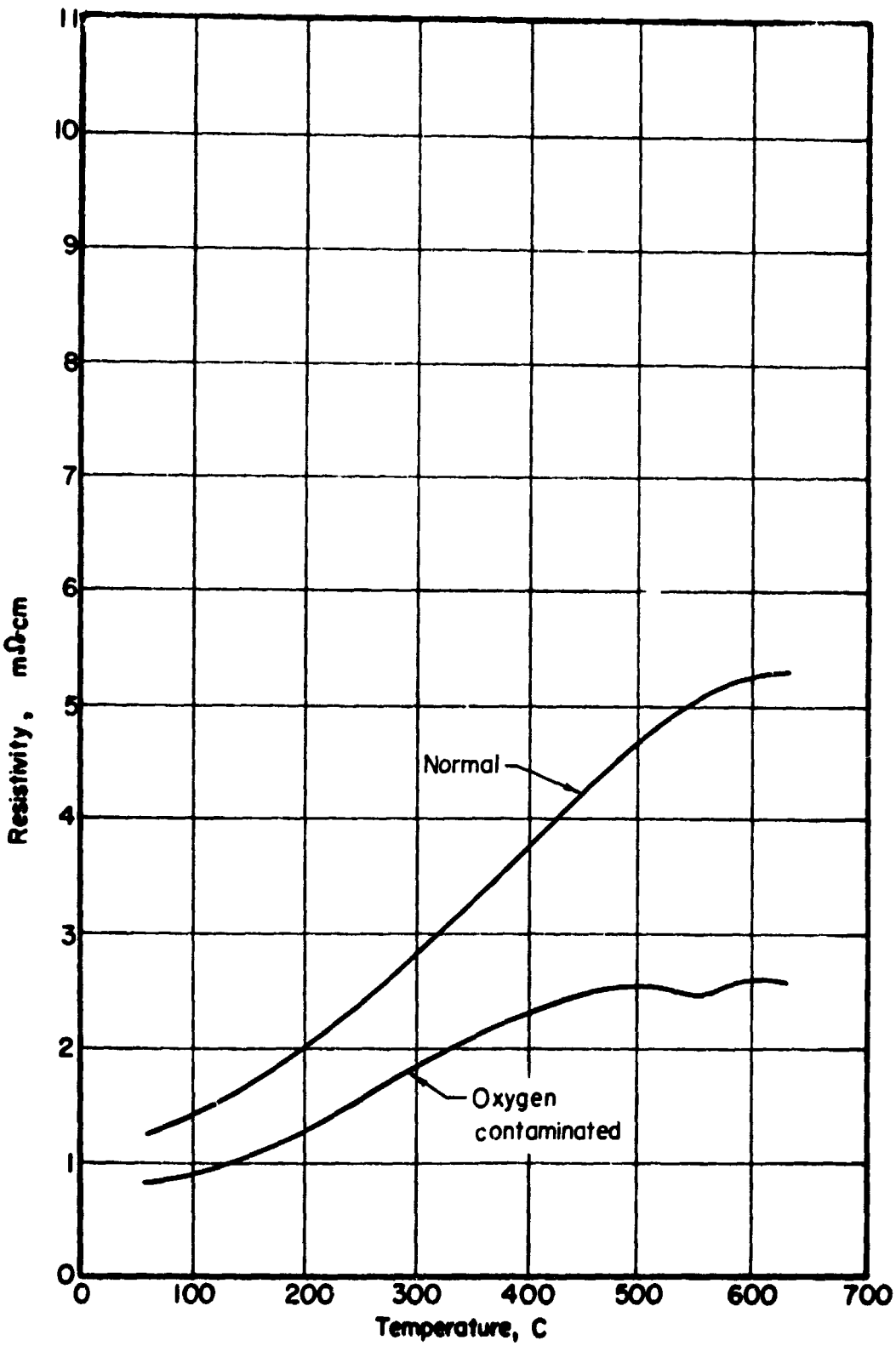

FIGURE 24. ELECTRICAL RESISTIVITY OF OXYGEN-CONTAMINATED AND NORMAL 3p-PbSnTe

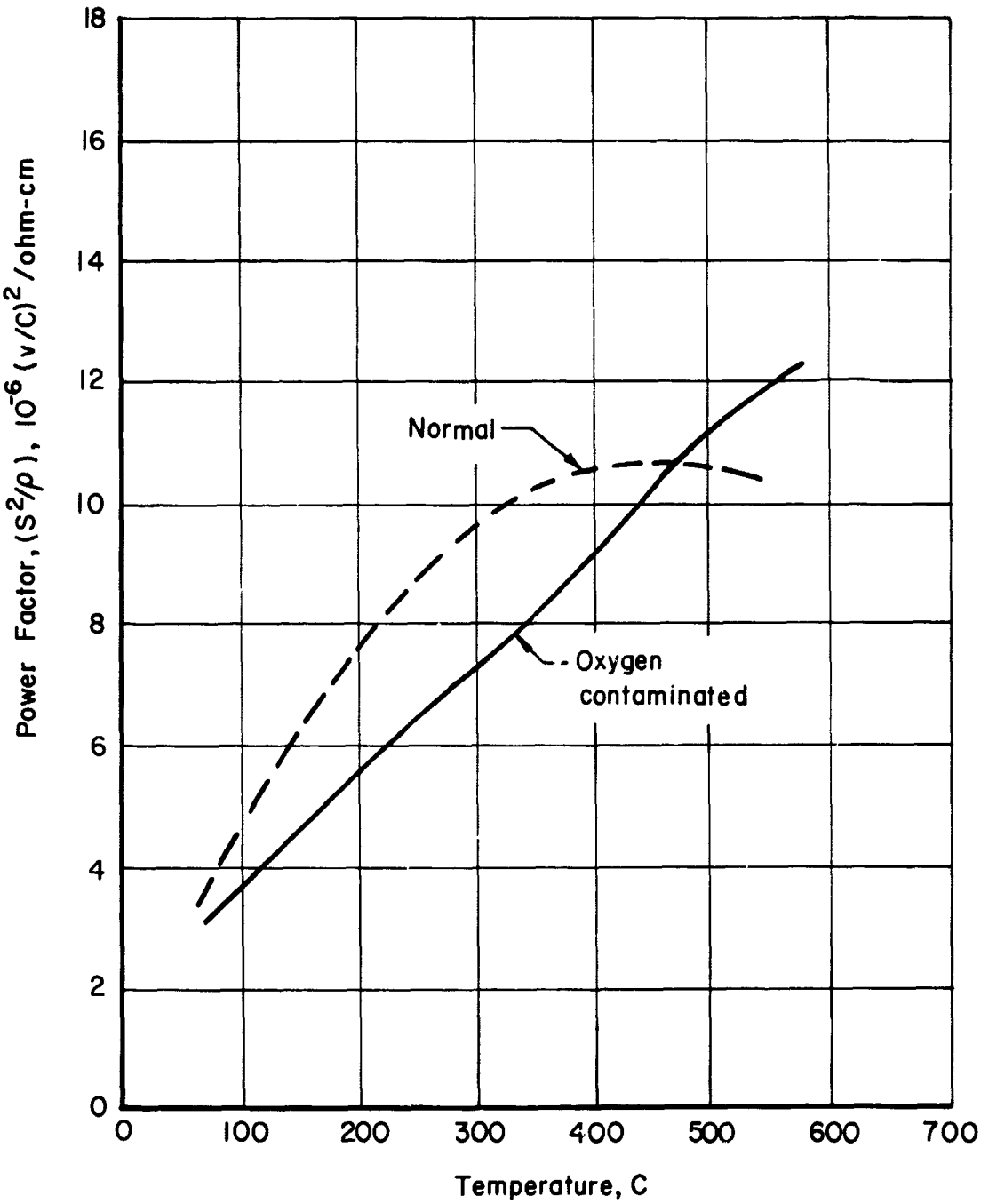

FIGURE 25. POWER FACTOR AS A FUNCTION OF TEMPERATURE FOR 3p-PbSnTe CONTAMINATED WITH OXYGEN

for the oxygen-contaminated and normal materials, respectively. The power-factor curves cross at about 450 C with the normal material having a lower power factor between 450 and 600 C.

Copper-Contaminated 2p-PbTe

The Seebeck-coefficient and electrical-resistivity data for the copper-contaminated condition of 2p-PbTe are summarized in Tables 12 and 13, respectively. Included in these tables are the calculated average values and maximum percent deviation of a single curve from the average curve at each 100 C increment of temperature. The maximum deviation from the mean property value is 9.7 percent for the Seebeck coefficient and 7.4 percent for the resistivity.

The average values of each property are plotted in Figures 26 and 27 with data for 2p-PbTe in normal uncontaminated condition. These data show effects which are smaller but similar to those produced by contamination with oxygen. The Seebeck coefficient is increased over most of the temperature range with the material becoming intrinsic at a temperature of about 400 C. The resistivity is increased over the entire range from room temperature to 550 C.

The calculated power factors (S^2/ρ) for the copper-contaminated and normal 2p-PbTe are compared in Figure 28. The power factor of the copper-contaminated material is depressed over most of the range from 100 to 500 C with the maximum difference occurring at the higher temperatures. The average power factors over the range 100 to 500 C are 9.2 and 15.6 $\left((\text{volts/C})^2/\text{ohm-cm} \times 10^{-6} \right)$ for the copper-contaminated and normal materials, respectively.

TABLE 12. SEEBECK COEFFICIENT OF 2p-PbTe CONTAINING 0.1 W/O COPPER

	Seebeck Coefficient (microvolts/C)				
	Temperature (C)				
Specimen	100	200	300	400	500
2269P2	113	194	269	302	283
2267P2	124	204	280	308	276
2279P2	125	212	290	314	282
2278P2	124	213	280	313	250
2280P2	124	210	285	312	278
Average	122	207	281	310	280
Maximum deviation from average (%)	-7.4	-6.3	-4.3	-2.6	-1.4

TABLE 13. ELECTRICAL RESISTIVITY OF 2p-PbTe CONTAINING 0.1 W/O COPPER

	Resistivity (microhm-cm)				
	Temperature (C)				
Specimen	100	200	300	400	500
2269P	1550	3850	7500	11,250	13,650
2267P	1550	3950	7950	12,000	13,550
2279P	1550	3600	7750	11,800	13,350
2278P	1550	3950	8250	11,850	12,800
2280P	1600	4150	8250	12,550	15,000
Average	1560	3900	7940	11,890	13,670
Maximum deviation from average (%)	+2.5	-7.7	-5.5	+5.6	+9.7

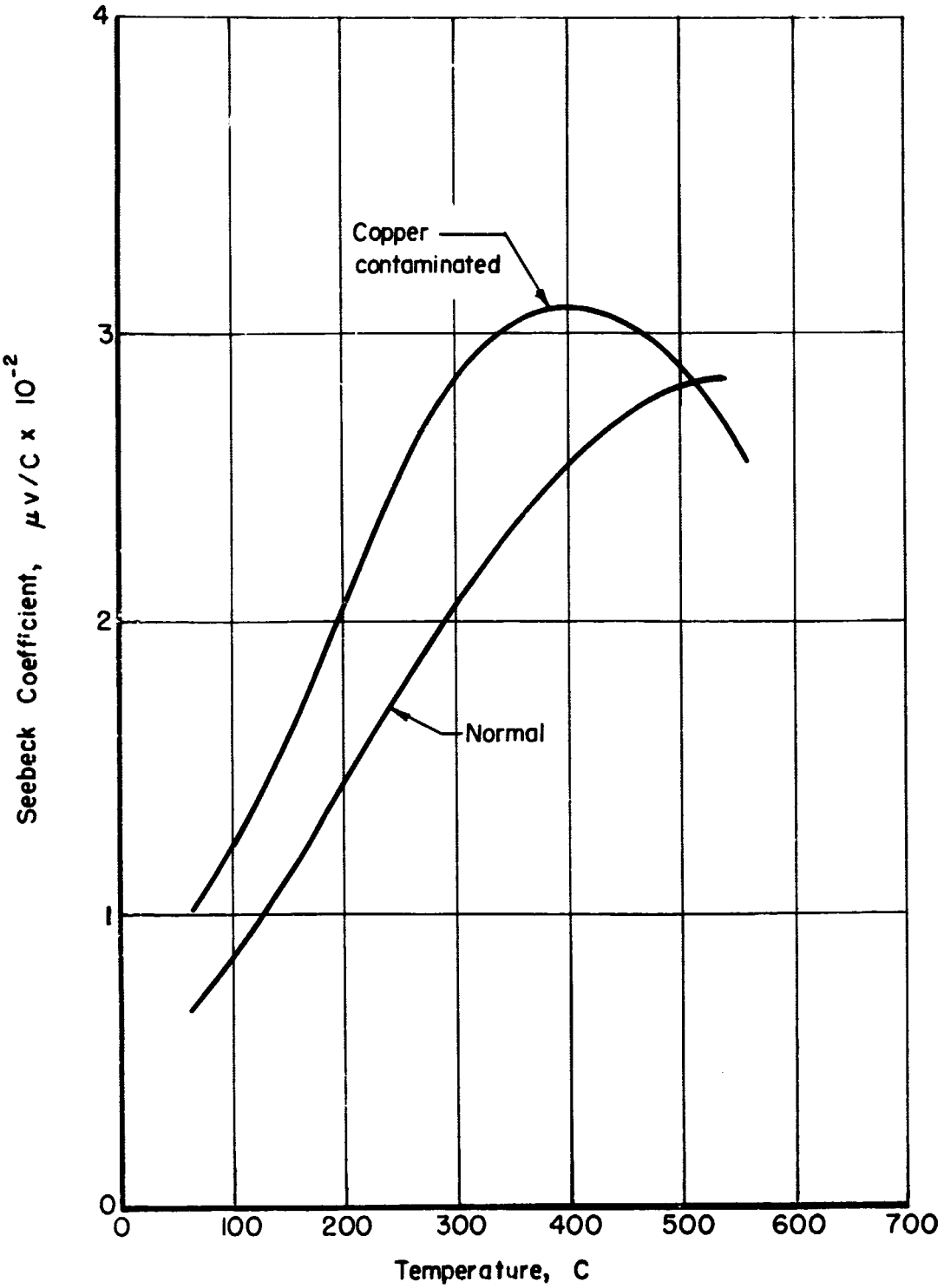

FIGURE 26. SEEBECK COEFFICIENT OF COPPER-CONTAMINATED AND NORMAL 2p-PbTe

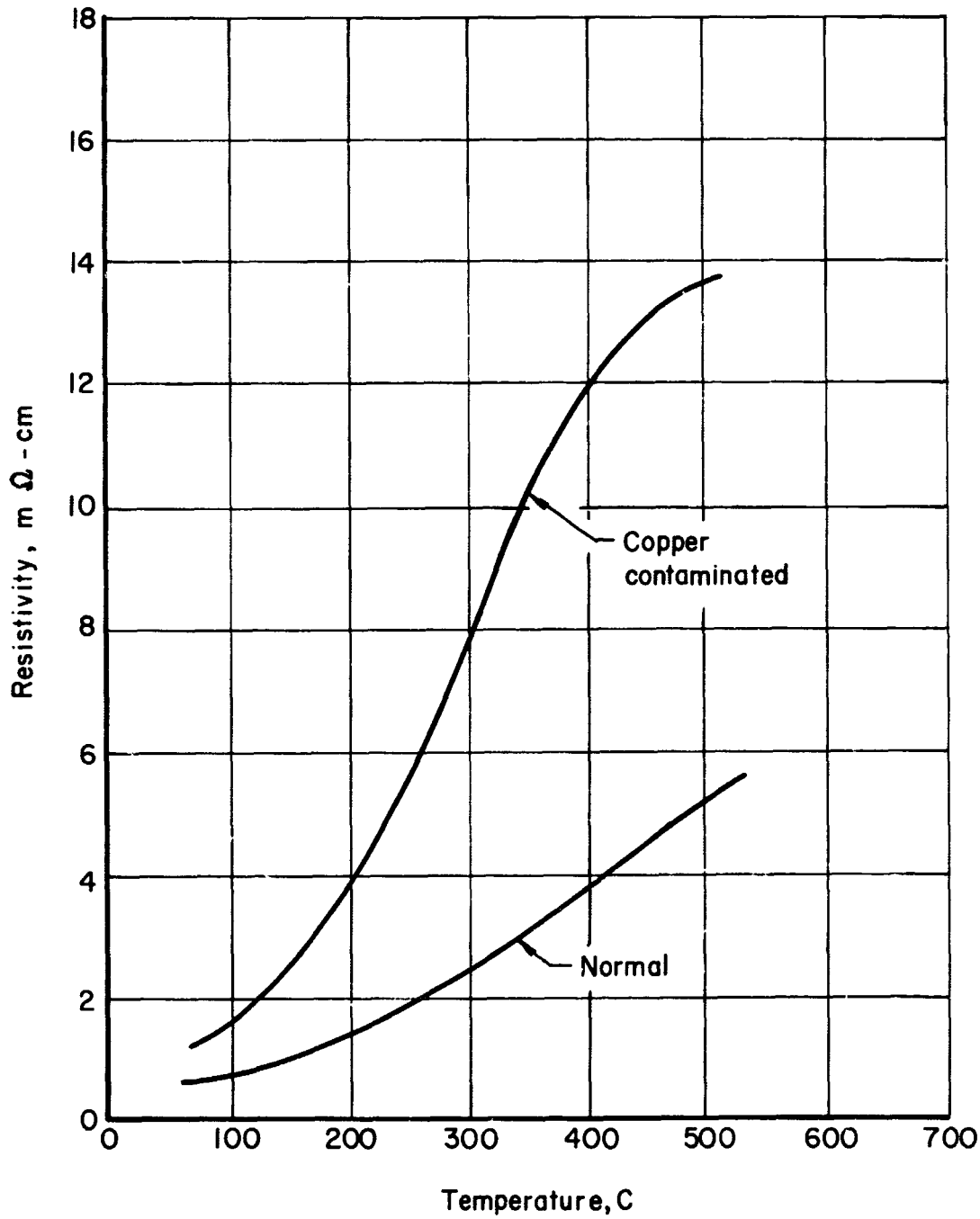

FIGURE 27. ELECTRICAL RESISTIVITY OF COPPER-CONTAMINATED AND NORMAL 2p-PbTe

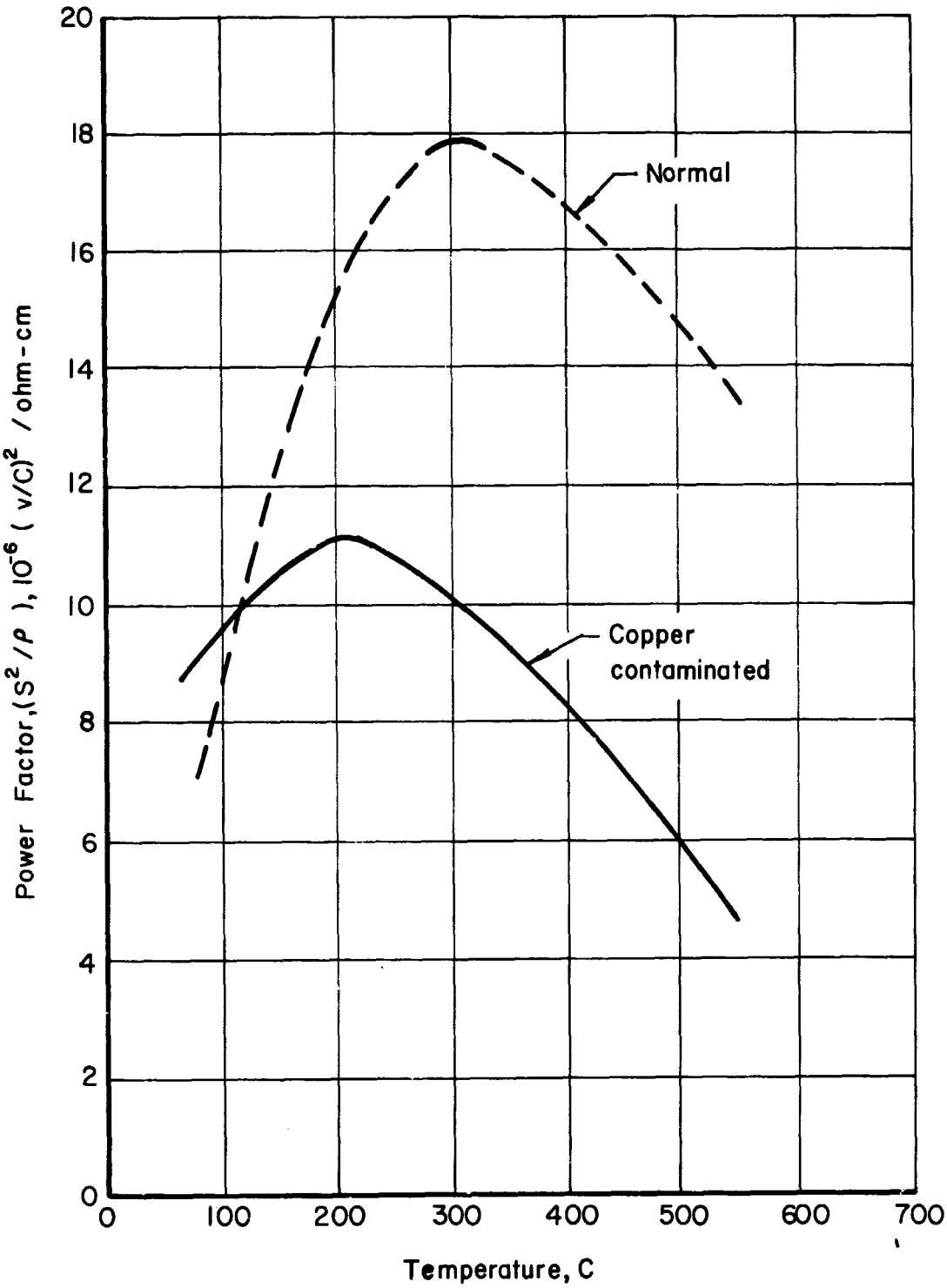

FIGURE 28. POWER FACTOR AS A FUNCTION OF TEMPERATURE FOR 2p-PbTe CONTAMINATED WITH 0.1 W/O COPPER

Thermal-Conductivity Determination

The thermal-conductivity values for the thermoelectric materials in nonstandard condition were determined by the laser diffusivity technique. This apparatus is described in Appendix IX. The specimens on which the thermal-diffusivity values were measured were nominally 0.04 in. thick by 0.30 in. in diameter. These specimens were cut from either an electrical-property-measurement element or one of the remaining elements of the group depending on the condition of the elements at the time of cutting. Particular attention was paid to obtaining specimens of uniform density which were free of cracks.

The diffusivity measurements were made from 200 to 550 C under static inert atmosphere. The thermal conductivity was computed as the product of diffusivity, specific heat, and density. Available data on the specific heat and thermal expansivity (for calculation of change in density with temperature) for the uncontaminated material were used in making these calculations. The change in both of these properties, viz., specific heat and thermal expansivity, resulting from the extremely small additions of the contaminants was considered negligible and was ignored. The densities of the specimens were determined by the water-immersion technique and were checked by geometric determinations. All of the specimens were in the range 85 to 90 percent of theoretical. The limits of accuracy determined for each thermal diffusivity measurement suggest that the calculated thermal conductivity values should be within about ±7 percent of true values.

The calculated values of thermal conductivity for the two 2p-PbTe materials and for the 3p-PbSnTe material are shown in Figures 29 and 30,

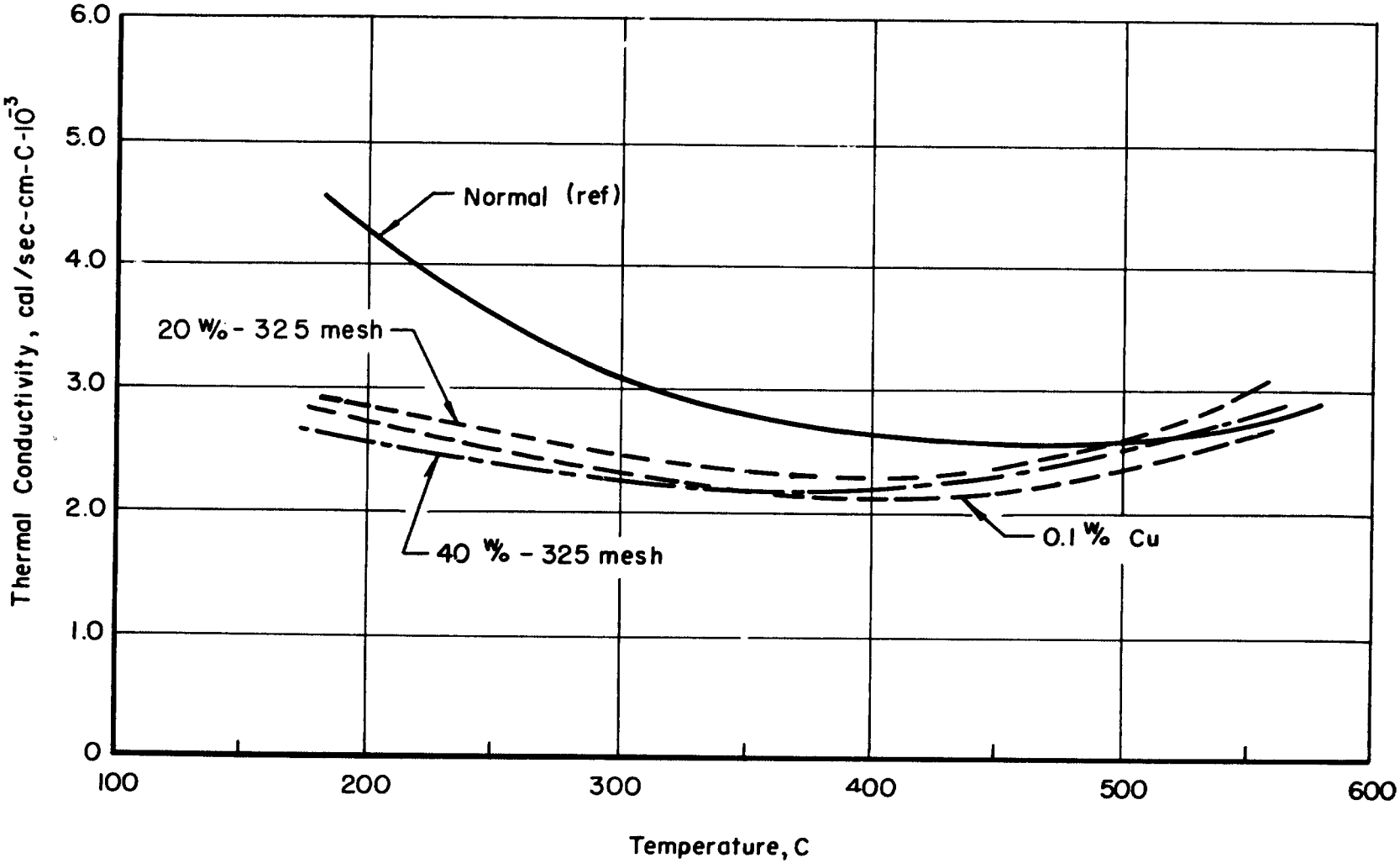

FIGURE 29. THERMAL CONDUCTIVITIES OF 2p-PbTe IN OXYGEN- AND COPPER-CONTAMINATED CONDITIONS

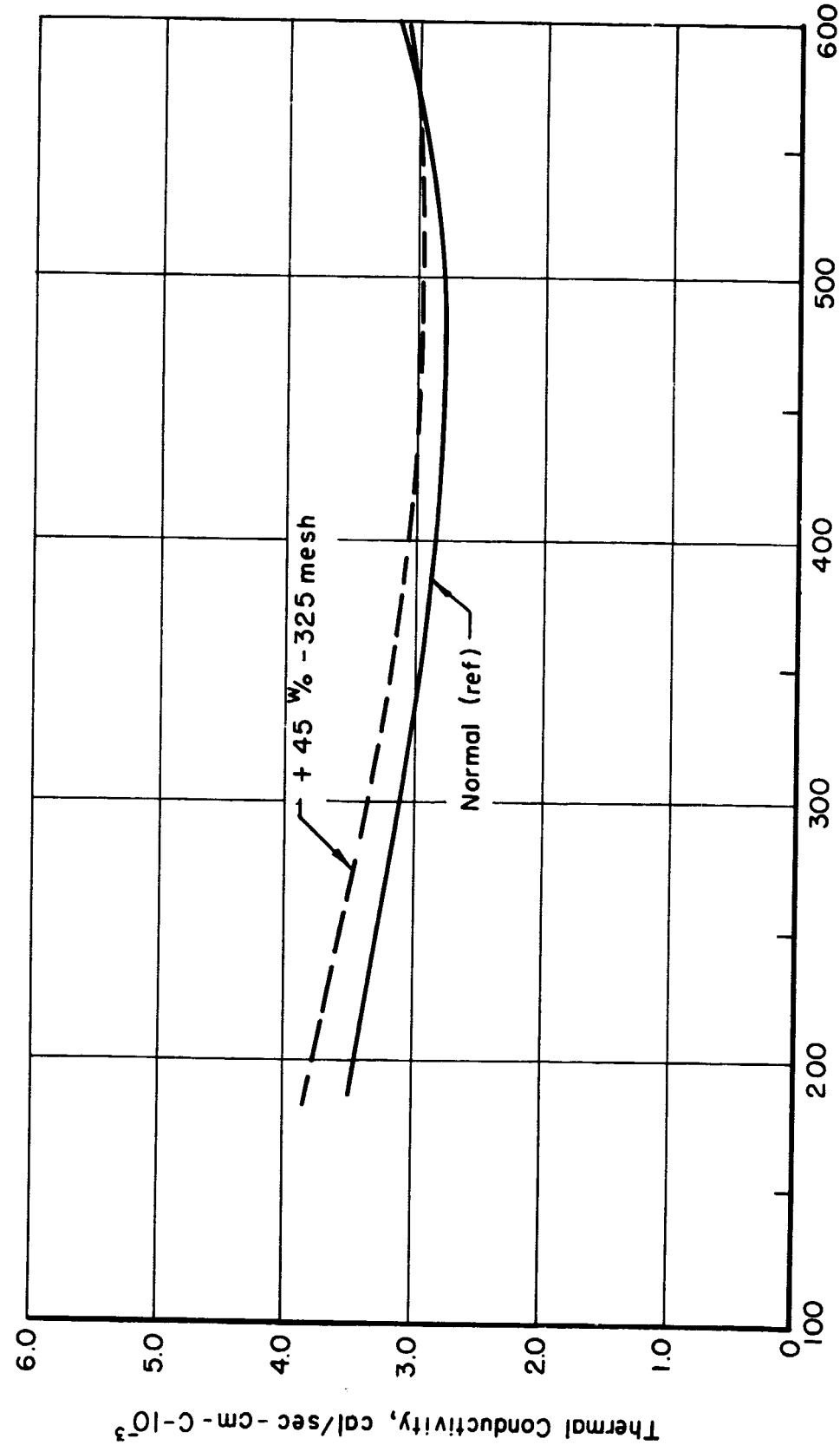

FIGURE 30. THERMAL CONDUCTIVITY OF OXYGEN-CONTAMINATED 3p-PbSnTe

respectively. Data for the normal or uncontaminated counterparts are included for comparison. The following generalizations can be drawn from the experimental results:

(1) The addition of oxygen or copper to 2p-PbTe (see Figure 29) resulted in a significant decrease in the thermal conductivity at the lower temperatures (about 40 percent at 200 C) but virtually no effect at about 500 to 550 C.

(2) The addition of oxygen to the 3p-PbSnTe (see Figure 30) resulted in an increase in the thermal conductivity of about 10 percent over most of the range from 200 to 550 C but virtually no effect above 550 C.

Figure of Merit of 2p-PbTe and 3p-PbSnTe

The figures of merit, Z, for each of the thermoelectric materials in nonstandard condition were calculated according to the relationship:

$$Z = S^2/\rho k \ ,$$

where S is the Seebeck coefficient in microvolts/C, ρ is the electrical resistivity in microhm-cm, and k is the thermal conductivity in watts/cm-C. The calculated values of Z for the 2p-PbTe materials and 3p-PbSnTe are shown in Figures 31 and 32, respectively. The figures of merit for the normal (uncontaminated) materials are included for comparison.

Both of the contaminated 2p-PbTe materials exhibit significant depressions in the values of figures of merit over most of the range from

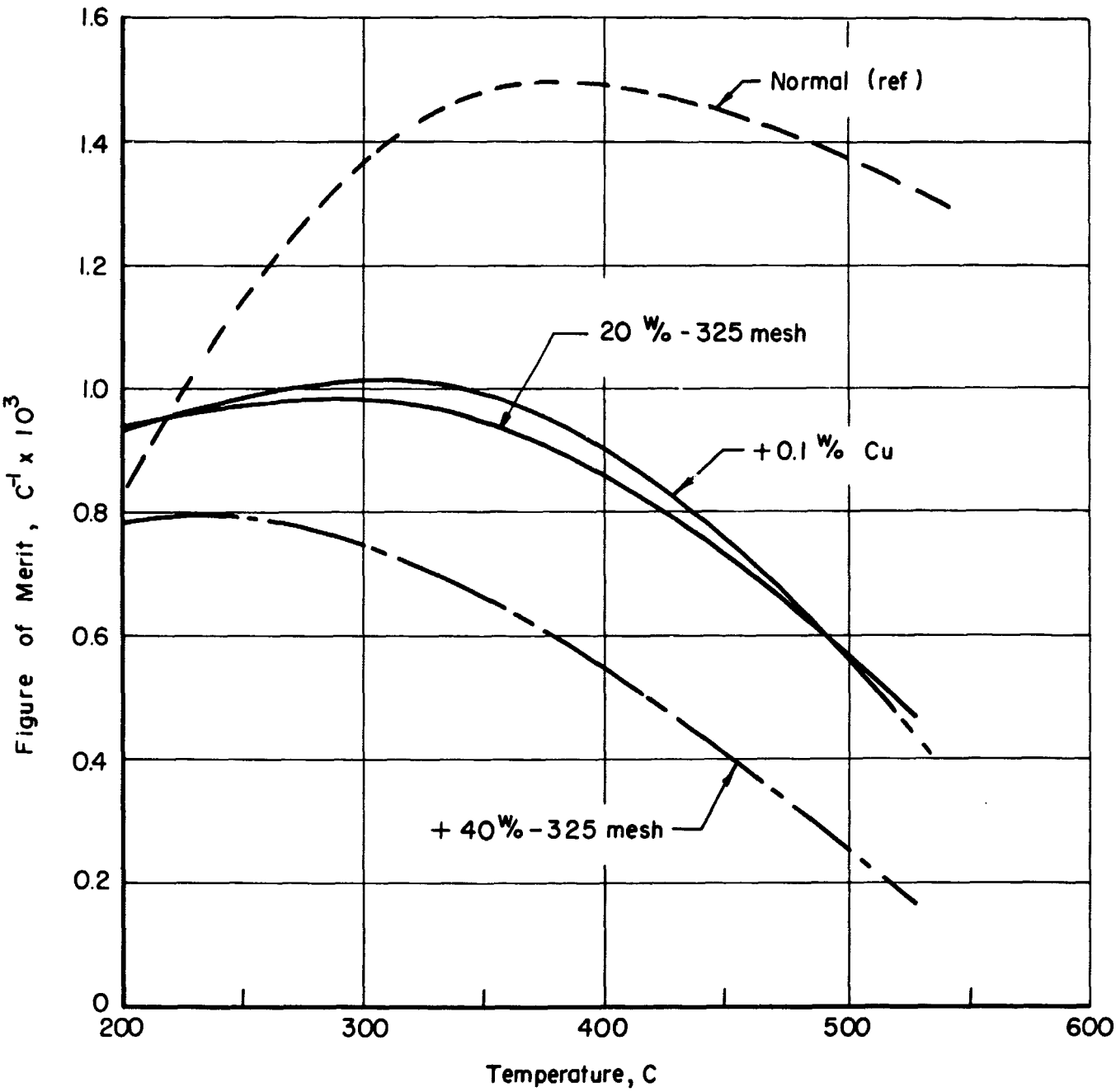

FIGURE 31. FIGURES OF MERIT FOR 2p-PbTe CONTAMINATED WITH OXYGEN OR COPPER

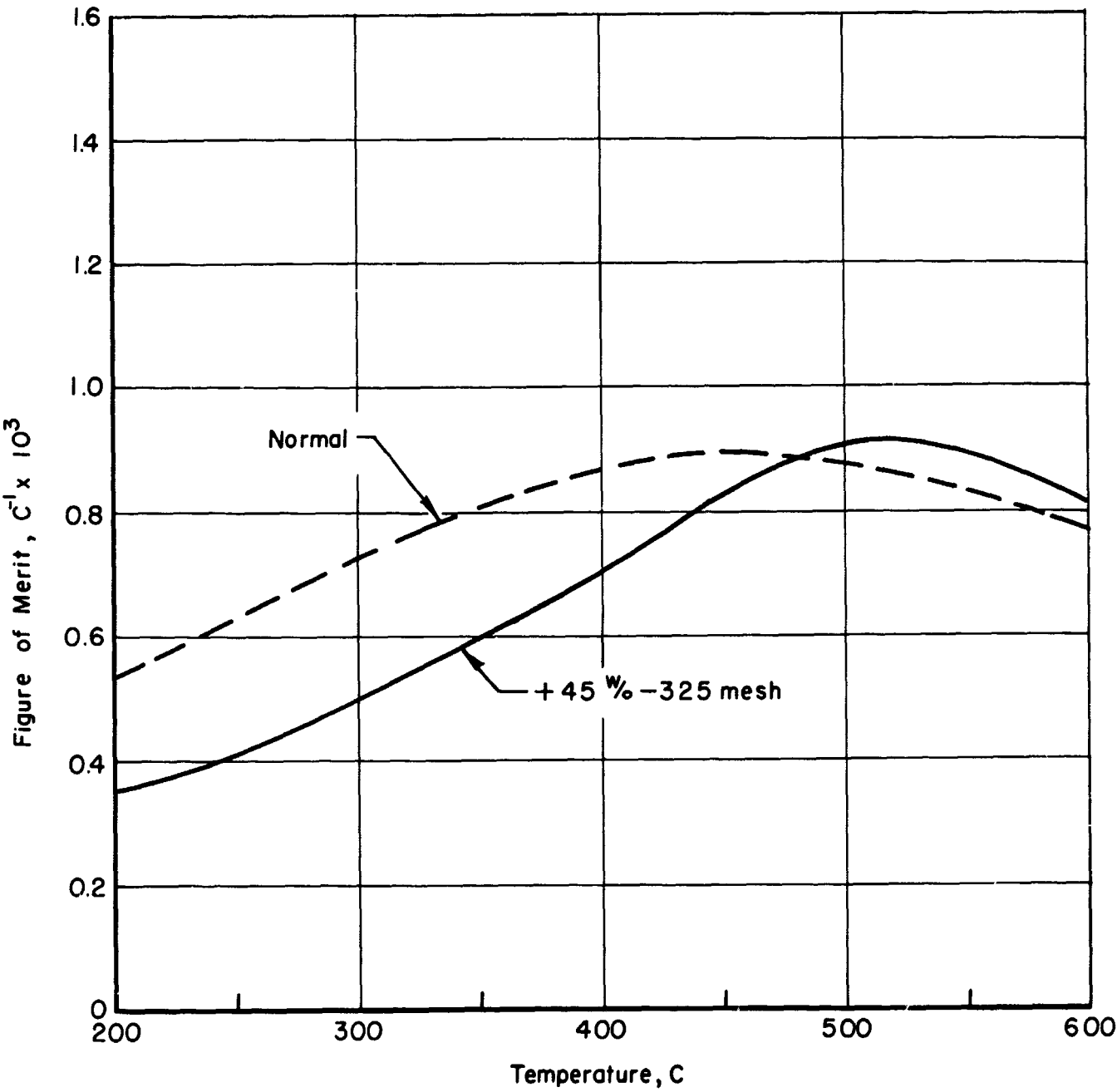

FIGURE 32. FIGURE OF MERIT OF 3p-PbSnTe CONTAMINATED WITH OXYGEN

200 to 550 C. At 200 C, the figures of merit are nearly equal to that of the normal 2p-PbTe. Based on a comparison of the data for 2p-PbTe containing 20 w/o, -325 mesh powder and 0.1 w/o copper, it is apparent that oxygen and copper produced essentially identical effects on both the electrical and thermal properties and, hence, result in nearly identical figure of merits in the range 200 to 550 C. Although the mechanisms of interaction between these contaminants and the 2p-PbTe are not known, some evidence exists which suggests that only one mechanism is operative, e.g., the reduction of the carrier concentration is a result of the depletion of the tellurium dopant. Since both of the contaminants form compounds with tellurium, it is possible that a simple chemical reaction may account for the observed effects.

The oxygen-contaminated 3p-PbSnTe yielded a figure of merit well below that of normal 3p-PbSnTe over the range 200 to 400 C but a slightly higher figure of merit between 450 and 600 C.

TASK IV. FABRICATION AND TESTING OF SiGe-PbTe THERMOELECTRIC COUPLES

Couple Design and Fabrication for Performance Testing

A segmented SiGe-PbTe couple configuration has been designed based on technology developed under a previous NASA-Goddard research program*. This design features a pressure-contacted junction between the PbTe segments and the tungsten shoe at the cold end of the SiGe segments (see Figure 33). The use of a pressure-contacted junction eliminates the problem of differential thermal expansivities encountered in previous SiGe-PbTe segmented couple development* and simplifies the couple fabrication schedule since the SiGe and PbTe segments can be processed separately and assembled in the life-test fixture. A spring-load pressure of 100 psi is maintained during the life test to effect a low resistance at the pressure-contacted junctions. A comparison of the computed conversion efficiencies for single-stage PbTe couples and the SiGe-PbTe segmented couples developed in this program indicates the significant advantages offered by joining SiGe to PbTe (see Figure 34). The segmenting of these two thermoelectric materials involves a mismatch between the thermal flux and current flux, e.g., optimizing the PbTe and SiGe segments for a common current flux results in a mismatch in the thermal flux. This mismatch has a significant effect on the temperature distribution which offsets the gains of segmenting these two materials. However, designing the segmented couple on the basis of matched thermal flux and mismatched current flux yields a significant gain in conversion efficiency as a result of the relative insensitivity of the conversion efficiency of the individual segments to the current flux. The latter approach was the basis for the design of the couples fabricated and tested in this program.

---

* Kortier, W. E., Mueller, J. J., Freas, D. G., and Eggers, P. E., "A Research and Development Program for Segmenting SiGe and PbTe Thermoelectric Materials", NAS5-10185, Final Summary Report dated December 15, 1966.

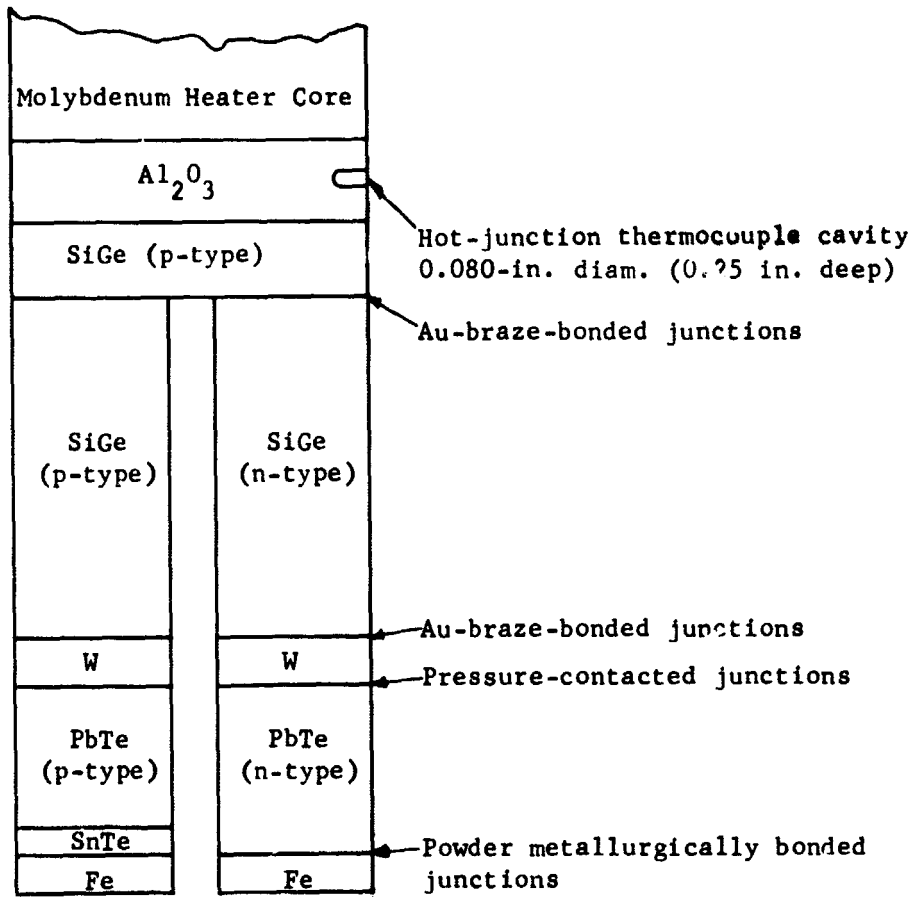

FIGURE 33. SEGMENTED COUPLE FOR PERFORMANCE TESTING

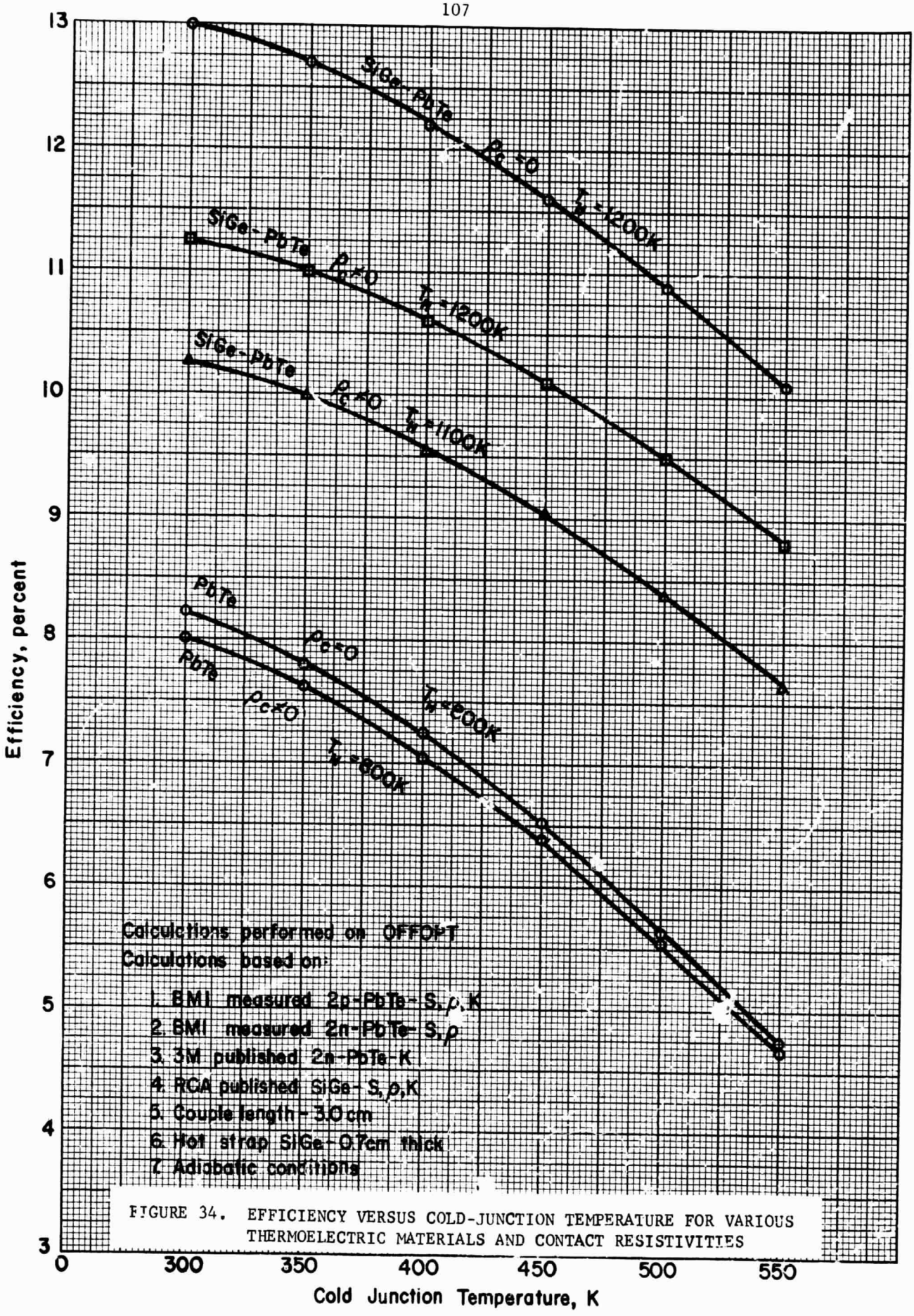

FIGURE 34. EFFICIENCY VERSUS COLD-JUNCTION TEMPERATURE FOR VARIOUS THERMOELECTRIC MATERIALS AND CONTACT RESISTIVITIES

Theoretical Analysis

A theoretical analysis was performed using the OFF-OPT computer program* to identify the dimensions of the SiGe and PbTe segments yielding maximum output power for a fixed couple length. The input data used for the PbTe segments were based on S, ρ, k, and ρ_c measurements performed on green-pressed and sintered material and the input data used for the SiGe segments were based on RCA-published ingot data. The results of the calculations are summarized in Table 14 in terms of (1) operating temperatures, (2) couple dimensions, and (3) output power and efficiency.

TABLE 14. COMPUTED DIMENSIONS AND PERFORMANCE PARAMETERS FOR SiGe-PbTe SEGMENTED COUPLES

T_c	= 300 K (80 F)
T_{INT}	= 800 K (980 F)
T_h	= 1200 K (1700 F)
A_P	= 0.578 cm^2 (0.0896 $in.^2$)
A_N	= 0.657 cm^2 (0.1020 $in.^2$)
L_N (SiGe)	= 2.021 cm (0.796 in.)
L_N (PbTe)	= 0.870 cm (0.343 in.)
L_P (SiGe)	= 2.044 cm (0.805 in.)
L_P (PbTe)	= 0.804 cm (0.317 in.)
Thickness (hot strap)	= 0.635 cm (0.250 in.)
I	= 7.25 amp (maximum power output)
P	= 1.300 watts(e)
$\eta_{T/E}$	= 11.20 percent

* Computer program, OFF-OPT, was developed under USAEC Thermoelectric Contract W-7405-eng-92, "Development of Segmented Thermoelectric Modules Fabricated by Hot Isostatic Pressing".

Fabrication of Segmented Couples

A total of eight segmented couples containing SiGe and PbTe segments were fabricated for performance testing according to the specifications presented in Table 14. The SiGe segments were bonded into a "U-shaped" couple with a p-type SiGe hot strap and tungsten shoes (see Figure 33). The PbTe segments were prepared as separate units for operation in pressure contact to the tungsten shoes of the SiGe couple.

The SiGe components and tungsten shoes were bonded into a couple by means of gold as a brazing agent. The brazing was accomplished using technology developed in earlier segmenting studies*. The gold was incorporated in the junctions in the form of foil. The assembled components were held in a differential thermal expansion bonding fixture and were brazed in vacuum for 1/2 hr at 1066 C (1950 F).

The PbTe segments were made by pressing PbTe powder and the cold-junction shoe into a composite body followed by sintering in hydrogen at 649 C (1200 F) for 1 hr under 100 psi spring loading. The n-type element was made with iron shoes bonded directly to the PbTe. The p-type element was made with a 1/32-in.-thick layer of tin telluride (SnTe) between the PbTe and iron shoe. The SnTe has been found to yield a stronger bonded element with lower effective contact resistivity than obtainable with iron bonded directly to the p-PbTe.

---

* Kortier, W. E., Mueller, J. J., Freas, D. G., and Eggers, P. E., "A Research and Development Program for Segmenting SiGe and PbTe Thermoelectric Materials", NAS5-11185, Final Summary Report dated December 15, 1966.

Performance Testing

Development of Test Apparatus

The life testing of SiGe-PbTe segmented couples in this program is being performed in test fixtures developed under a previous NASA-Goddard contract*. The heater design (shown in Figure 35) is based on a low-current (<10 amp), nonrefractory resistance heating element. This choice permits the use of low-amperage voltage regulators and electrical wiring. The heater consists of Kanthal** heater wire wound on a high-purity alumina tube (4 x 2-in. diameter) with a molybdenum heater core (5 x 1.5-in. diameter). This heater unit is insulated by 2.5 in. of Fiberfrax insulation and is designed to operate for extended periods (>10,000 hr) at 1275 C (1550 K) in argon.

The life-test apparatus used to measure couple power and open-circuit voltage as a function of time is shown in Figures 35 and 36. The life-test fixture features a spring-loaded cold-junction assembly to permit application of couple-loading pressures over the range 0 to 100 psi.

Test Procedure

The couple life test includes the measurement of cold-, intermediate-, and hot-junction temperatures, couple voltage (open and closed circuit), and the operating current under load. The couple output power is calculated from

---

* Kortier, W. E., Mueller, J. J., Freas, D. G., and Eggers, P. E., "A Research and Development Program for Segmenting SiGe and PbTe Thermoelectric Materials", NAS5-10185, Final Summary Report dated December 15, 1966, page 49.

** Kanthal is an Fe-Cr-Al alloy supplied by the Kanthal Corporation, Bethel, Connecticut.

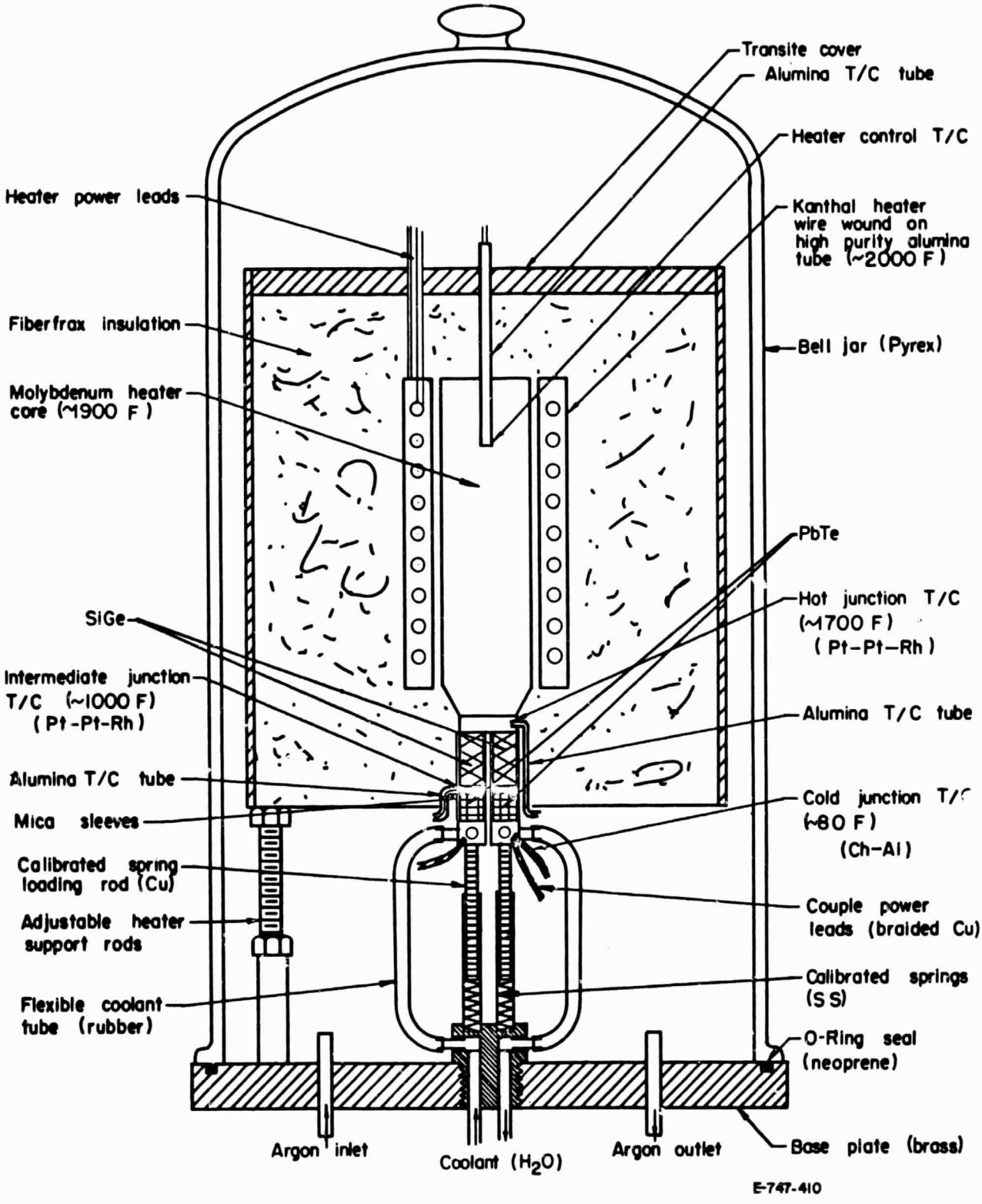

FIGURE 35. DIAGRAM OF LIFE-TESTING APPARATUS

35057

FIGURE 36. PHOTOGRAPH OF LIFE-TESTING APPARATUS

the measured couple voltage and current. Observed changes in open-circuit voltage indicate changes in thermoelectric materials properties, while changes in couple power indicate changes of the junction resistance and/or thermoelectric materials properties.

Each segmented couple is mounted onto copper cold sinks with low-melting-point In-Sn solder (MP = 117 C). Thermocouples are affixed to the cold, intermediate, and hot junction of the couple. The couple is installed in the life-test apparatus and a pressure of 100 psi is applied by spring loading. After evacuation (25 microns Hg), the bell-jar test apparatus is backfilled with argon (or hydrogen) at atmospheric pressure. The couple is brought to operating temperature at a heatup rate not exceeding 5 C/min, which has been found to minimize thermal-shock effects. After a 50-100-hr stabilization period at temperature, the external load resistance is varied to obtain the maximum power output from the couple. This load setting establishes initial conditions for the couple and is fixed for the duration of the test. The life test is terminated when the power degradation exceeds 10 percent. The couple is then removed from the test apparatus and subjected to posttest examination.

Test Results

The life-test results of eight SiGe-PbTe segmented couples have identified three principal problems, their effect, and their solution and are briefly summarized in Table 15. Early test results indicated the need for a more reliable hot-junction temperature measurement technique. Therefore, a study was performed (following the failure of the alumina vapor-sprayed W-vs-W-Rh thermocouple used in Couple PG-68-1) to ascertain

TABLE 15. SUMMARY OF SiGe-PbTe SEGMENTED COUPLE PROBLEM AREAS

Couple No.	Defined Problem	Resultant Effect(s)	Design Alteration
PG-68-1	Brittleness of Al_2O_3 vapor-sprayed coating on hot-junction thermocouple	Loss of protective coating of Al_2O_3 with subsequent reaction between thermocouple and SiGe (p-type) hot strap	Replace Al_2O_3 vapor-sprayed coating with high-purity Al_2O_3 thermocouple holder positioned above the SiGe hot strap
PG-68-2	Parasitic heat loss from PbTe section of couple due to insufficient thermal insulation	Intermediate junction (SiGe-W-PbTe) operates significantly below the designed temperature resulting in high resistance at the pressure-contacted junction	Increase the amount of thermal insulation used in the cold region of couple and increase the length of the PbTe segments
PG-68-3 through PG-68-8	Oxide formation on W shoe at intermediate junction	Increase of contact resistivity of intermediate junction with attendant decrease output power(e)	Minimize background level of O_2 and H_2O vapor in test fixture or hermetically seal thermoelectric couple

the chemical compatibility of high-purity alumina (McDanel AP-35) with the p-type SiGe hot strap at 1050 C in argon. This temperature was selected since during life testing, an operating temperature of 1050 C at the surface of the SiGe hot strap corresponds to a temperature of ~927 C at the hot-strap - SiGe element interface, i.e., the "hot junction" of the segmented couple. No reaction was detected when p-type SiGe was pressure contacted to the high-purity alumina sample and maintained in argon at 1050 C for 60 hr. Based on this result, high-purity alumina straps were positioned above the p-type SiGe hot strap (as shown in Figure 33) in order to (1) provide a nonreactive environment for the hot-junction thermocouple attachment and (2) prevent the reaction between the p-type SiGe hot strap and molybdenum heater core. However, the introduction of an insulator, i.e., alumina, as the hot-junction thermocouple holder (which was originally designed to function as the voltage tap) prevents the measurement of individual n-leg and p-leg performance since the center tap must be in electrical contact with the hot strap of the couple. Consequently, the modified design will permit the measurement of (1) hot-junction temperature, (2) cold-junction temperature, (3) couple open-circuit voltage, (4) couple closed-circuit voltage, (5) operating current, and (6) couple output power. The test results and posttest examination of SiGe-PbTe segmented couples indicated that no visible reaction had occurred between the SiGe hot strap and the alumina thermocouple holder which had operated at ~1050 C for periods up to 3000 hr.

The remaining seven couples (PG-68-2 through -8) all exhibited similar trends in performance, viz., (1) the open-circuit voltage was stable with respect to time, (2) the couple output power(e) was relatively stable with respect to time, (3) the output power was ~10 percent lower than calculated, and (4) the surface of the tungsten intermediate shoe adjacent to the PbTe became heavily oxidized after 500 to 1000 hr on test. The reduction in output power is attributed to (1) an improper temperature distribution on the couple resulting from parasitic heat losses from the lower region of the couple (see Figure 35) and (2) high-resistance oxide layers present on the surface of the tungsten shoes adjacent to the PbTe segments. The control of the formation of oxide layers on the surface of the tungsten shoe is complicated by the presence of Fiberfrax thermal insulation which releases significant amounts of water vapor when operated at elevated temperatures. The life-test data for six of these couples (Couples PG-68-1 and -2 not shown) are reported in the form of normalized output power plotted as a function of time and are accompanied by a brief description of the test conditions (see Figures 37, 38, and 39). The significant rate of decrease of output power at certain periods during their lifetime is attributed to an increase in the contact resistivity of the intermediate PbTe-W junctions (n-leg and/or p-leg). In most cases, the couples experiencing significant rates of degradation were rejuvenated by (1) introducing hydrogen into the argon atmosphere (to form a 10 hydrogen - 90 argon mixture) for 50 to 100 hr in order to reduce any oxide(s) formed at the junction and (2) increasing the cold-junction temperature from 27 C to 125 C for 50 to 100 hr allowing the intermediate temperature to increase and, hence, effect a low-resistance pressure-contacted junction.

DESCRIPTION OF EXPERIMENT

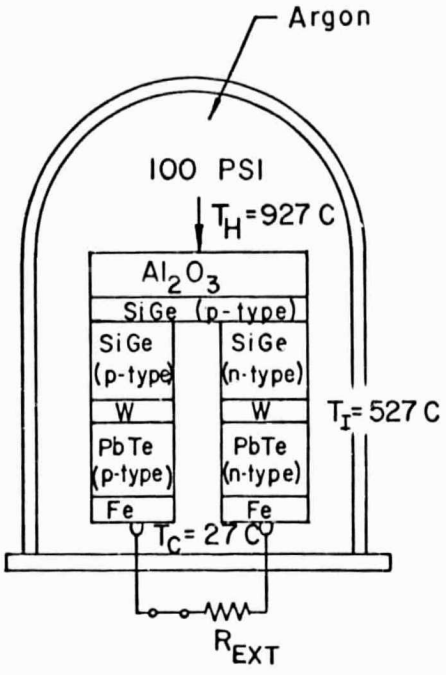

NORMALIZED OUTPUT POWER VS. TIME

Couple No. PG-68-3
P (calculated) 1.30 watts (e)
P_o (measured) 1.23 watts (e)

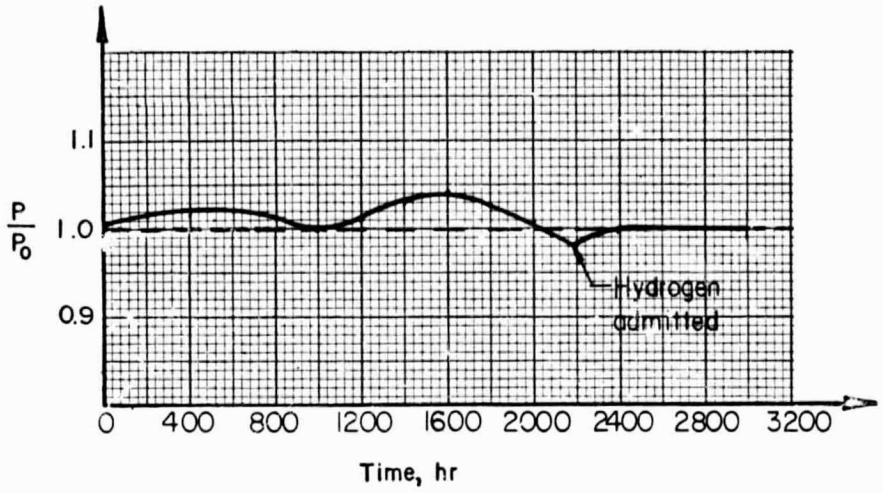

DESCRIPTION OF EXPERIMENT

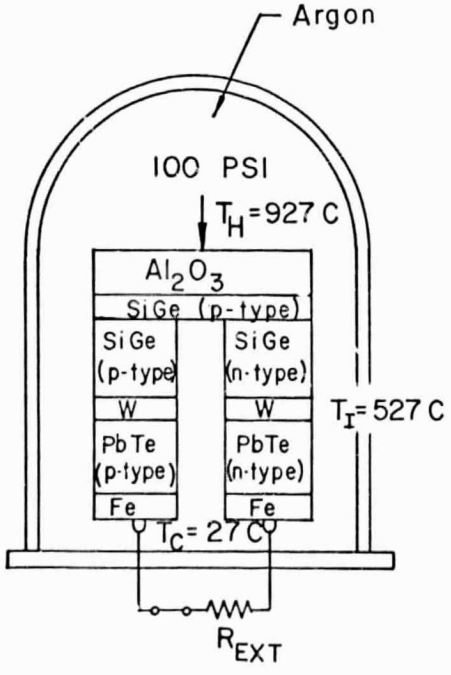

NORMALIZED OUTPUT POWER VS. TIME

Couple No. PG-68-4
P (calculated) 1.30 watts (e)
P_o (measured) 1.05 watts (e)

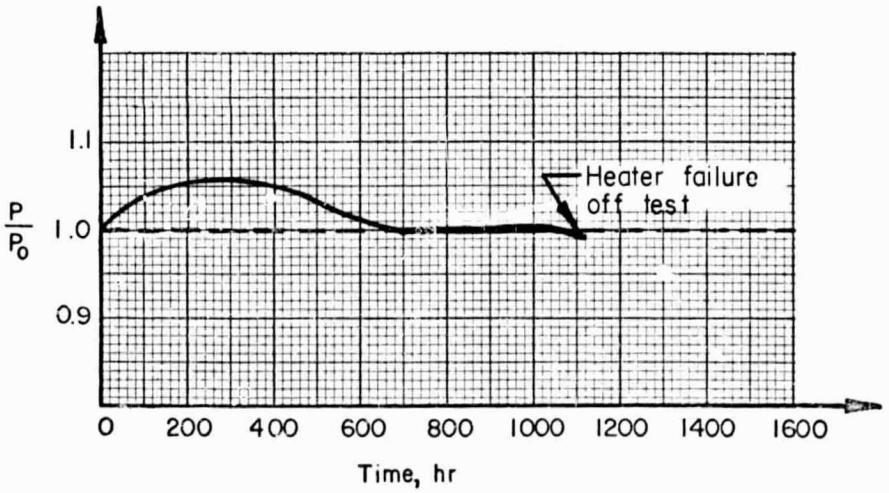

FIGURE 37. NORMALIZED OUTPUT POWER VERSUS TIME FOR SiGe-PbTe SEGMENTED COUPLE (PG-68-3 AND -4)

DESCRIPTION OF EXPERIMENT

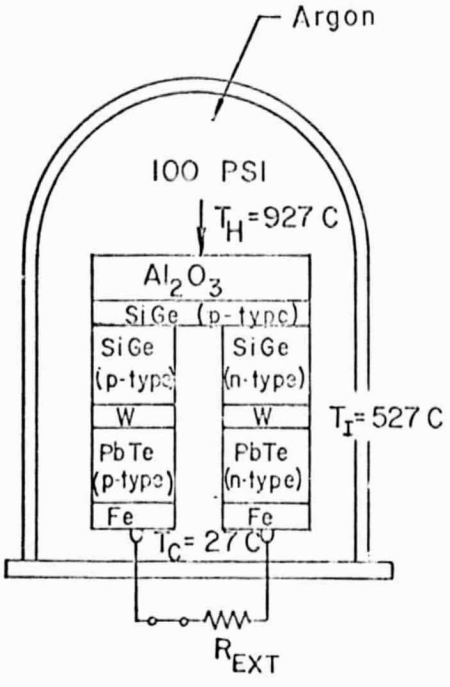

NORMALIZED OUTPUT POWER VS. TIME

Couple No. PG-68-5
P (calculated) 1.30 watts (e)
P_0 (measured) 1.13 watts (e)

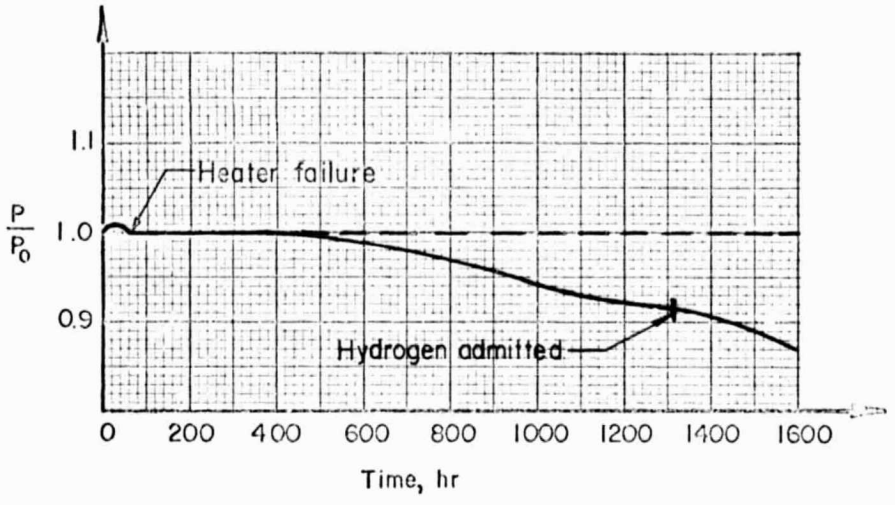

DESCRIPTION OF EXPERIMENT

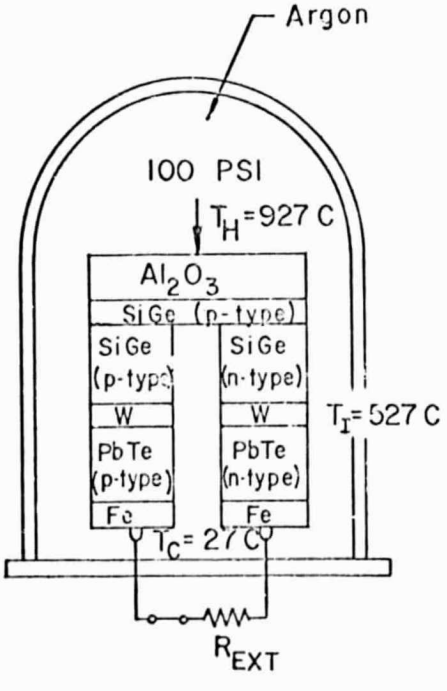

NORMALIZED OUTPUT POWER VS. TIME

Couple No. PG-68-6
P (calculated) 1.30 watts (e)
P_0 (measured) 1.06 watts (e)

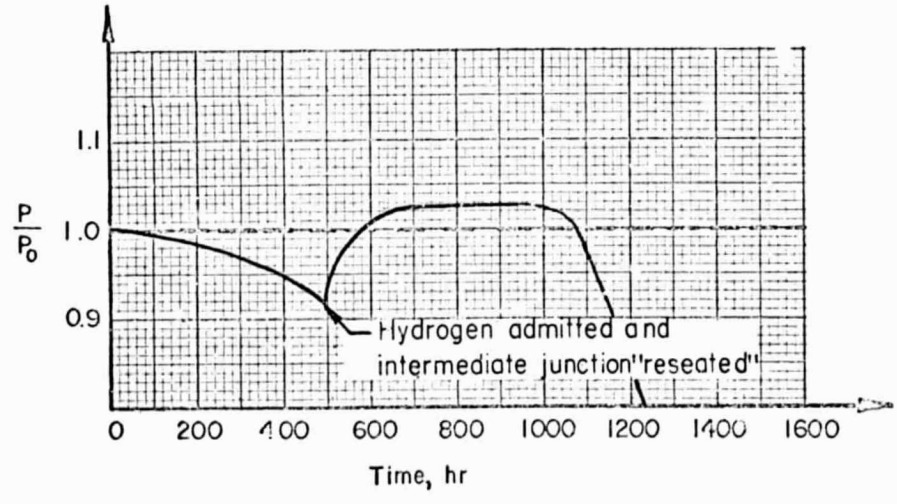

FIGURE 38. NORMALIZED OUTPUT POWER VERSUS TIME FOR SiGe-PbTe SEGMENTED COUPLE (PG-68-5 AND -6)

DESCRIPTION OF EXPERIMENT

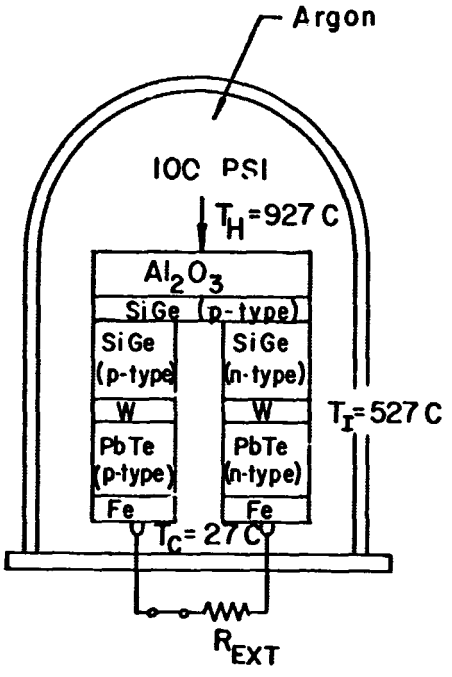

NORMALIZED OUTPUT POWER VS. TIME

Couple No. PG-68-7
P (calculated) 1.30 watts (e)
P_0 (measured) 1.18 watts (e)

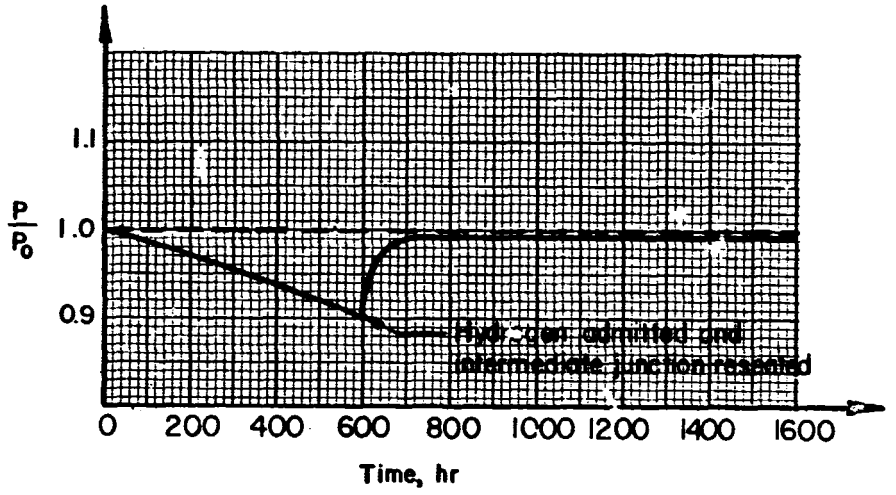

DESCRIPTION OF EXPERIMENT

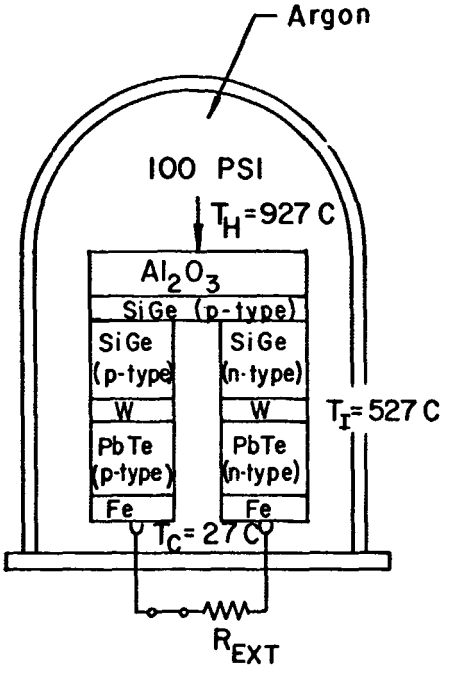

NORMALIZED OUTPUT POWER VS. TIME

Couple No. PG-68-8
P (calculated) 1.30 watts (e)
P_0 (measured) 1.16 watts (e)

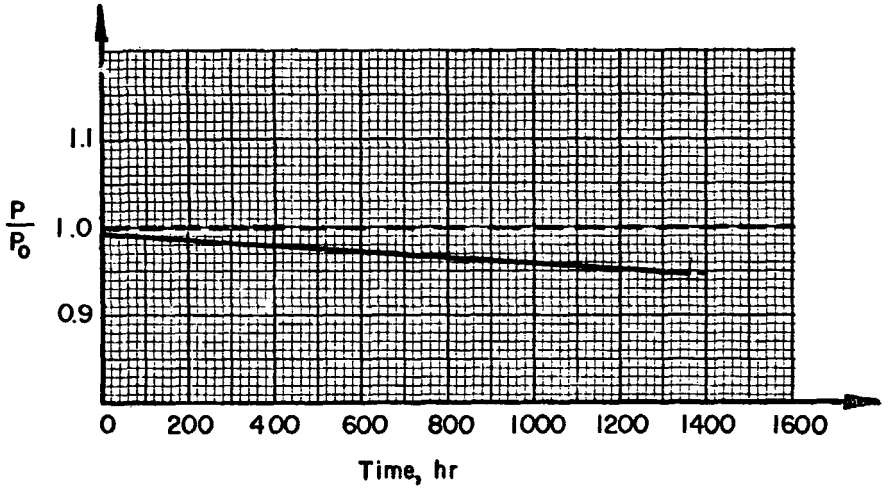

FIGURE 39. NORMALIZED OUTPUT POWER VERSUS TIME FOR SiGe-PbTe SEGMENTED COUPLE (PG-68-7 AND -8)

Posttest Examination Results

A visual posttest examination of the SiGe-PbTe segmented couples has revealed that (1) little or no sublimation of PbTe has occurred for periods up to 3000 hr, (2) thermal cycling of couples from operating temperature down to room temperature has no apparent effect on the junctions, (3) an oxide layer was present on the surface of the tungsten adjacent to the n-type and p-type PbTe, and (4) no visible reaction had occurred between the alumina thermocouple holder and the p-type SiGe hot strap.

CONCLUSIONS AND RECOMMENDATIONS

Under Task I, Development of Uniform Procedures for Tests and Measurements of Thermoelectric Materials and Components, a study of the Seebeck coefficient and electrical resistivity revealed that high-precision and high-accuracy measurements can be performed within the framework of conventional techniques. The experimental evaluation of candidate calibration standards for these measurements is considered a significant step towards the establishment of laboratory reference(s) which would provide for the direct comparison of experimental results obtained by various research groups.

Based on an analysis of the results of (1) life-testing studies (Task I) and (2) a sensitivity analysis involving radioisotope thermoelectric generator (RTG) performance under conditions simulating typical modes of degradation (Task II), it can be concluded that life testing performed under conditions of constant or controlled thermal input power (in contrast to conventional techniques involving constant hot- and cold-junction temperatures) will provide data which are directly applicable to the prediction of RTG performance.

The results of the theoretical and experimental development of test and measurement procedures satisfy the overall objective of Task I in that they provide a guideline for the precise, accurate measurement of parameters associated with thermoelectric materials and components. In addition, it is also significant that the measurement techniques have been developed in sufficient detail to allow NASA to (1) establish their own thermoelectric test and measurement capability and (2) specify

established test and measurement procedures in the course of thermoelectric research performed in their contractors' laboratories.

It is recommended that the life-testing and efficiency-measurement techniques studied in this task be undertaken experimentally including the development of (1) a method for the precise measurement of thermal input power (life test), (2) a method for the accurate measurement of thermal input power (efficiency measurement), and (3) a calibration standard (for thermal input power measurement) which would serve as a laboratory reference permitting the direct comparison of experimental results obtained by various research groups.

In Task II, RTG Analysis and Design, the gross simplification of the input/output formats for the existing RTG computer program (GESPGN) will offer the user a significant decrease in the time required and probability of error associated with the input data compilation and output data reduction. Also, an analysis of the results of three-dimensional heat-transfer analyses confirmed the validity of the mathematical model used in the RTG computer program and, hence, improved the "confidence limits" associated with the computations performed in the GESPGN program. Any additional analysis of the mathematical model or further simplification of the input/output formats would yield only marginal gains and are, therefore, not recommended.

The results of the study performed under Task III, Thermoelectric Materials Studies, are significant in that they have provided heretofore unavailable information regarding the effects of contaminants on the thermal properties of the popularly used 2p-PbTe and 3p-PbSnTe materials. In addition, the interrelationships of the electrical and thermal properties have

provided insight into the effects of contaminants on the operating characteristics of thermoelectric components including their power and efficiency. The results are especially relevant to the diagnosis of failure modes since the contaminants used in this study are frequently present in the construction of thermoelectric devices. It is, therefore, recommended that these studies be continued and that the results be used in conjunction with specialized diagnostic techniques, e.g., Seebeck coefficient traverse techniques, in order to (1) establish systematic procedures for the identification of the most probable source(s) of degradation based on thermopile performance and limited posttest examination and (2) advance the understanding of degradation phenomena associated with thermoelectric materials.

Under Task IV, Fabrication and Testing of SiGe-PbTe Thermoelectric Couples, the feasibility of pressure-contacted junctions between the PbTe segments and the tungsten shoe at the cold end of SiGe segments has been successfully demonstrated. The use of a pressure-contacted junction in the transition from SiGe to PbTe has eliminated the problem of differential thermal expansion encountered in previous SiGe-PbTe segmented couple development and has simplified the couple fabrication schedule since the SiGe and PbTe segments can be processed separately and assembled in the life-test fixture. However, an analysis of the life-test results has revealed that the pressure-contacted intermediate junction is highly sensitive to oxygen and water vapor since the formation of an oxide layer on the tungsten adjacent to the PbTe will result in a significant increase in the junction resistance. It is, therefore, recommended that, in order to realize the advantages of this couple configuration, long-term testing

be performed in hermetically sealed containers or in ultraclean test fixtures. The use of hermetically sealed containers is preferred since the problems associated with the control of environmental contamination of the test fixture, particularly oxygen and water vapor, are eliminated.

BIBLIOGRAPHY

1. Cusack, N. and Kendall, P., The Absolute Scale of Thermoelectric Power at High Temperature, Proceedings of the Physical Society of London, 72, page 898 (1958).

2. Christian, J. W., Jan, J. P., Pearson, W. B., and Templeton, I. M., Thermoelectricity at Low Temperatures, Proceedings of the Royal Society A, 245, pages 213-221 (1958).

3. Norén, Björn and Beckman, Clof, Measurement of Thermoelectric Power and Thermal Conductivity According to the Absolute Method, Arkiv För Fysik, 25, pages 567-575 (1964).

4. Eisner, R., Apparatus for Accurate Measurement of Thermoelectric Power, Rev. Sci. Instr., 31, page 462 (1960).

5. Berglund, C. N. and Beairstro, R. C., An Automatic Technique for Accurate Measurements of Seebeck Coefficient, Rev. Sci. Instr., 38, pages 66-68 (1967).

6. Shelykh, A. I. and Chukanov, V. Z., Methods of Measuring Thermo-Emf's and Description of Apparatus for Measuring the Integral Thermoelectric Power of Semiconductors, Proceedings of the First and Second Conferences on Thermoelectricity, Academy of Sciences Press, page 34 (1964).

7. Agayev, Ya and Mikhaylov, A. R., Thermoelectric Parameter Measurement Technique, Geliotekhnika, 6, Tashkent, pages 41-46 (1966).

8. Ioffe, A. F., Physics of Semiconductors, Academic Press, Inc., New York (1957).

9. Heikes, R. R. and Ure, R. W., Thermoelectricity: Science and Engineering, Interscience Publishers, New York (1961).

10. Frankl, D. R., Electrical Properties of Semiconductor Surfaces, Pergamon Press, New York (1967).

11. Harmon, T. C. and Honig, J. M., Thermoelectric and Thermomagnetic Effects and Applications, McGraw-Hill, Inc., New York (1967).

12. Russell, C. R., Elements of Energy Conversion, Pergamon Press, London (1967).

13. Hannay, N. B., Semiconductors, Reinhold Publishing Corporation, New York, page 542 (1960).

14. Ioffe, A. F., Physics of Semiconductors, Academic Press, Inc., New York (1960).

15. Heikes, R. R. and Ure, R. W., Thermoelectricity: Science and Engineering, Interscience Publishers, New York (1961).

16. Ehrenberg, W., Electric Conduction in Semiconductors and Metals, Clarendon Press, Oxford (1958).

17. Antonov, V. B. and Nani, R. Kh., Method for the Rapid Determination of the Temperature Dependence of the Electrical Conductivity of Semiconductors, Proceedings of the First and Second Conferences on Thermoelectricity, Academy of Sciences Press, page 23 (1964).

18. Winslow, J. W., et al., A High Precision System for Measuring Seebeck Coefficient, Electrical Resistivity, and Hall Coefficient in Inhomogeneous Thermoelectric Materials, U.S. Naval Radiological Defense Laboratory, Report No. USNRDL-TR-850 (1965).

19. Egli, P. H., Thermoelectricity, John Wiley and Sons, Inc., New York (1960).

20. Harmon, T. C. and Honig, J. M., Thermoelectric and Thermomagnetic Effects and Applications, McGraw-Hill, Inc., New York (1967).

21. Tentative Method of Test for Resistivity of Semiconductor Materials, 1967 Book of ASTM Standards, ASTM Designations F43-67T and F46-64T.

22. Mengali, O. J. and Seiler, M. R., Contact Resistance Studies on Thermoelectric Materials, Advanced Energy Conversion, Vol 2, pp 59-68 (1962).

23. Jain, G. C. and Berry, W. B., Contact Resistivity Temperature Dependence of Iron-Plated Lead Telluride, Advanced Energy Conversion, Vol 4, pp 159-168 (1964).

24. Goodman, A. M., Metal-Semiconductor Barrier Height Measurement by the Differential Capacitance Method Without an Ohmic Reference Contact--One Carrier System, Journal of Applied Physics, Vol 36, No. 4, pp 1411-1414 (April, 1965).

25. Nichols, K. G. and Vernon, E. V., Transistor Physics, Chapman and Hall Ltd., London, pp 227-235 (1965).

26. Kramer, G., Eggers, P. E., Mueller, J. J., and Shilliday, T. S., Bonding Evaluation Study of HPD Thermoelectric Program Optimum-Length Investigation, Technical Report, Contract No. DA-44-009-AMC-1824(X), prepared by Battelle Memorial Institute (June-November, 1966).

APPENDIX I

STATISTICAL ANALYSIS OF SEEBECK COEFFICIENT DATA

L E A S T - S Q U A R E S P O L Y N O M I A L S

NUMBER OF POINTS = 88
MEAN VALUE OF X = 596.344
MEAN VALUE OF Y = 231.797
STD ERROR OF Y = 55.2213

NOTE: CODE FOR 'WHAT NEXT?' IS:

0 = STOP PROGRAM
1 = COEFFICIENTS ONLY
2 = ENTIRE SUMMARY
3 = FIT NEXT HIGHER DEGREE

POLYFIT OF DEGREE 1 INDEX OF DETERM = .982654 WHAT NEXT? 3

POLYFIT OF DEGREE 2 INDEX OF DETERM = .99617 WHAT NEXT? 3

POLYFIT OF DEGREE 3 INDEX OF DETERM = .999014 WHAT NEXT? 3

POLYFIT OF DEGREE 4 INDEX OF DETERM = .999064 WHAT NEXT? 3

POLYFIT OF DEGREE 5 INDEX OF DETERM = .999125 WHAT NEXT? 3

POLYFIT OF DEGREE 6 INDEX OF DETERM = .999135 WHAT NEXT? 3

POLYFIT OF DEGREE 7 INDEX OF DETERM = .999146 WHAT NEXT? 2

TERM	COEFFICIENT
0	-17449.8
1	224.801
2	-1.22108
3	3.63893 E-3
4	-6.42299 E-6
5	6.72873 E-9
6	-3.88054 E-12
7	9.51399 E-16

Temperature X-ACTUAL	Seebeck Coefficient Y-ACTUAL	Y-CALC	DIFF	PCT-DIFF
410.5L7	133.968	132.754	1.21419	.914614
490.463	177.429	177.407	2.18344 E-2	1.23075 E-2
520.778	195.268	196.016	-.727808	-.371301
542.283	207.745	209.043	-1.29782	-.620838
572.863	224.859	226.83	-1.9705	-.868713
594.4	235.98	238.643	-2.66325	-1.116
636.917	257.49	259.861	-2.37057	-.912245
690.841	280.503	281.891	-1.3875	-.492214
750.141	294.558	298.692	-4.13862	-1.38558
760.913	297.344	301.143	-3.79867	-1.26142
474.97	167.99	168.025	-3.50857 E-2	-2.08812 E-2
502.221	184.396	184.618	-.221859	-.120172
531.649	201.362	202.64	-1.27814	-.630742
550.606	212.608	213.985	-1.37686	-.64344
578.847	228.773	230.176	-1.40336	-.60969
634.411	255.893	258.695	-2.80155	-1.08296
684.85	275.892	279.754	-3.86249	-1.38067
737.7	290.838	295.735	-4.89726	-1.65596
761.268	298.926	301.224	-2.29757	-.762746
380.933	118.144	118.603	-.458539	-.386618
485.546	174.557	174.41	.147179	8.43871 E-2
514.614	192.106	192.237	-.130816	-6.80496 E-2
534.127	202.94	204.14	-1.19974	-.587705
566.578	222.701	223.263	-.562214	-.251817
634.414	257.334	258.695	-1.36079	-.526023
682.662	275.789	278.955	-3.16596	-1.13493
731.132	292.656	294.081	-1.42493	-.484538
761.268	300.653	301.224	-.570572	-.189418
404.026	128.235	129.582	-1.34673	-1.03929
414.616	134.161	134.749	-.587718	-.436159
490.48	179	177.418	1.58224	.891819
521.796	196.729	196.639	9.01144 E-2	4.58273 E-2
537.114	205.649	205.942	-.292712	-.142133
568.017	224.318	224.084	.233863	.104364
612.304	248.169	247.94	.228967	9.23477 E-2
638.937	260.297	260.79	-.4931	-.189079
692.764	282.419	282.558	-.139106	-4.92309 E-2
744.259	298.226	297.319	.907183	.305121
775.722	304.001	304.582	-.581092	-.190783
398.72	129.276	127.045	2.23089	1.75599
482.849	172.251	172.773	-.522163	-.302225
536.384	205.787	205.502	.285383	.138871
568.68	225.664	224.461	1.2026	.535773
611.928	248.614	247.75	.864213	.348825
638.831	260.309	260.741	-.432364	-.165821
690.737	281.927	281.855	7.23853 E-2	2.56818 E-2
735.753	296.429	295.252	1.17699	.398638
773.182	303.341	303.972	-.631413	-.20772
392.724	123.04	124.203	-1.16255	-.936008
483.202	172.932	172.987	-5.51522 E-2	-3.18822 E-2
519.007	194.987	194.932	5.53594 E-2	2.83994 E-2
542.503	209.983	209.174	.808775	.386651
569.782	226.366	225.088	1.27848	.56799
614.186	249.67	248.888	.782335	.314333
639.891	262.965	261.228	1.73712	.664985
690.995	284.405	281.944	2.46051	.872693
733.29	298.473	294.632	3.84138	1.30379

Temperature X-ACTUAL	Seebeck Coefficient Y-ACTUAL	Y-CALC	DIFF	PCT-DIFF
770.283	304.979	303.289	1.69033	.557335
424.531	139.14	139.754	-.614181	-.439472
508.833	189.049	188.684	.365345	.193628
533.511	204.689	203.767	.922002	.452478
562.049	221.344	220.662	.68189	.30902
573.963	228.186	227.448	.737819	.32439
610.256	247.724	246.902	.821687	.332798
640.316	262.793	261.422	1.37134	.52457
708.568	289.234	287.715	1.51913	.527997
752.594	301.956	299.254	2.70173	.90282
775.163	306.337	304.446	1.89138	.621255
397.787	127.052	126.602	.450407	.355767
497.535	181.51	181.739	-.229441	-.126247
536.384	206.085	205.502	.583382	.283882
557.782	218.536	218.19	.346028	.15859
594.239	239.663	238.557	1.10578	.463528
631.326	258.336	257.245	1.09143	.424278
638.619	262.247	260.645	1.60201	.614633
683.291	280.941	279.186	1.75548	.628788
720.385	293.1	291.188	1.91241	.656762
760.25	304.171	300.995	3.17643	1.05531
349.397	101.765	101.666	9.86792 E-2	9.70618 E-2
430.666	143	142.945	5.53894 E-2	3.87489 E-2
508.547	188.833	188.508	.324608	.172198
542.503	209.661	209.174	.486775	.232713
564.872	223.323	222.286	1.03678	.466415
612.735	249.078	248.157	.921078	.371168
634.842	260.417	258.896	1.52125	.587591
698.524	284.685	284.506	.179263	6.30084 E-2
737.958	298.448	295.799	2.64939	.895672
779.937	305.533	305.63	-9.68523 E-2	-3.16894 E-2

STD ERROR OF ESTIMATE FOR Y = 1.683

APPENDIX II

ERROR ANALYSIS OF SEEBECK COEFFICIENT MEASUREMENT TECHNIQUE

APPENDIX II

ERROR ANALYSIS OF SEEBECK COEFFICIENT MEASUREMENT TECHNIQUE

The uncertainty limits for the Seebeck coefficient measurement were calculated using simple differential calculus to identify the variables and their effect upon the total uncertainty of the measurement system. The approach is one of obtaining the total differential of the equation which describes the parameter being investigated.

In the subject case, the equation for S, the Seebeck coefficient, is expressed in terms of the measurement parameters.

$$S = \frac{V}{T_2 - T_1} \quad , \tag{1}$$

where

V = voltage drop measured across the specimen

$T_2 - T_1$ = temperature differential across the specimen.

Using a technique developed in literature*, the exact differential for the S equation is:

$$DS = \frac{\partial S}{\partial V} dV + \frac{\partial S}{\partial T_1} dT_1 + \frac{\partial S}{\partial T_2} dT_2 \quad . \tag{2}$$

---

* Baird, D. C., An Introduction to Measurement Theory and Experiment Design, Prentice-Hall, 1962.

Approximating this differential equation with a finite difference equation,

$$\Delta S = \frac{\partial S}{\partial V}\,\delta V + \frac{\partial S}{\partial T_1}\,\delta T_1 + \frac{\partial S}{\partial T_2}\,\delta T_2 \quad , \tag{3}$$

where ΔS represents the plus or minus value of the uncertainty limit assigned to each point. The partial differential equations listed below are obtained by differentiating Equation 1.

$$\frac{\partial S}{\partial V} = \frac{1}{T_2 - T_1} \quad . \tag{4}$$

$$\frac{\partial S}{\partial T_1} = \frac{V}{(T_2 - T_1)^2} \quad . \tag{5}$$

$$\frac{\partial S}{\partial T_2} = -\frac{V}{(T_2 - T_1)^2} \quad . \tag{6}$$

Substituting Equations 4 through 6 into Equation 3,

$$\Delta S = \left| \frac{\delta V}{T_2 - T_1} \right| + \left| \frac{V\,\delta T_1}{(T_2 - T_1)^2} \right| + \left| \frac{-V\,\delta T_2}{(T_2 - T_1)^2} \right| + \delta S', \tag{7}$$

where $\delta S'$ is the error resulting from the drift associated with the dynamic measurement of T_1, T_2, and V during a 7-second time interval.

The δ values are those uncertainty values associated with the measurement apparatus. This uncertainty is derived from thermocouple calibration error and digital voltmeter error.

The resultant δ values used in the determination of the uncertainty limit equations are listed below for each piece of equipment.

δ Factor Affected	Equipment Item
δT_1, δT_2	Voltmeter - ±6 microvolts or ±0.6 C for Pt-vs-Pt-Rh thermocouple (calibration + reading error)
δT_1, δT_2	Thermocouples - ±0.1 C (relative error)
δV	Voltmeter - ±6 microvolts (calibration error)

Factoring the above values into Equation 7, the final equations to be used in determining the uncertainty limit for the S measurements are:

$$\Delta S = \pm \left[\frac{1}{\Delta T} \left(6 + 2(0.1 + 0.67) \frac{V}{\Delta T}\right)\right] + \delta S'$$

$$\text{or } \Delta S = \pm \left[\frac{1}{\Delta T} \left(6 + 1.54 \cdot S\right)\right] + \delta S'$$

where

$$\Delta T = T_2 - T_1$$

$$S = \frac{V}{\Delta T} \text{ (Seebeck coefficient at } (T_1 + T_2)/2).$$

APPENDIX III

STATISTICAL ANALYSIS OF ELECTRICAL-RESISTIVITY DATA

POLFTB 11:38 CY THU 07/11/68

L E A S T - S Q U A R E S P O L Y N O M I A L S

NUMBER OF POINTS = 81
MEAN VALUE OF X = 545.816
MEAN VALUE OF Y = 2529.23
STD ERROR OF Y = 1739.04

NOTE: CODE FOR 'WHAT NEXT?' IS:

0 = STOP PROGRAM
1 = COEFFICIENTS ONLY
2 = ENTIRE SUMMARY
3 = FIT NEXT HIGHER DEGREE

POLYFIT OF DEGREE 6 INDEX OF DETERM = .999819 WHAT NEXT? 3

POLYFIT OF DEGREE 7 INDEX OF DETERM = .999821 WHAT NEXT? 3

POLYFIT OF DEGREE 8 INDEX OF DETERM = .999821 WHAT NEXT? 2

TERM	COEFFICIENT
0	-176990.
1	2894.45
2	-20.2911
3	7.98969 E-2
4	-1.93253 E-4
5	2.93850 E-7
6	-2.73859 E-10
7	1.42887 E-13
8	-3.19541 E-17

Temperature (Deg. K)	Electrical Resistivity (microhm-cm)			
X-ACTUAL	Y-ACTUAL	Y-CALC	DIFF	PCT-DIFF
304.79	556.776	578.749	-21.973	-3.79664
396.693	740.108	770.53	-30.422	-3.9482
448.198	1002.01	1043.9	-41.8887	-4.01272
491.051	1341.83	1388.03	-46.2008	-3.32851
548.152	2007.67	2032.83	-25.1601	-1.23769
621.114	3094.17	3119.51	-25.3381	-.812245
674.532	3931.77	3972.16	-40.3858	-1.01672
702.616	4364.26	4396.05	-31.792	-.723195
737.733	4857.67	4887.63	-29.9633	-.613043
758.388	5134.96	5159.21	-24.2531	-.470094
304.79	556.73	578.749	-22.019	-3.80459
372.256	661.6	689.1	-27.4999	-3.99069
479.715	1238.46	1285.77	-47.3076	-3.67933
515.227	1624.19	1634.58	-10.3906	-.635672
554.276	2094.31	2114.46	-20.1512	-.953017
606.276	2853.21	2883.37	-30.164	-1.04614
651.735	3569.34	3612.02	-42.6849	-1.18174
683.092	4076.94	4104.06	-27.1196	-.660799
714.705	4542.53	4570.12	-27.5906	-.603717
746.334	4973.99	5002.03	-28.0427	-.560626
764.199	5218.42	5233.89	-15.4687	-.295548
303.979	579.14	577.455	1.68468	.291742
350.423	640.831	640.21	.62055	9.69291 E-2
388.896	751.745	741.308	10.4369	1.4079
444.788	1022.44	1021.29	1.14581	.112192
538.306	1888.73	1906.38	-17.6477	-.925718
592.736	2690.13	2672.53	17.6034	.65868
669.613	3923.96	3895.4	28.5569	.733093
722.328	4721.41	4677.16	44.2459	.945999
761.652	5234.9	5201.3	33.6002	.645996
303.979	579.14	577.455	1.68468	.291742
356.302	668.718	651.357	17.3606	2.66529
426.012	909.67	908.571	1.0992	.120981
471.459	1217.84	1216.49	1.35098	.111056
543.796	1956.39	1976.12	-19.733	-.998574
601.413	2826.71	2807.03	19.6751	.700921
690.481	4252.04	4216.08	35.9609	.852946
751.957	5108.74	5075.81	32.9287	.648738
766.644	5290.68	5265.08	25.5994	.486211
304.79	586.712	578.749	7.96298	1.37589
416.306	872.808	857.862	14.9459	1.74223
532.457	1859.2	1834.18	25.0225	1.36424
646.768	3552.43	3532.38	20.054	.56772
733.425	4852.4	4829.55	22.8531	.473194
765.32	5258.78	5248.19	10.5913	.201808
311.533	586.969	588.365	-1.3955	-.237183
398.527	792.64	777.852	14.7877	1.90109
516.595	1678.88	1649.68	29.1957	1.76977

Temperature (Deg. K)	Electrical Resistivity (microhm-cm)			
X-ACTUAL	Y-ACTUAL	Y-CALC	DIFF	PCT-DIFF
584.346	2569.62	2544.98	24.6373	.968075
653.318	3657.42	3637.33	20.088	.552272
677.562	4036.76	4019.06	17.7026	.440467
756.245	5146.37	5131.52	14.8536	.289459
314.859	595.429	592.566	2.86333	.483208
354.303	663.925	647.413	16.5122	2.55048
401.528	809.419	790.207	19.2122	2.43129
454.734	1125.92	1089.12	36.8006	3.37893
519.441	1708.76	1681.56	27.1958	1.61729
594.801	2713.8	2704.31	9.48579	.350765
644.756	3497.74	3500.02	-2.28051	-.065157
693.286	4255.04	4258.1	-3.06279	-7.19285 E-2
732.297	4808.17	4814.25	-6.07707	-.126231
329.861	615.924	610.249	5.67522	.929985
377.456	710.322	703.955	6.36668	.904415
428.385	941.995	921.745	20.2504	2.19696
479.832	1316.63	1286.78	29.8549	2.32013
604.764	2861.39	2859.57	1.82066	6.36691 E-2
661.217	3758.3	3763.09	-4.79424	-.127402
707.581	4463.01	4468.15	-5.14333	-.115111
740.499	4908.92	4924.65	-15.7265	-.319342
766.338	5237.73	5261.18	-23.4468	-.445656
350.423	614.586	640.21	-25.6245	-4.0025
417.828	833.922	865.48	-31.5577	-3.64627
493.374	1410.28	1410.03	.254852	1.80743 E-2
673.695	3990.97	3959.1	31.8672	.80491
475.123	1273.86	1246.71	27.1525	2.17794
725.825	4747.45	4725.65	21.7959	.461226
765.014	5224.61	5244.33	-19.7201	-.376027
533.471	1861.85	1846.53	15.3207	.829703
304.79	586.712	578.749	7.96298	1.37589
303.329	592.419	576.391	16.0284	2.78082
304.466	583.661	578.234	5.42662	.938482

STD ERROR OF ESTIMATE FOR Y = 24.5038

APPENDIX IV

ERROR ANALYSIS OF ELECTRICAL-RESISTIVITY-MEASUREMENT TECHNIQUE

The uncertainty limits for the electrical-resistivity measurement were calculated using simple differential calculus to identify the variables and their effect upon the total uncertainty of the measurement system. The approach is one of obtaining the total differential of the equation which describes the parameter being investigated.

In the subject case, the equation for ρ, the electrical resistivity, is expressed in terms of the measurement parameters.

$$\rho = \frac{VA}{IL} \quad , \tag{1}$$

where

V = voltage drop measured across the specimen

A = cross-sectional area of the specimen

L = voltage-probe separation

I = a-c current flow.

Using a technique developed in literature*, the exact differential for the ρ equation is:

$$D\rho = \frac{\partial \rho}{\partial V} dV + \frac{\partial \rho}{\partial A} dA + \frac{\partial \rho}{\partial L} dL + \frac{\partial \rho}{\partial I} dI \ . \tag{2}$$

---

* Baird, D. C., An Introduction to Measurement Theory and Experiment Design, Prentice-Hall, 1962.

Approximating this differential equation with a finite difference equation,

$$\Delta\rho = \frac{\partial\rho}{\partial V}\,\delta V + \frac{\partial\rho}{\partial A}\,\delta A + \frac{\partial\rho}{\partial L}\,\delta L + \frac{\partial\rho}{\partial I}\,\delta I \quad , \tag{3}$$

where $\Delta\rho$ represents the plus or minus value of the uncertainty limit assigned to each point. The partial differential equations listed below are obtained by differentiating Equation 1.

$$\frac{\partial\rho}{\partial V} = \frac{A}{LI} \quad , \tag{4}$$

$$\frac{\partial\rho}{\partial A} = \frac{V}{LI} \quad , \tag{5}$$

$$\frac{\partial\rho}{\partial L} = -\frac{AV}{L^2 I} \quad , \tag{6}$$

$$\frac{\partial\rho}{\partial I} = -\frac{AV}{LI^2} \quad . \tag{7}$$

Substituting Equations 4 through 7 into Equation 3,

$$\Delta\rho = \left|\frac{A\delta V}{LI}\right| + \left|\frac{V\delta A}{LI}\right| + \left|-\frac{AV\delta L}{L^2 I}\right| + \left|-\frac{AV\delta I}{LI^2}\right| + \delta\rho' \quad , \tag{8}$$

where $\delta\rho'$ is the error resulting from the drift associated with the dynamic measurement of T, I, and V during a 7-second time interval. The δ values are those uncertainty values associated with the measurement apparatus. This uncertainty is derived from thermocouple calibration error and digital voltmeter error.

The resultant δ values used in the calculation of the uncertainty limits are listed below for each piece of equipment and parameter measured.

δ Factor Affected	Equipment Item
δV	Voltmeter - ±0.10 percent of reading and ±0.05 percent of full scale
δI	Voltmeter and standard resistor - ±0.0018 amp
δA	Micrometer and specimen dimensional control - ±0.0021 cm^2
δL	Micrometer and area of probe point contact - ±0.008 cm

Factoring the above values into Equation 8, the final equations to be used in determining the uncertainty limit for the ρ measurements are:

$$\Delta\rho(\text{microhm-cm}) = \left(\frac{0.680}{0.635}\right)\delta V + V\left(\frac{0.0021}{0.635}\right) + \frac{(0.680)V(0.008)}{(0.635)^2} + \frac{(0.680)V(0.0018)}{(0.635)} + \delta\rho' \ . \tag{9}$$

Reducing, we have

$$\Delta\rho(\text{microhm-cm}) = (1.07)\delta V + (18.7 \times 10^{-3})V + \delta\rho' \ , \tag{10}$$

where V is the measured value of the voltage drop across the specimen.

APPENDIX V

TEST PROCEDURE SPECIFICATIONS

A. Seebeck Coefficient Measurement Procedure Specifications

1. Measurement Apparatus

a. Use only low-vapor-pressure, low-porosity materials in the construction of apparatus in order to minimize contamination of specimen with volatiles or entrapped gases (air).

b. Thermocouples and voltage probes should be selected based on high-temperacure stability and reproducibility. The pair of thermocouples used to measure the temperature difference across the specimen should be extracted from adjacent locations on a given roll of thermocouple wire in order to minimize relative difference in temperature readings. These differences are caused by inhomogeneities in the thermocouple wire which result in variations in the thermal emf at a given temperature as well as effecting the response of the thermocouple material to thermal aging.

c. Thermoelectric specimen should be supported between a high-thermal-conductivity heat source and heat-sink material which provides a uniform thermal contact with the specimen over its entire cross-sectional area and is known to be chemically compatible with the thermoelectric material over the entire range of measurement.

d. The direct contact of the voltage probes and thermocouple probes with the thermoelectric specimen should include only the use of materials which are known to be chemically compatible with the thermoelectric materials.

e. The hermetic seals of the apparatus should result in a leak rate of $<1 \times 10^{-9}$ atm-cc/sec.

2. Measurement Procedure

a. The Seebeck coefficient specimen heatup rate should not exceed 3 C/min (at an assumed digital voltmeter readout rate of ~3 channels/7 sec) for semiconductors materials (e.g., PbTe, BiXTe) and should be ~0 C/min for metals (e.g., Constantan calibration standard).

b. Measurements should be performed in inert gas atmospheres (<10 ppm 0_2) following a 24-hr bakeout of the system in vacuum at 250 to 300 C. The pressure should be ~1 atmosphere in order to minimize sublimation of semiconductor material.

c. Thermocouples and voltage taps should be attached to the specimen such that no significant heat is transferred between the thermocouple and the specimen. This minimizes the magnitude of the temperature drop due to thermal contact resistance. The placement of thermocouples on the side of the specimen is preferred (see Figure 1).

d. The temperature difference between the thermocouples, i.e., the ΔT, should be maintained at or above ~30 C for the entire range of Seebeck coefficient measurements.

e. The surface on which voltage probes and thermocouple probes are to be placed should be free of gross surface oxide and imperfections.

f. Mean specimen temperature measurement should be accurate to within ±1.0 C.

3. Instrumentation Specifications

a. Thermocouples (preferably Pt-vs-Pt-Rh) should be calibrated and accurate to within ±0.2 percent.

b. Dynamic measurement of Seebeck coefficient requires an integrating digital voltmeter with microvolt resolution and accurate to within ±6 microvolts over the entire range of measurement ±(0.01 percent of reading + 0.005 percent of full scale). The effective noise-rejection capability of the voltmeter should be 120 to 140 db and a common mode rejection of 120 db or more. The integrating capability of the digital voltmeter reduces superimposed noise by averaging out the random signal. Equilibrium measurement of Seebeck coefficient can be accomplished using a Leeds and Northrup K-2 or K-3 potentiometer.

c. Ice-bath thermocouple reference should be accurate to within ±0.1 C.

B. Electrical-Resistivity and Electrical-Contact-Resistivity-Measurement Procedure Specifications

1. Measurement Apparatus

a. Use only low-vapor-pressure, low-porosity materials in the construction of apparatus in order to minimize contamination of specimen with volatiles or entrapped gases (air).

b. The thermocouple used to measure specimen temperature should be selected based on high-temperature stability and reproducibility.

c. The thermoelectric specimen should be supported between high-electrical-conductivity metal electrodes in order to minimize Joulean heating of the adjacent specimen. In addition, the resistance between the specimen and the electrodes must be uniform and low over the entire area of contact in order to provide a uniform current distribution. The metal electrodes should be greater than one diameter (cylindrical specimens) or one diagonal (rectangular specimens) in order to provide uniform current distribution throughout the specimen.

d. The direct contact of the electrodes, voltage probes, and thermocouple probe with the thermoelectric specimen should include only the use of materials which are known to be chemically compatible with the thermoelectric materials.

e. The hermetic seals of the apparatus should result in a leak rate of $<1 \times 10^{-9}$ atm-cc/sec.

2. Measurement Procedure

a. The electrical-resistivity-versus-temperature measurements should be performed using a heatup rate not exceeding 3 C/min (at an assumed digital voltmeter readout rate of ~3 channels/7 sec).

b. Measurements should be performed in inert gas atmospheres containing <10 ppm O_2 for short-term (<100 hr) measurements or <1 ppm O_2 for long-term measurements (>100 hr). This requirement can be met by baking out the system in vacuum for 24 hr at 250 to 300 C followed by a "pregettering" of the inert gas using suitable gettering materials, e.g., tantalum. A gettering material may be used in the hot zone of the apparatus in order to maintain a low level of oxygen throughout the course of measurements, particularly for electrical-contact-resistivity-versus-time measurements.

c. Alternating current should be used in the resistivity measurements in the frequency range 100 to 200 Hz. Direct-current or very-low-frequency measurements should be avoided in order to (1) minimize thermal gradients in the specimen which result from Peltier cooling effects and (2) minimize the effect of a thermal-gradient-induced Seebeck voltage component on the ohmic potential drop measured between the voltage probes. High signal frequencies should be avoided, particularly in polycrystalline specimens, since the contact resistance between the crystal grains may result in the superposition of a significant capacitive component onto the resistance being measured.

d. The current flux should not exceed 1.5 amp/cm^2 in order to minimize Joulean heating in the specimen which may otherwise result in errors in the measurement of specimen temperature.

e. For the measurement of electrical resistivity versus temperature and electrical contact resistivity versus time, the ratio of voltage-probe separation to specimen-cross-sectional area should be ≥ 2 cm^{-1} in order to achieve the desired level of accuracy.

f. For the measurement of electrical resistivity versus temperature, the distance between a given voltage probe and the specimen-electrode interface should be no less than one diameter (cylindrical specimens) or one diagonal (rectangular specimens) in order to provide uniform current distribution throughout the specimen.

g. For measurement of electrical contact resistivity versus temperature using the traverse method, an increment step of 4 to 5 mils should be used to define the voltage profile in the vicinity of the metal-semiconductor junction.* In addition, the voltage probes should have a nominal tip radius of 0.5 mil.**

h. The surface on which the voltage probes are to be placed should be free of gross surface oxide and imperfections which would significantly affect the resistivity measurement.

---

* Posttest microscopic examination used to locate position of junction relative to known traversing probe positions.

** This tip radius can be obtained by using electrolytic etching techniques (see H. C. Torrey, et al., Crystal Rectifiers, McGraw-Hill Book Company, New York, N.Y., page 319 (1948).

i. Adequate shielding shall be used for all voltage and current leads in order to minimize the effects of spurious electromagnetic pickup from any a-c field. In addition, particular care must be used in the design of the voltage-measurement circuit since induced a-c ground currents, i.e., common mode pickup, usually at power line frequency, can generate a potential of several volts between the signal source ground and the voltmeter chassis ground. If not blocked, these currents will cause an erroneous voltage larger than the signal to appear at the input.

3. Instrumentation Specifications

a. Thermocouples (preferably Pt vs Pt-Rh) should be calibrated and accurate to within ±0.2 percent.

b. The specimen a-c current should be measured using a standard four-terminal resistor with a maximum error of less than ±0.03 percent.

c. The a-c signal should be supplied by a precision a-c power supply with less than (1) 0.05 percent distortion, (2) 0.01 percent amplitude instability, and (3) 1.5 milliwatts of noise.

d. The specimen current and voltage measurements should be performed using an integrating digital voltmeter in conjunction with an a-c/d-c converter with microvolt resolution and accurate to within ±(0.10 percent of reading + 0.05 percent of full scale).

e. Ice-bath thermocouple reference should be accurate to within ±0.1 C.

C. Life Testing and Efficiency-Measurement Procedure Specifications

1. Measurement Apparatus

a. Use only low-vapor-pressure, low-porosity materials in the construction of apparatus in order to avoid contamination of specimen with volatiles or entrapped gases (air). However, fibrous-type thermal insulations will probably be necessary in the construction of the thermal insulation system and must be baked out in vacuum in order to remove volatiles, entrapped gases, and water vapor. In addition, the use of volatile and/or reactive materials in the life-test apparatus which are not otherwise present in RTG systems may result in misleading performance stability and, thus, should be avoided.

b. The thermocouples used to measure specimen temperatures should be selected based on high-temperature stability and reproducibility.

c. The direct contact of voltage probes and thermocouples with the thermoelectric materials should be avoided at elevated temperatures (>100 C) in order to avoid long-term "poisoning" effects, i.e., chemical reaction and subsequent changes in electrical properties.

d. The hermetic seals of the apparatus should result in a leak rate of $<1 \times 10^{-9}$ atm-cc/sec.

2. Test and Measurement Procedure

a. Life testing should be performed under conditions of constant or controlled (in order to simulate radioisotope decay) thermal input power. The monitoring of thermal input power using electrical input power measurements may be feasible if the ratio of the heat flow through the thermoelectric couple(s) to the total heat input can be maintained above about 0.85 to 0.90. In addition, the parasitic heat losses would have to remain nearly constant with time (less than 5 percent variation).

b. The hot-, intermediate- (optional), and cold-junction temperatures should be monitored during either life test or efficiency measurement. The cold-junction temperature should be maintained nearly constant to simulate actual operating conditions of a thermoelectric generator.

c. Output power, P, of the thermoelectric couple should be computed using the relation $P = I \cdot V_{cc}$ under conditions of fixed external load (where I and V_{cc} are the measured current and closed-circuit voltage).

d. The monitoring of thermal input power (efficiency measurement) may be accomplished using calibrated heat-flux transducers at the cold end of the thermoelectric legs. However, calibration of this heat-monitoring technique is necessary to correct for unavoidable parasitic heat losses from the periphery of the thermoelectric couple. This calibration can be accomplished using a Pyroceram 9606 thermal-conductivity standard whose

dimensions, emissivity, and thermal conductivity are closely matched to those of the thermoelectric couple to be tested.

e. In making efficiency measurements, care must be exercised to minimize parasitic losses from the periphery of the thermoelectric couple even though these losses may be accurately known. This minimization is necessary since the electrical output power of an individual couple operating at fixed hot- and cold-junction temperatures will increase with increasing parasitic heat losses from the periphery of the thermoelectric elements. The increase in electrical output power is the result of a decrease in the internal resistance caused by a parasitic heat-loss-induced change in the temperature distribution along the length of the thermoelectric elements.

3. Instrumentation Specifications

a. Thermocouples should be accurate to within ±0.5 percent.

b. Thermal-flux transducers (efficiency measurement only) should be calibrated and accurate to within ±4 percent or less.

c. Constant thermal input power can be achieved using a regulated d-c input electrical power supply (±0.25 percent line and load regulation).

d. Direct-current flow through thermoelectric couple should be monitored using a calibrated four-terminal resistor with a maximum error of less than ±0.3 percent.

e. The thermoelectric couple current, voltage, and thermocouple emf measurements should be performed using an integrating digital voltmeter accurate to within ±6 microvolts over the entire range of measurement ±(0.01 percent of reading + 0.005 percent of full scale).

APPENDIX VI

ERROR ANALYSIS OF ELECTRICAL-CONTACT-RESISTIVITY TRAVERSE MEASUREMENT TECHNIQUE

The uncertainty limits for the electrical-contact-resistivity traverse measurement were calculated using simple differential calculus to identify the variables and their effect upon the total uncertainty of the measurement system. The approach is one of obtaining the total differential of the equation which describes the parameters being investigated.

In the subject case, the equation for the contact resistivity, ρ_c, is expressed in terms of the measured parameters:

$$\rho_c = \frac{(V_1 - V_2)\, A}{I} \quad , \tag{1}$$

where

V_1 and V_2 = the voltages measured adjacent to either side of the bond interface

A = cross-sectional area of the specimen

I = a-c current flow.

The total differential for the contact-resistivity equation is:

$$D\rho_c = \frac{\partial \rho_c}{\partial V_1} dV_1 + \frac{\partial \rho_2}{\partial V_2} dV_2 + \frac{\partial \rho_c}{\partial A} dA + \frac{\partial \rho_c}{\partial I} dI \quad . \tag{2}$$

Approximating this differential equation with a finite difference equation gives:

$$\Delta\rho_c = \frac{\partial \rho_c}{\partial V_1} \delta V_1 + \frac{\partial \rho_c}{\partial V_2} \delta V_2 + \frac{\partial \rho_c}{\partial A} \delta A + \frac{\partial \rho_c}{\partial I} \delta I \quad , \tag{3}$$

where $\Delta\rho_c$ represents the plus or minus value of the uncertainty limit assigned to the mean value of contact resistivity. Carrying out the partial differentiation of Equation 1 in Equation 3 yields:

$$\Delta\rho_c = \left|\frac{A\,\delta V_1}{I}\right| + \left|-\frac{A\,\delta V_2}{I}\right| + \left|\frac{(V_1 - V_2)\delta A}{I}\right| + \left|-\frac{(V_1 - V_2)A\delta I}{I^2}\right| + \delta\rho_c' \quad , \tag{4}$$

where $\delta\rho_c'$ is the error resulting from the uncertainty associated with the location of the semiconductor-metal junction. The δ values are those uncertainty values associated with the measurement apparatus.

The resultant δ values used in the calculation of the uncertainty limits are listed in Table VI-1 for each piece of equipment and parameter measured. Since V_1 and V_2 are usually not significantly different in magnitude and are used to determine a difference, V_1 and V_2 may, in this measurement, be considered independent of the instrument error and only the reading error (±1 μvolt) need be considered.

The principal source of error in the measurement of contact resistivity is associated with the actual location of the metal-semiconductor interface in relation to the location of the measuring probe on either side of it. The nature of this error can be understood by referring to Figure VI-1. The measurements were made with the probe positioned at 5.0-mil intervals. There was no visual access to the sample during measurement. The point of measurement in the metal (tungsten) closest to the junction and the point of measurement in the semiconductor (PbTe) closest to the junction can be identified from observed differences in voltage drop. However, there is no way of knowing the location of the metal-semiconductor interface in relation

TABLE VI-1. UNCERTAINTIES ASSOCIATED WITH MEASURED PARAMETERS

δ Factor Affected	Equipment Item
δV_1 and δV_2	Voltmeter reading error only - ±1 μvolt
δI	Voltmeter and standard resistor - ±0.0018 amp
δA	Micrometer and specimen dimensional control - ±0.0021 cm^2
δ_c' (without posttest microscopic examination of junction)	Uncertainty associated with location of semiconductor-metal interface - $\pm 1/2\rho_B \cdot L$ (L = 5 mils)
δ_c' (with posttest microscopic examination of junction)	Uncertainty associated with location of semiconductor-metal interface - $\pm 1/2\rho_B \cdot L$ (L = 1 mil)

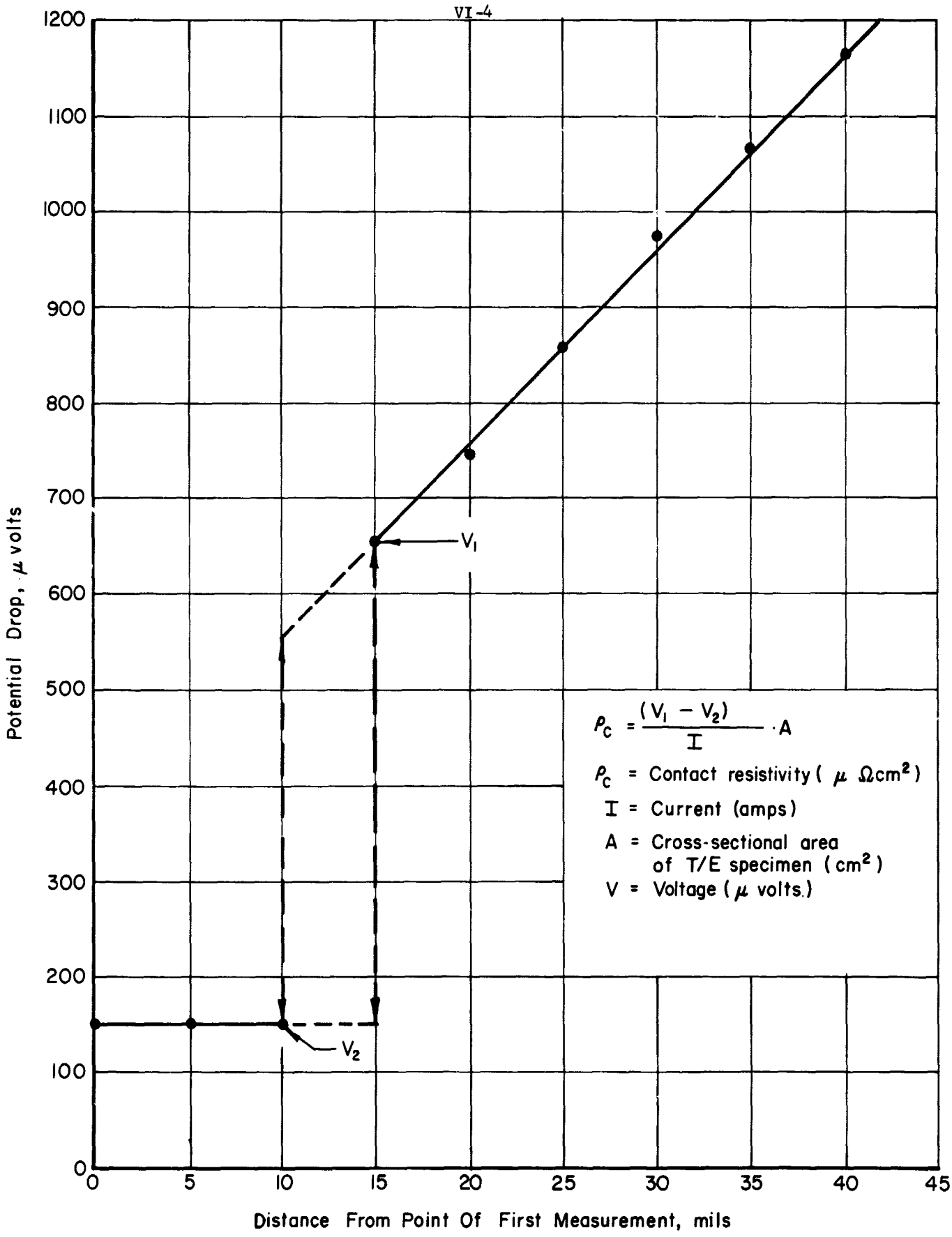

FIGURE VI-1. POTENTIAL PROFILE OF W-2p-PbTe PRESSURE-CONTACTED JUNCTION

to these two points. Because of the uncertainty in location, one must assume that the interface could lie at V_1 (see Figure VI-1) essentially coincident with the position of the first measurement in the semiconductor, or at V_2 essentially coincident with the first measurement in the metal, or anywhere in between. It can be seen that tne magnitude of error arising from uncertainty in the interface location, i.e., $\pm 50\ \mu\Omega\text{-cm}^2$ for the example shown, is substantially larger than the magnitude of error associated with parameter measurements. It can be readily shown that the magnitude of this error is equal to $\pm 1/2\rho_B \cdot L$, where ρ_B is the resistivity of the thermoelectric material in the vicinity of the junction, and L is the spacing between probe measurements. The surface deformation of the semiconductor resulting from voltage probe contact and voltmeter resolution prohibit traverse increment sizes less than about 4 or 5 mils. This component of error can be minimized, however, by performing a single traverse (normally at elevated temperature) across the metal-semiconductor junction followed by a post-test microscopic examination in the vicinity of the junction to identify the exact position of the metal-semiconductor interface relative to Points V_1 and V_2.

Factoring the above values into Equation 4, the final equations to be used in determining the uncertainty limit for the ρ_c measurements are:

$$\Delta\rho_c \text{ (without microscopic examination)} = \left(\frac{0.680 \times 1.0}{1.000}\right) + \left(\frac{0.680 \times 1.0}{1.000}\right) + \left(\frac{0.605 \times 0.0021}{1.000}\right) + \left(\frac{0.605 \times 0.680 \times 0.0018}{(1.000)^2}\right) + 1/2\rho_B \cdot L$$

$$= 37.4\ \mu\Omega\text{-cm}^2$$

$$\Delta\rho_c \text{ (with microscopic examination)} = 10.1\ \mu\Omega\text{-cm}^2.$$

APPENDIX VII

STANDARD INPUT DATA FORMS

FORTRAN FIXED 10 DIGIT DECIMAL DATA

DECK NO. _____ PROGRAMMER _____ DATE _____ PAGE 1 of _____ JOB NO. _____

	NUMBER	IDENTIFICATION	DESCRIPTION DO NOT KEY PUNCH
1		Radiator Fin Inputs	Radiator material I.D. number(1)* (Col. 1) and material name (e.g. beryllium)
13		Note: Last three inputs on this card required only if data other than that in library are desired.	Number of radiator fins
25			Radiator fin emissivity
37			Fin-length parameter, $\emptyset(cm^2 - {}^\circ K^4/W)$
49			Fin-thickness parameter, $\varphi(cm^3 - {}^\circ K^5/W^2)^{1/2}$
61		73 80 1	Fin-weight parameter, $\mu(cm^2 - lb - {}^\circ K^9/W^3)^{1/2}$
1		Thermopile Inputs	Thermoelectric material (e.g., PbTe, GeSi, etc.)
13			Thermoelectric hardware material (e.g., S.S. 304)
25			Thermoelectric hot-shoe material (e.g., tungsten, iron, etc.)
37			Thermoelectric cold-shoe material (e.g., tungsten, iron, etc.)
49			Interelement thermal and electrical insulation material (e.g., mica)
61		73 80 2	Module cladding material (e.g., S.S. 304)
1			Thermoelectric element length assumed (cm)
13			Closed-circuit voltage per couple output of thermoelectrics (volt)
25			Thermoelectric current(2) (amp)
37			Number of modules(3)
49			
61		73 80 3	
1		Note:	Length-to-area ratio of Phase I n-element (cm^{-1})
13		Phase I - cold end	Length-to-area ratio of Phase I p-element (cm^{-1})
25		Phase II - middle	Length-to-area ratio of Phase II n-element (cm^{-1})
37		Phase III - hot end	Length-to-area ratio of Phase II p-element (cm^{-1})
49			Length-to-area ratio of Phase III n-element (cm^{-1})
61		73 80 4	Length-to-area ratio of Phase III p-element (cm^{-1})

* See Input Data References at end of Appendix I.

FORTRAN FIXED 10 DIGIT DECIMAL DATA

DECK NO. _____ PROGRAMMER _____ DATE _____ PAGE 2 of _____ JOB NO. _____

	NUMBER	IDENTIFICATION	DESCRIPTION DO NOT KEY PUNCH
1			Density of Phase I n-type segment (lb/cc)
13			" " " I p-type " "
25			" " " II n-type " "
37			" " " II p-type " "
49		73 80	" " " III n-type " "
61		5	" " " III p-type " "
1			Number of thermoelectric element segments (1,2, or 3)
13			Element distribution in module width[4] (0 - odd or even, 1 - even only)
25			Density of thermoelectric hardware (hot and cold platens, etc.) (lb/cc)
37			Density of module cladding material (lb/cc)
49		73 80	Density of thermoelectric shoe material (lb/cc)
61		6	Density of thermal and electrical insulation between elements (lb/cc)
1			Thermoelectric hardware thickness in conductive mode (cm)
13			Thermoelectric hardware thickness in radiative mode (cm)
25			Radiation gap between heat source and module (cm)
37			Thickness of element shoes (cm)
49		73 80	Thickness of module periphery material (cm)
61		7	Thickness of module peripheral gap for radiation-loss analysis (cm)
1			
13			
25			
37			
49		73 80	
61			

FORTRAN FIXED 10 DIGIT DECIMAL DATA

DECK NO. _____ PROGRAMMER _____ DATE _____ PAGE 3 of _____ JOB NO. _____

	NUMBER	IDENTIFICATION	DESCRIPTION DO NOT KEY PUNCH
1			Thickness of thermal and electrical insulation between elements (cm)
13			Effective thermal conductivity of module periphery (watts/cm/°C)
25			Effective thermal conductivity of thermal and electrical insulation
37			(watts/cm/°C)
49		73 80	
61		8	
1		Fuel-Form Impact Cladding Inputs	Fuel-form cladding material (e.g., Inconel 716)
13			Inner-liner cladding material (e.g., tantalum)
25			Outer-shell cladding material (e.g., molybdenum)
37			Fuel-tube material (e.g., molybdenum)
49		73 80	Toughness parameter of cladding(5) (lb/cm^2)
61		9	Thickness of inner-liner cladding (cm)
1			Thickness of outer-shell cladding (cm)
13			Thickness of fuel tube (cm)
25			Density of fuel-form cladding (lb/cc)
37			Density of inner-liner cladding (lb/cc)
49		73 80	Density of outer-shell cladding (lb/cc)
61		10	Density of fuel tube (lb/cc)
1		Fuel-Form Inputs	Fuel-form material (e.g., plutonium)
13			Fuel-block material (e.g., graphite)
25			Fuel-form power density(6) (watts/cc)
37			Fuel-pin density in close-packing matrix(7) (decimal)
49		73 80	
61		11	Fuel-pin array option* (0 - locus of all fuel-pin centers is a circle; 1 - close packing of fuel pins)

* Kortier, W. E., "An Advanced Thermoelectric Component Program Final Summary Report", February 18, 1966, page 6, NAS5-9160.

FORTRAN FIXED 10 DIGIT DECIMAL DATA

DECK NO. _____ PROGRAMMER _____ DATE _____ PAGE 4 of _____ JOB NO. _____

	NUMBER	IDENTIF'CATION	DESCRIPTION DO NOT KEY PUNCH
1			Fuel pin - fuel tube separation[8] (cm)
13			Fuel-pin separation (cm)
25			Number of fuel pins
37			"Effective" surface-power-density available for module[9] (watts/cm^2)
49		73 80	Heat-transfer mode between heat source and module (1 - conductive 2 - radiative)
61		12	Density of fuel block (lb/cc)
1			Density of fuel form[10] (lb/cc)
13			Density of fuel pin (lb/cc)
25			Limiting aspect ratio of fuel form
37			Limiting aspect ratio of fuel pin
49		73 80	
61		13	
1		Heat-Source Support Inputs	Heat-source-support material for ends (e.g., Min-K 2000)
13			Heat-source-support material for radial portion (e.g., Min-K 2000)
25			Thermal insulation material for ends
37			Thermal insulation material for radial portion
49		73 80	Absolute end support option (0 - all support on ends; 1 - some support on radial portion)
61		14	Absolute radial support option (0 - all support on radial portion 1 - some support on ends)
1			Elastic modulus[11] (compression) of end heat-source support (lb/cm^2)
13			Elastic modulus (compression) of radial heat-source support (lb/cm^2)
25			Elastic modulus (shear) of end heat-source support (lb/cm^2)
37			Elastic modulus (shear) of radial heat-source support (lb/cm^2)
49		73 80	Heat-source-support end-deflection neglection[12]
61		15	(0 - deflection controls generator length; 1 - generator length independent of deflection)

FORTRAN FIXED 10 DIGIT DECIMAL DATA

DECK NO. _____ PROGRAMMER _____ DATE _____ PAGE 5 of _____ JOB NO. _____

	NUMBER	IDENTIFICATION	DESCRIPTION DO NOT KEY PUNCH
1			Heat-source-support foil separation on end support (cm)
13			Heat-source-support foil separation on radial support (cm)
25			End-insulation-foil separation (cm)
37			Radial-insulation-foil separation (cm)
49		73 80	Thermal conductivity of end heat-source support (watts/cm/°C)
61		16	Thermal conductivity of radial heat-source support (watts/cm/°C)
1			Thermal conductivity of end insulation (watts/cm/°C)
13			Thermal conductivity of radial insulation (watts/cm/°C)
25			Density of the end heat-source support (lb/cc)
37			Density of the radial heat-source support (lb/cc)
49		73 80	Density of the end insulation (lb/cc)
61		17	Density of the radial insulation (lb/cc)
1			Maximum tolerable deflection of end heat-source support[13] (cm)
13			Maximum tolerable deflection of radial heat-source support[13] (cm)
25			
37			
49		73 80	
61		18	
1		Generator Shell Inputs	Generator shell material (e.g., beryllium)
13			Final overall generator length (cm)
25			Normal increment step-size for generator length (cm)
37			Initial overall generator length (cm)
49		73 80	Density of generator shell (lb/cc)
61		19	Thickness of ablator on end (cm)

FORTRAN FIXED 10 DIGIT DECIMAL DATA

DECK NO. _____ PROGRAMMER _____ DATE _____ PAGE 6 of _____ JOB NO. _____

	NUMBER	IDENTIFICATION	DESCRIPTION DO NOT KEY PUNCH
1			Thickness of ablator on radial portion (cm)
13			Thermal conductivity of generator shell (watts/cm/°C)
25			Limiting aspect ratio of generator envelope
37			Limiting aspect ratio of generator shell
49		73 80	Percent of total heat-dump capability of generator ends[14] (decimal)
61		20	
1		RTG Analysis Computation Options (Note: See end of Appendix I for description of these options)	Thermoelectric-array computation sequence (1,2,3)
13			Generator-length computation sequence (0,1)
25			Thermoelectric-element-length computation sequence (0,-1)
37			Fuel-form geometry option (0,1)
49		73 80	Heat-source-support computation option (-1,0,1)
61		21	End-insulation computation option (-1,0)
1			Insulation and heat-source-support option (0,1)
13			Insulation and heat-source-support material option (0,1)
25			Print option for output data[15] (0 - abstract, 1 - detailed, 2 - super-detailed)
37			Plot option (1 - plot component weights vs generator length;
49			2 - plot component weights vs radiator temperature;
61		73 80	3 - no plot)
		22	Output format option[15] (0 - abstract, 1 - detailed)
1		Temperatures[16]	Temperature of thermoelement cold junction (K)
13			Temperature at cold end of insulation (K)
25			Temperature of thermoelement hot junction (K)
37			Temperature at hot end of insulation (K)
49			Temperature at heat-source surface (that surface which is adjacent to module) (K)
61		73 80	
		23	Temperature of radiator fin and generator shell (K)

FORTRAN FIXED 10 DIGIT DECIMAL DATA

DECK NO _____ PROGRAMMER _____ DATE _____ PAGE 7 of _____ JOB NO. _____

	NUMBER	IDENTIFICATION	DESCRIPTION DO NOT KEY PUNCH
1		General Design Inputs	Assumed engineering efficiency[17] (decimal form)
13			Minimum thermoelectric element length to be considered by generator[18] (cm)
25			Maximum element length to be considered by generator[18] (cm)
37			"g"-loading axially (dimensionless)
49		73 80	"g" loading radially (dimensionless)
61		24	Generator power level (watts(e))
1			Impact velocity of heat source[5] (cm/sec)
13			End-of-life thermoelectric efficiency (decimal)
25			Data set index for component weight versus cold-junction temperature option
37			
49		73 80	
61		25	
1			
13			
25			
37			
49		73 80	
61			
1			
13			
25			
37			
49		73 80	
61			

Input Data Reference

(1) Radiator Material Designation

The following radiator material numbering code may be used to extract the radiator fin parameters from the input data library:

Radiator Material I.D. Number	Radiator Material
1	Magnesium
2	Beryllium
3	Magnesium M1A
4	Magnesium HM21-T8
5	Aluminum A356-T6
6	Copper (ETPC)
7	Chromium-copper

(2) Thermoelectric Current and Voltage

The selection of the operating current establishes the shape factor of the thermoelectric elements. The current may be selected on the basis of power level, voltage level, or shape-factor preference. The voltage per couple and shape factor may be obtained from the thermoelectric-input analysis.

(3) Selection of Module Number

The selection of the number of modules is a tradeoff between module peripheral losses and desired number of fins. For maximum utilization of radiator fins, the number of modules should match the number and position of the fins. Therefore, this selection will be subject to the selection of the number of fins discussed.

(4) Thermoelectric-Array Option

The choice of module-width array is affected by the requirements imposed by equipment used in the vicinity of the generator. For example, for magnetometers, extraneous fields produced by current-carrying wires must be arranged so that they are self-cancelling. This is achieved by an array with equal numbers of n- and p-elements across the width of the module, and this can be introduced into the program by means of the input value set equal to 1.0.

(5) Toughness Parameter and Impact Velocity

This parameter is used in the cladding analyses subroutine of the program. The selection of this term is discussed in the final report of NASA Contract NAS5-3697, page 25. Also in this reference appears a discussion of the impact velocity and how the cladding analyses establish a cladding thickness sufficient for intact impact with an unyielding surface.

(6) Fuel-Form Power Density

This power density is usually found in the properties table of a candidate fuel form. However, when fission gas must be accommodated by void space, the fuel-form power density is reduced to an effective power density. This power density is used to determine the volume the fuel form will occupy, including the void volume.

(7) Fuel-Pin Packing Density

This parameter defines the packing density of the fuel pins in the fuel-block matrix. The maximum packing fraction is about 70 percent and will have to be determined prior to the computer run. This number, when divided into the total cross-sectional area of the fuel pins, will give the total cross-sectional area of the fuel-form cross section. The value is used when an undefined array is specified.

(8) Separation Between the Fuel Pin-Fuel Tube and Between Fuel Pins

This input permits the operator to choose the fuel-block thickness between a fuel pin and the fuel tube which supports the fuel block plus fuel pins. This only applies to the symmetric fuel-pin array which is selected by the input value for FPA, the fuel-pin-array option.

The separation between fuel pins along a line connecting the fuel-pin centers allows the packing density to be controlled. Note that the fuel block is optional in the case of radiation heat transfer. In this case, the fuel pins would be supported by a frame whose weight would be included under the heading of the fuel block.

(9) Heat-Source-Surface Power Density

The heat-source-surface power density is selected on the basis of maximum-power-density capability. This value is found from two-dimensional heat-flow considerations of the fuel form, fuel block, cladding, and fuel-tube composite. The term is then used in the computer to determine whether the designed thermoelectric module requires a surface power density greater

than that practical for a particular heat-source design. A surface-power-density deficiency will result in an escalation of the heat-source surface temperature which will increase parasitic heat losses through the insulation and heat-source support.

(10) Fuel-Form Density

The fuel-form density may be expressed as an effective value if void volumes are incorporated into the fuel form. For example, if a fuel requires an additional 100 percent void volume due to fission-gas release, then the effective fuel-form density, RHOFF, would be one-half the actual fuel-form density for the weight calculation.

(11) Modulus of Elasticity for Heat-Source Support

The compressive- and shear-modulus inputs are necessary for the determination of heat-source support required for a maximum allowed deflection. The values will often be supplied with homogeneous materials. However, for more complex support structures, such as honeycomb, special data reports must be consulted. Since heat-source support is a basic necessity, the support medium may have to be designed for a required modulus.

(12) Heat-Source-Support End-Deflection Neglection

This option permits the code to consider or ignore longer generators when a deficiency of end-support bearing area exists. Longer generators are attended by decreasing end areas, which serves to increase the bearing-area deficiency.

(13) Maximum Tolerable Deflections

The module, heat source, or support may be limited in deflection because of preservation of electrical or thermal contacts of the thermoelectrics, excessive shear forces on thermoelectrics or heat-source support, or increase in heat transfer through heat-source support or insulation due to reduction in heat path.

(14) Heat Dissipation by Generator Ends

The particular mission of a generator may allow all, part, or none of the end area of the generator shell to dissipate heat. This may be introduced into the program by specifying the percentage of the total dissipative capability available for heat dump.

(15) Output Options

The print option for output data controls the frequency of the display of output data, e.g., the user may choose to (1) print the calculated data after a change in each component (super-detailed mode), (2) print the calculated data after each component has been optimized (detailed), and (3) print only the optimum generator design case (abstract).

The output format option permits the user to specify (1) an output format containing all dimensions, weights, etc. (detailed) or (2) an output format containing only the principal parameters (abstract). A description of both types of output format is given in Appendix II.

(16) Generator Profile Temperatures

The temperatures of the cold junction of the thermoelectrics, cold junction of the insulation, and the radiator surface may all be specified independently to accommodate the temperature differentials present in the heat path for the thermoelectric cold junction to the radiator surface. The same procedure is used at the hot junction.

(17) Initial Assumption of Engineering Efficiency

This program is designed to construct mathematically a generator based on assumed thermoelectric and engineering efficiencies. Therefore, the operator must select a practical value of engineering efficiency for the program. The program will analyze and iterate on engineering efficiency until a heat balance is achieved. Thus, the proper selection of this parameter will greatly reduce the computer run time.

(18) Element-Length Limits

These limits are imposed to avoid impractical element shapes and sizes due to the element-length iterations taking place in the program. The limits may be based on fabricability or insulation capability, since insulation thickness and heat-source-support thickness follows the element length.

(19) RTG Analysis Computation Options

(a) Thermoelectric-array computation sequence

1 - Limited by heat-source diameter

2 - Limited by heat-source length

3 - Investigates Cases 1 and 2

Geometry of module based on geometry of heat source

(b) Generator length computation sequence

0 - Iterate using normal increments

1 - Iterate using large increments and then small increments

(c) Thermoelectric-element-length computation sequence

0 - Element length is fixed

1 - Element length is varied in order to trade off thermoelectric weight vs other generator components (viz., heat source, insulation, shell, etc.)

(d) Fuel-form geometry option

0 - Right-cylindrical geometry for single fuel form

1 - Right-cylindrical geometry for subfuel form or fuel pins and overall right-cylindrical for fuel block

(e) Heat-source-support computation option

1 - Maximum support by ends

0 - Support by both end and radial portion

1 - Maximum support by radial portion

(f) End-insulation computation option

1 - Tradeoff end-insulation thickness against other generator components

0 - End-insulation thickness is fixed

(g) Insulation and heat-source-support option

0 - Solid-type insulation and support

1 - Foil- and honeycomb-type insulation and support

(h) Insulation and heat-source-support material option

0 - Treat insulation and heat-source support as independent components

1 - Assume insulation and heat source are same and calculate deflection of support material on the basis of total bearing area available

APPENDIX VIII

INPUT/OUTPUT FORMAT

INPUT DATA
****

RADIATOR FIN INPUTS

RADIATOR MATERIAL I.D.	MAGHM21A-T8	NO. OF FINS	5.00
FIN EMISSIVITY	.90	FIN LENGTH PARAMETER	6.1526
FIN THICKNESS PARAMETER	1.6516	FIN WEIGHT PARAMETER	0.405E-01

THERMOPILE INPUTS

THERMOELECTRIC MATERIAL	PBTE(2P-2N)	THERMOELECTRIC HARDWARE MATERIAL	SS304
THERMOELECTRIC HOT-SHOE MATERIAL	IRON	THERMOELECTRIC COLD-SHOE MATERIAL	IRON
THERMAL AND ELECTRICAL INSULATION MATERIAL	MICA	MODULE CLAD MATERIAL	NONE USED
ASSUMED ELEMENT LENGTH	1.40	CLOSED-CIRCUIT VOLTAGE PER COUPLE	.0910
THERMOELECTRIC CURRENT	2.00	NO. OF MODULES	5.00
L/A FOR STAGE-1 N-ELEMENT	4.00	L/A FOR STAGE-1 P-ELEMENT	3.84
L/A FOR STAGE-2 N-ELEMENT	0.00	L/A FOR STAGE-2 P-ELEMENT	0.00
L/A FOR STAGE-3 N-ELEMENT	0.00	L/A FOR STAGE-3 P-ELEMENT	0.00
DENSITY FOR STAGE-1 OF N-ELEMENT	.0179	DENSITY FOR STAGE-1 OF P-ELEMENT	.0179
DENSITY FOR STAGE-2 OF N-ELEMENT	0.0000	DENSITY FOR STAGE-2 OF P-ELEMENT	0.0000
DENSITY FOR STAGE-3 OF N-ELEMENT	0.0000	DENSITY FOR STAGE-3 OF P-ELEMENT	0.0000
NO. OF SEGMENTS FOR T/E ELEMENTS	1.00	EVEN,1,OR EITHER,0,NO. OF ELEMENTS IN MODULE WIDTH	0.00
DENSITY OF HARDWARE RELATED TO THE T/E S	.0176	DENSITY OF MODULE CLAD MATERIAL	0.0000
DENSITY OF T/E SHOE MATERIAL	.0173	DENSITY OF INTER-ELEMENT INSULATION MATERIAL	.0071
T/E HARDWARE THICKNESS FOR CONDUCTION MODE OF HT TRN	1.100	T/E HARDWARE THICKNESS FOR RADIATION MODE OF HT TRAN	0.000
RADIATION GAP BETWEEN HEAT SOURCE AND MODULE	0.000	THICKNESS OF T/E ELEMENT SHOES	.127
MODULE CAN WALL THICKNESS	0.000	SEPARATION BETWEEN MODULE WALL AND GENERATOR INS.	.025
THICKNESS OF INTER-ELEMENT INSULATION	.013	EFFECTIVE THERMAL CONDUCTIVITY OF MODULE CAN WALL	0.0000
EFFECTIVE THERMAL CONDUCTIVITY OF INTER-ELEMENT INS	.0050		

FUEL-FORM IMPACT CLAD INPUTS

FUEL-FORM CLAD MATERIAL	HASTELLOY C	INNER LINER CLAD MATERIAL	NONE USED

OUTER-SHELL CLAD MATERIAL	NONE USED	FUEL TUBE MATERIAL	MOLYBDENUM
TOUGHNESS PARAMETER FOR FUEL FORM CLAD	0.321E+04	THICKNESS OF CLAD INNER LINER	0.000
THICKNESS OF OUTER SHELL CLAD	0.000	THICKNESS OF FUEL TUBE	.200
DENSITY OF FUEL FORM CLAD	.0201	DENSITY OF CLAD INNER LINER	0.0000
DENSITY OF OUTER SHELL CLAD	0.0000	DENSITY OF FUEL TUBE	.0195

FUEL-FORM INPUTS

FUEL FORM MATERIAL	PU-238 METAL	FUEL BLOCK MATERIAL	GRAPHITE
FUEL FORM POWER DENSITY	3.60	NORMALIZED MATRIX DENSITY FOR FUEL PIN ARRAY	.60
FUEL PIN EFFECTIVENESS FACTOR	1.00	FUEL PIN ARRAY OPTION (0-CIRCLE,1-CLOSE PACK)	1.00
FUEL PIN TO FUEL TUBE SEPARATION	.500	FUEL PIN SEPARATION	.50
NO. OF FUEL PINS	10.00	EFFECTIVE SURFACE PWR. DENS. AVAILABLE FOR MODULE	10.00
HEAT TRANSFER TO MODULE (1-CONDUCTION,2-RADIATION)	1.00	DENSITY OF FUEL BLOCK	.0198
DENSITY OF FUEL FORM	.0251	DENSITY OF FUEL PIN	.0251
LIMITING ASPECT RATIO FOR FUEL FORM	2.50	LIMITING ASPECT RATIO FOR FUEL PIN	4.00

HEAT SOURCE SUPPORT INPUTS

END HEAT SOURCE SUPPORT MATERIAL	MIN-K 2000	RADIAL HEAT SOURCE SUPPORT MATERIAL	MIN-K 2000
END THERMAL INSULATION MATERIAL	MIN-K 2000	RADIAL THERMAL INSULATION MATERIAL	MIN-K 2000
ABSOLUTE END SUPPORT (0-ALL END OR 1-SOME RADIAL)	1.00	ABSOLUTE RADIAL SUPPORT (0-ALL RADIAL OR 1-SOME END)	1.00
END SUPPORT ELASTIC MODULUS (COMPRESSION)	0.20E+04	RADIAL SUPPORT ELASTIC MODULUS (COMPRESSION)	0.20E+04
END SUPPORT ELASTIC MODULUS (SHEAR)	0	RADIAL SUPPORT ELASTIC MODULUS (SHEAR)	0
GEN LENGTH INDEPENDENT OF END DEFLECTION,0-NO,1-YES	1.00	END SUPPORT FOIL SEPARATION	0.000
RADIAL SUPPORT FOIL SEPARATION	0.000	END INSULATION FOIL SEPARATION	0.000
RADIAL INSULATION FOIL SEPARATION	0.000	END SUPPORT THERMAL CONDUCTIVITY	.0008
RADIAL SUPPORT THERMAL CONDUCTIVITY	.0008	END INSULATION THERMAL CONDUCTIVITY	.0008
RADIAL INSULATION THERMAL CONDUCTIVITY	.0008	END SUPPORT DENSITY	.0009
RADIAL SUPPORT DENSITY	.0009	END INSULATION DENSITY	.0009
RADIAL INSULATION DENSITY	.0009	MAX ALLOWED END SUPPORT DEFLECTION	.0508

MAX ALLOWED RADIAL SUPPORT DEFLECTION	.0508		
		GENERATOR SHELL INPUTS	
GENERATOR SHELL MATERIAL	MAGHM21A-T8	FINAL VALUE FOR GENERATOR LENGTH	300.00
NORMAL GENERATOR LENGTH INCREMENT	20.000	INITIAL VALUE FOR GENERATOR LENGTH	120.00
DENSITY OF GENERATOR SHELL	.0039	THICKNESS OF END ABLATOR	0.000
RADIAL ABLATOR THICKNESS	0.000	THERMAL CONDUCTIVITY OF GENERATOR SHELL	1.370
LIMIT FOR GENERATOR ENVELOPE ASPECT RATIO	30.00	LIMIT FOR GENERATOR SHELL ASPECT RATIO	25.000
TOTAL HEAT DUMP CAPABILITY FOR ENDS (PERCENT)	.500	GENERATOR SHELL THICKNESS	.50
		RTG ANALYSIS COMPUTATION OPTIONS	
T/E ARRAY COMPUTATION SEQUENCE	1.00	GENERATOR LENGTH COMPUTATION SEQUENCE	0.00
T/E ELEMENT LENGTH COMPUTATION SEQUENCE	0.00	FUEL FORM GEOMETRY OPTION	1.000
HEAT SOURCE SUPPORT COMPUTATION OPTION	0.00	END INSULATION COMPUTATION OPTION	0.00
INSULATION AND HEAT SOURCE SUPPORT OPTION	0.00	INSULATION AND HEAT SOURCE SUPPORT MATERIAL OPTION	1.00
PRINT OPTION FOR OUTPUT DATA	1.00	PLOT OPTION	1.00
		TEMPERATURES	
T/E COLD JUNCTION TEMPERATURE	500.0	THERMAL INSULATION COLD SIDE TEMPERATURE	485.0
T/E HOT JUNCTION TEMPERATURE	800.0	THERMAL INSULATION HOT SIDE TEMPERATURE	813.0
HEAT SOURCE SURFACE TEMPERATURE	813.0	RADIATOR FIN AND GENERATOR SHELL TEMPERATURE	484.0
		GENERAL DESIGN INPUTS	
ASSUMED ENGINEERING EFFICIENCY	.900	MIN ALLOWED T/E ELEMENT LENGTH	.800
MAX ALLOWED T/E ELEMENT LENGTH	3.000	AXIAL G-LOAD	30.00
RADIAL G-LOAD	30.00	GENERATOR POWER LEVEL	250.0
HEAT SOURCE IMPACT VELOCITY	98.4	END OF MISSION T/E EFFICIENCY	.0617

THE PRINT OUT FOLLOWING THIS PAGE APPEARS AFTER EACH GENERATOR LENGTH ITERATION.

THE PRINT OUT APPEARS ONLY IF GENERATOR LENGTH REMAINS INDEPENDENT OF HEAT SOURCE SUPPORT DEFLECTION.

(I.E. THE INPUT VARIABLE ZP WAS SET EQUAL TO 0 OR THE HEAT SOURCE SUPPORT

DID NOT REACH THE MAXIMUM ALLOWED DEFLECTION)

WARNING HEAT SOURCE LENGTH EXCEEDS MODULE LENGTH BY MORE THAN ONE HEAT SOURCE DIAMETER

FOR LOW THERMAL CONDUCTIVITY HEAT SOURCES THE MODULE HEAT SOURCE MISMATCH MAY RESULT IN A LOWER ENGINEERING EFFICIENCY THAN HAS BEEN CALCULATED HERE

HEAT SOURCE SURFACE TEMPERATURES MAY ALSO EXCEED DESIRED LIMITS

PAGE 1

SUMMARY OF OUTPUT DATA

GENERATOR LENGTH = 180.0

I GEOMETRIC DESIGN DATA	(CM)	(IN)
OVER ALL GENERATOR LENGTH	180.0	70.9
RADIATOR FIN HEIGHT	18.2	7.2
DIAMETER OF GENERATOR SHELL (O.D.)	11.67	4.59
DIAMETER OF GENERATOR SHELL (I.D.)	10.67	4.20
BASE THICKNESS OF RADIATOR FIN	.272	.107
DIAMETER OF HEAT SOURCE	5.67	2.23
DIAMETER OF FUEL BLOCK	5.67	2.23
LENGTH OF HEAT SOURCE	173.99	68.50
LENGTH OF SEGMENT OF HEAT SOURCE	3.70	1.46
DIAMETER OF FUEL PIN	1.17	.46
DEPTH OF MODULE	1.654	.651
WIDTH OF MODULE	3.15	1.24
LENGTH OF MODULE	67.89	26.73
LENGTH OF T/E ELEMENTS	1.400	.551
NO. OF HEAT SOURCE SEGMENTS	47	
NO. OF FUEL PINS	470	
NO. OF T/E COUPLES IN GENERATOR	1374	
NO. OF T/E COUPLES PER MODULE	275	
NO. OF T/E ELEMENTS IN WIDTH OF MODULE	5.0	

II COMPONENT WEIGHTS	(LB)	(KG)
TOTAL GENERATOR WEIGHT	164.5	74.7
HEAT SOURCE WEIGHT	93.3	42.4
MODULE WEIGHT	28.9	13.1
RADIATOR FIN WEIGHT	8.7	4.0
END HEAT SOURCE SUPPORT WEIGHT	.11	.05
RADIAL HEAT SOURCE SUPPORT WEIGHT	1.12	.51
GENERATOR SHELL WEIGHT	12.66	5.75

III HEAT BALANCE AND THERMAL INVENTORY	(WATTS)
GENERATOR OUTPUT POWER (E)	250.0
GENERATOR INPUT POWER (TH)	4328.9
HEAT DUMPED BY RADIATOR (TH)	2931.9
HEAT DUMPED BY ENDS (TH)	29.9
GENERATOR ENGINEERING EFFICIENCY(DECIMAL)	.936
T/E COUPLE EFFICIENCY (DECIMAL)	.0617

GENERATOR LENGTH = 180.0

OUTPUT DATA

I GEOMETRIC DESIGN DATA

	(CM)	(IN)
1 MODULE AND T/E		
DEPTH OF MODULE	1.654	.651
WIDTH OF MODULE	3.15	1.24
LENGTH OF MODULE	67.89	26.73
T/E ELEMENT LENGTH	1.400	.551
STAGE 1 LENGTH FOR SEGMENTED N-TYPE T/E ELEMENT	1.400	.551
STAGE 1 LENGTH FOR SEGMENTED P-TYPE T/E ELEMENT	1.400	.551
STAGE 2 LENGTH FOR SEGMENTED N-TYPE T/E ELEMENT	0.000	0.000
STAGE 2 LENGTH FOR SEGMENTED P-TYPE T/E ELEMENT	0.000	0.000
STAGE 3 LENGTH FOR SEGMENTED N-TYPE T/E ELEMENT	0.000	0.000
STAGE 3 LENGTH FOR SEGMENTED P-TYPE T/E ELEMENT	0.000	0.000
DEPTH OF N-TYPE ELEMENT	.579	.228
DEPTH OF P-TYPE ELEMENT	.604	.238
WIDTH OF N-TYPE ELEMENT	.604	.238
WIDTH OF P-TYPE ELEMENT	.604	.238
AREA OF MODULE PERPINDICULAR TO HEAT FLOW	213.7	33.1
HEAT LOSS AREA FOR MODULE ELECTRICAL AND THERMAL INSULATION	83.45	12.94
HEAT LOSS AREA FOR MODULE PERIPHERY	0.00	0.00
NO. OF T/E COUPLES IN GENERATOR	1374	
NO. OF T/E COUPLES PER MODULE	275	
T/E ELEMENT LENGTH ITERATION NO.	1	
NO. OF COUPLES IN LENGTH OF MODULE	55.0	
NO. OF COUPLES IN WIDTH OF MODULE	5.0	

2 HEAT SOURCE AND FUEL FORM	(CM)	(IN)
HEAT SOURCE DIAMETER	5.67	2.23
FUEL BLOCK DIAMETER	5.67	2.23
HEAT SOURCE LENGTH	174.0	68.5
HEAT SOURCE SEGMENT LENGTH	3.70	1.46
FUEL PIN CENTER TO CENTER SEPARATION	0.00	0.00
FUEL PIN DIAMETER	1.17	.46
THICKNESS OF FUEL FORM CLAD	.102	.040
THICKNESS OF FUEL FORM CLAD LINER	0.000	0.000
THICKNESS OF FUEL FORM OVER-CLAD	0.000	0.000
THICKNESS OF FUEL TUBE	.200	.079
DIAMETER OF FUEL FORM	.97	.38
LENGTH OF FUEL FORM	164.4	64.7
NO. OF FUEL PINS	470	
NO. OF CLAD ITERATIONS	10	

OUTPUT DATA (CONTINUED)

GENERATOR LENGTH = 180.0

I GEOMETRIC DESIGN DATA (CONTINUED)

2 HEAT SOURCE AND FUEL FORM (CONTINUED)	(CM)	(IN)
LENGTH OF FUEL FORM SEGMENT	3.50	1.38
LENGTH INCREMENT TO SIZE FUEL FORM	.030	.012
TOLERENCE ON LENGTH OF FUEL FORM	.030	.012
FUEL FORM VOLUME	1202.5	73.3
FUEL PIN VOLUME	2.56	.16
RATIO OF FUEL FORM LENGTH TO DIAMETER	3.63	
NO. OF FUEL FORM SEGMENTS	47	
FUEL FORM LENGTH ITERATION NO.	26	

3 RADIATOR FIN AND GENERATOR SHELL	(CM)	(IN)
OVER ALL GENERATOR LENGTH	180.0	70.9
RADIATOR FIN HEIGHT	18.22	7.17
RADIATOR FIN BASE THICKNESS	.272	.107
OUTSIDE DIAMETER OF GENERATOR SHELL	11.67	4.59
INSIDE DIAMETER OF GENERATOR SHELL	10.67	4.20
NO. OF LARGE ITERATIONS FOR RADIATOR ANALYSIS	15	
NO. OF SMALL ITERATIONS FOR RADIATOR ANALYSIS	1	

4 INSULATION AND HEAT SOURCE SUPPORT	(CM)	(IN)
END SEPARATION BETWEEN HEAT SOURCE AND SHELL	2.507	.987
RADIAL SEPARATION BETWEEN HEAT SOURCE AND SHELL	2.500	.984
HEAT SOURCE DEFLECTION AGAINST END SUPPORT	.139	.055
HEAT SOURCE DEFLECTION AGAINST RADIAL SUPPORT	.017	.007
HEAT LOSS AREA FOR RADIAL INSULATION	675.6	104.7
HEAT LOSS AREA FOR END INSULATION	0.00	0.00
END AREA AVAILABLE FOR SUPPORT	25.2	3.9
AREA REQUIRED FOR END SUPPORT	69.1	10.7
RADIAL AREA AVAILABLE FOR SUPPORT	1020.0	158.1
RADIAL AREA REQUIRED FOR SUPPORT	344.4	53.4
HEAT LOSS AREA FOR END HEAT SOURCE SUPPORT	25.2	3.9
HEAT LOSS AREA FOR RADIAL HEAT SOURCE SUPPORT	344.4	53.4
NO. OF END INSULATION ITERATIONS	1.0	

OUTPUT DATA(CONTINUED)

GENERATOR LENGTH = 180.0

II COMPONENT WEIGHTS	(LB)	(KG)
TOTAL GENERATOR WEIGHT	164.53	74.70
1 MODULE AND T/E		
WEIGHT OF T/E MATERIALS	28.93	13.13
WEIGHT OF T/E HARDWARE	15.91	7.22
WEIGHT OF MODULE CAN	0.00	0.00
WEIGHT OF T/E MODULE	28.93	13.13
2 HEAT SOURCE AND FUEL FORM		
FUEL FORM WEIGHT	30.18	13.70
FUEL FORM SEGMENT WEIGHT	.64	.29
FUEL PIN WEIGHT	.06	.03
CLAD FUEL PIN WEIGHT	.09	.04
FUEL TUBE WEIGHT	11.65	5.29
FUEL BLOCK WEIGHT	38.17	17.33
WEIGHT OF CLAD LINER	0.00	0.00
WEIGHT OF OUTER CLAD	0.00	0.00
PRIMARY CLAD WEIGHT	13.30	6.04
WEIGHT OF REENTRY ABLATOR	0.00	0.00
HEAT SOURCE TOTAL WEIGHT	93.31	42.36

	(LB)	(KG)
3 RADIATOR FIN AND GENERATOR SHELL		
RADIATOR FIN WEIGHT	8.74	3.97
GENERATOR SHELL WEIGHT	12.66	5.75
4 INSULATION AND HEAT SOURCE SUPPORT		
END INSULATION WEIGHT	.29	.13
RADIAL INSULATION WEIGHT	3.47	1.57
END HEAT SOURCE SUPPORT WEIGHT	.11	.05
RADIAL HEAT SOURCE SUPPORT WEIGHT	1.12	.51

OUTPUT DATA(CONTINUED)

GENERATOR LENGTH = 180.0

III HEAT BALANCE AND THERMAL INVENTORY (WATTS)

1 MODULE AND T/E

T/E COUPLE EFFICIENCY (1)	.0617
HEAT LOSS THROUGH MODULE CAN	0.00
HEAT LOSS THROUGH ELECTRICAL INSULATION	75.68
SURFACE POWER DENSITY (2)	4.15

2 HEAT SOURCE AND FUEL FORM

HEAT SOURCE THERMAL INVENTORY	4328.94
FUEL FORM POWER DENSITY (3)	3.6000

3 RADIATOR FIN AND GENERATOR SHELL

HEAT DUMPED BY RADIATOR FINS	2931.89
HEAT DUMPED BY GENERATOR SHELL ENDS	29.93

4 INSULATION AND HEAT SOURCE SUPPORT

HEAT LOSS THROUGH END INSULATION	6.71
HEAT LOSS THROUGH RADIAL INSULATION	98.90
HEAT LOSS THROUGH MODULE WEDGE INSULATION	.65
HEAT LOSS BY RADIATION FROM MODULE PERIPHERY	39.03
HEAT LOSS THROUGH END HEAT SOURCE SUPPORT	5.28
HEAT LOSS THROUGH RADIAL HEAT SOURCE SUPPORT	50.42
TOTAL PARASITIC HEAT LOSS	276.67

5 GENERAL

CALCULATED ENGINEERING EFFICIENCY (1)	.9360
GENERATOR POWER LEVEL	250.00

(1) DECIMAL UNITS
(2) WATTS (TH) PER SQ. CM.
(3) WATTS (TH) PER CUBIC CM.

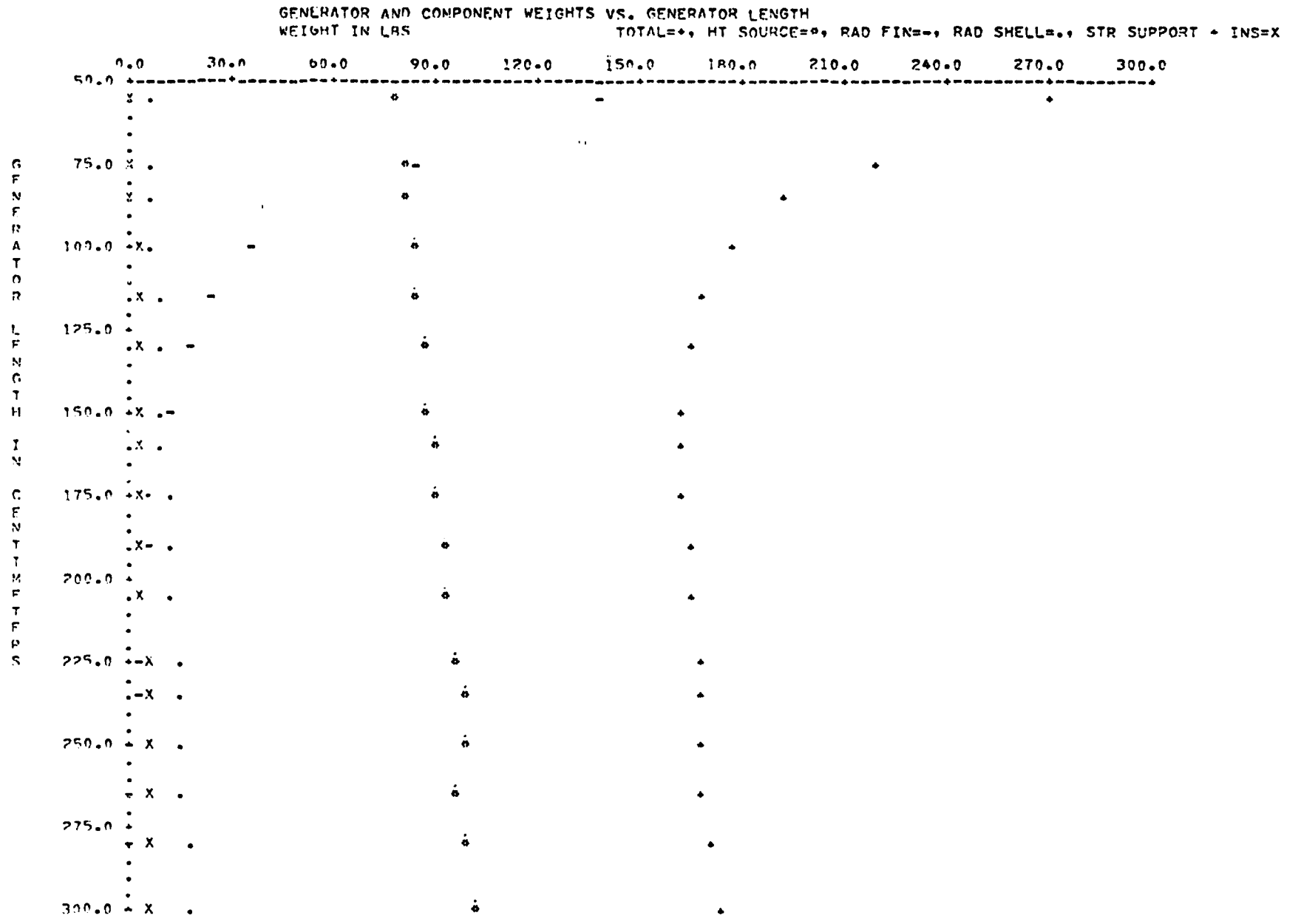
GENERATOR AND COMPONENT WEIGHTS VS. GENERATOR LENGTH
WEIGHT IN LBS
TOTAL=+, HT SOURCE=*, RAD FIN=-, RAD SHELL=., STR SUPPORT + INS=X
0.0
30.0
60.0
90.0
120.0
150.0
180.0
210.0
240.0
270.0
300.0
50.0
75.0
100.0
125.0
150.0
175.0
200.0
225.0
250.0
275.0
300.0
GENERATOR LENGTH IN CENTIMETERS

APPENDIX IX

PROPERTY-TEST EQUIPMENT

Seebeck Coefficient Probe

The Seebeck voltage probing apparatus used to measure the Seebeck voltage of the surface of an element is shown schematically in Figure IX-1 and as photographed in Figure IX-2.

The apparatus consists of two reservoirs with copper electrodes attached to the base of the reservoir as shown in Figure IX-1. The two reservoirs are maintained at 0 C (using a mixture of ice and water) and at 100 C (using the boiling point of water), respectively. A digital voltmeter is connected to the electrodes to measure the potential difference. A voltage (Seebeck voltage) is generated between the electrodes when brought into contact with the surface of a thermoelement. The effective temperature difference during such a measurement is determined by contacting the two electrodes against a Constantan standard which is sized appropriately to yield a heat-sink capacity similar to that of the thermoelement which has much lower thermal conductivity. The voltage generated during this check is referred to the tabulated Seebeck characteristics of Constantan to obtain the corresponding temperature difference. The Seebeck coefficient of the thermoelement is determined by dividing the measured Seebeck voltage of the element by the temperature difference determined using the Constantan reference material.

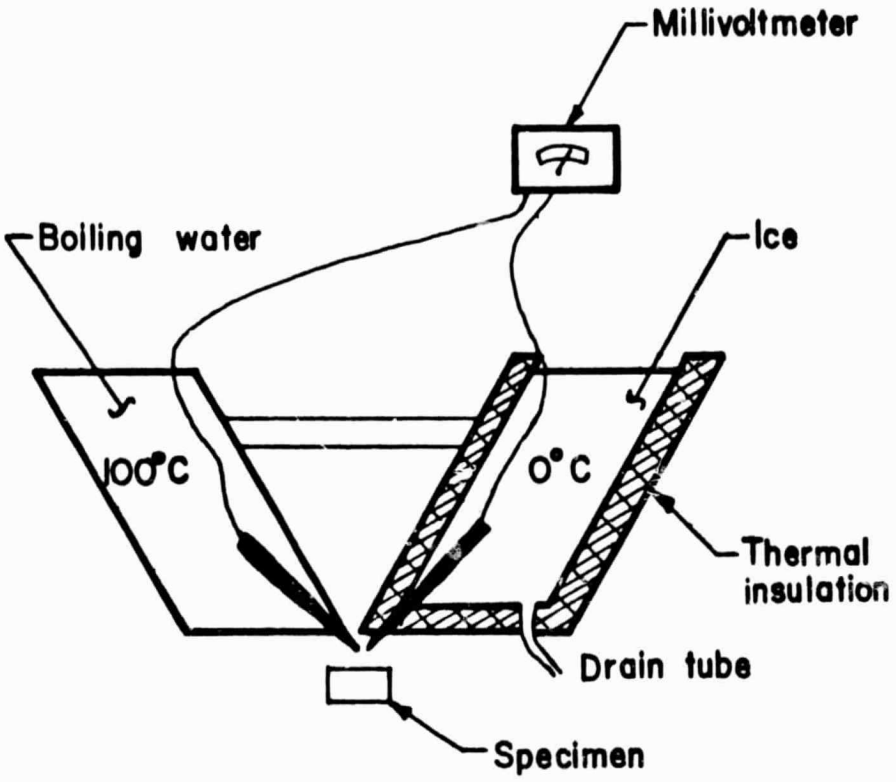

FIGURE IX-1. SKETCH OF SEEBECK VOLTAGE PROBE APPARATUS

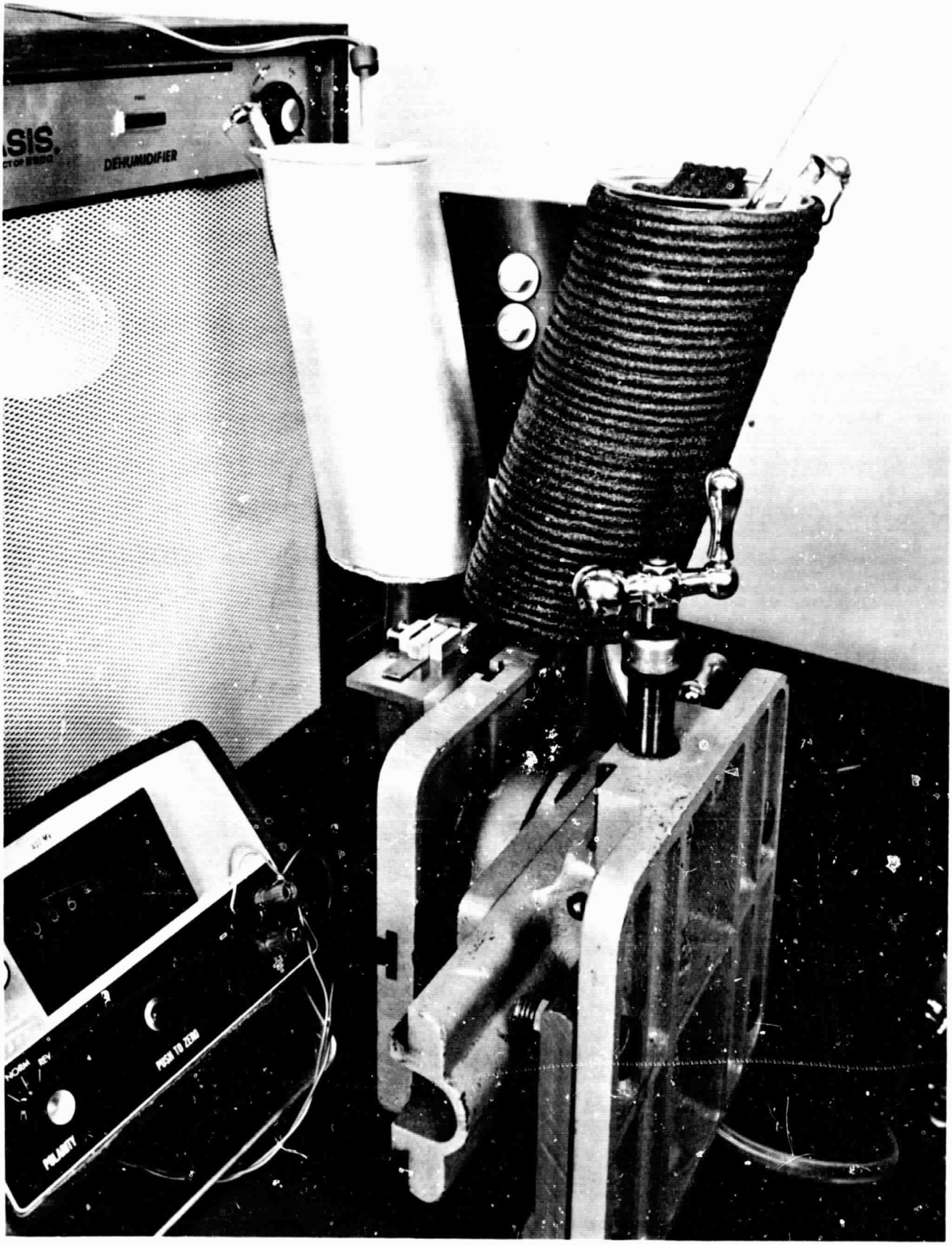

FIGURE IX-2. SEEBECK VOLTAGE PROBE APPARATUS 39947

Thermal-Diffusivity Measurement Apparatus

A photograph of the thermal-diffusivity apparatus is shown in Figure IX-3 and a schematic of the principal parts of the system in Figure IX-4. This thermal-diffusivity equipment involves the single-heat-wave of flash method, employing a laser source for the heat pulse. Basically, the method consists of subjecting one face of a thin specimen to a short-duration thermal impulse and measuring the time-temperature history of the back face of the specimen. The thermal diffusivity is calculated from the specimen thickness and the time required for the back face of the specimen to reach one-half temperature amplitude ($t_{1/2}$) from the instant of thermal input from the laser. The back face of the specimen is monitored by a lead sulfide radiation receiver using suitable optics. The specimen is a small disk nominally 3/8 in. in diameter and from 0.01 to 0.07 in. thick. A furnace is used in the environmental chamber to raise the temperature to the desired level prior to the thermal input.

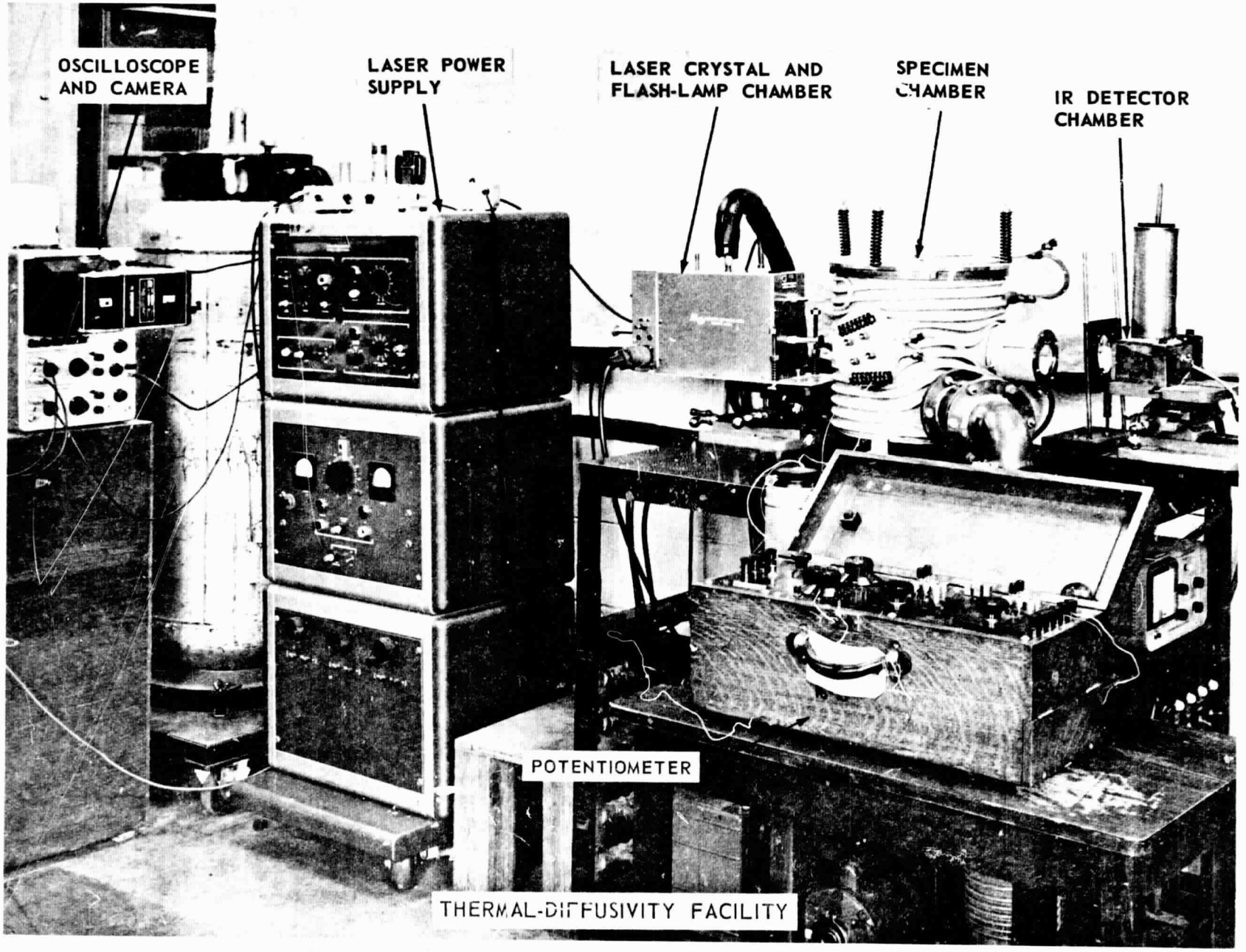

FIGURE IX-3. PHOTOGRAPH OF THERMAL-DIFFUSIVITY APPARATUS

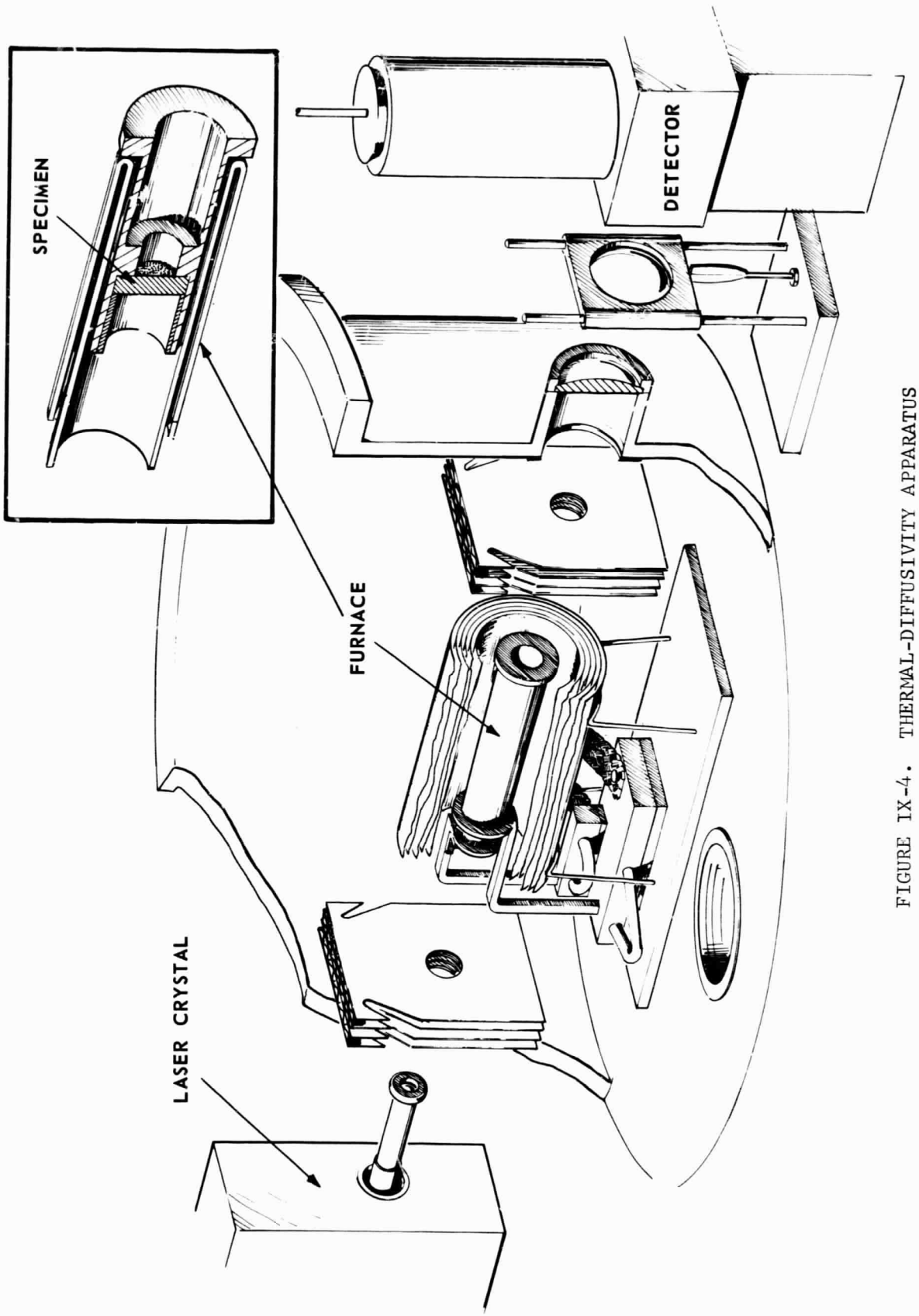

FIGURE IX-4. THERMAL-DIFFUSIVITY APPARATUS